

University of Leoben
Department of Applied Geosciences



**Geology of the Fanjiabauzi Talc
Deposit, Liaoning Province, China**

by
David Misch, BSc

Eidesstattliche Erklärung

Ich erkläre an Eides statt, dass ich diese Arbeit selbstständig verfasst, andere als die angegebenen Quellen und Hilfsmittel nicht benutzt und mich auch sonst keiner unerlaubten Hilfsmittel bedient habe.

Affidavit

I declare in lieu of oath, that I wrote this thesis and performed the associated research myself, using only literature cited in this volume.

Leoben, September 2012

David Misch

Abstract

The talc deposits of China are world class concerning size and quality of mineralization. The largest deposit of China is located near the village of Mafeng in the Eastern Liaoning Province (Fanjiabauzi). Mineralizations of talc occur in Early Proterozoic Mg-rich carbonates. The region also hosts some of the world's largest magnesite deposits. Talc from Fanjiabauzi is remarkably pure and shows only minor impurities compared to other deposit types, especially compared to alpine talc deposits. Genesis of talc and host rock was heavily discussed in the past, new data concerning rock chemistry, isotopic composition and composition of fluid inclusions strengthens the widespread thesis of primary magnesite formation in an Early Proterozoic, shallow marine or lagoonal environment with significant freshwater influence. Later multiple deformation events formed large, high-quality magnesite marble deposits along an E-W-trending belt in the Eastern Liaoning Province. The age of hydrothermal talc formation responsible for the high-quality talc deposit of Fanjiabauzi remains unclear, as the deformation history in the region is very complex. Multiple deposit forming processes occurred in several mineralization periods throughout the geologic history from the Early Proterozoic until the young Himalayan orogenic event. Nevertheless, chemical analysis of talc shows no evidence for multiple generations of talc formation. Several other hydrothermal deposits in the Eastern Liaoning Province are attributed to the Triassic (Indosinian) metallogenic period, correlation of the Fanjiabauzi deposit with other locations in the region requires further investigation.

Zusammenfassung

Die Talk-Vorkommen Chinas zählen zu den weltweit bedeutendsten Talk-Lagerstätten hinsichtlich Qualität und Größe der Mineralisation. Einige der wichtigsten chinesischen Talk-Lagerstätten befinden sich im sogenannten Haicheng-Dashiqiao-Talk-Magnesit-Belt im Nordosten des Landes. Hier ist auch die Talklagerstätte Fanjiabauzi lokalisiert. Talk wurde hier in Mg-reichen Karbonaten des frühen Proterozoikums im Zuge hydrothermalen Alteration des Nebengesteins gebildet. Neben Talk befinden sich auch einige weltweit bedeutende Magnesitlagerstätten innerhalb des Haicheng-Dashiqiao-Belts. Eine Besonderheit des Talks aus Fanjiabauzi ist die außerordentliche Reinheit und der hohe Weißegrad des Produkts im Vergleich zu anderen Lokalitäten. Die Magnesitgenese ist bis heute Teil heftiger Kontroversen, das häufig vertretene syngenetisch-sedimentäre Bildungsmodell steht einem epigenetisch-metasomatischen Ansatz gegenüber. Die in dieser Arbeit gesammelten Daten sprechen für das syngenetisch-sedimentäre Modell, welches traditionell als Erklärung der außergewöhnlich mächtigen Magnesitabfolgen der Region herangezogen wird. Isotopenverteilung, Spurenelementgehalte und Zusammensetzung von Flüssigkeitseinschlüssen aus dem Magnesit sprechen für ein frühproterozoisches, flachmarines Bildungsmilieu mit signifikantem Süßwassereinfluss. Spuren biogener Aktivität (Stromatolithen) sowie sedimentäre Marker wie Trockenrisse bestätigen dieses Modell. Spätere Metamorphoseevents führten zu einer nahezu vollständigen Rekristallisation des primären Magnesitsediments, dieser Prozess ist für die Bildung der bedeutenden Magnesitlagerstätten des E-W-streichenden Haicheng-Dashiqiao-Belts verantwortlich. Bildungszeitraum und Genesemodell der Talkvorkommen der östlichen Liaoning-Provinz sind weiterhin nicht eindeutig geklärt. Grund dafür ist die komplexe metamorphe Tektonik in der Region. Lagerstättenbildende Prozesse fanden laufend statt und sind in verschiedenen metallogenetischen Perioden vom frühen Proterozoikum bis zur jungen Himalaya-Orogenese eingeteilt. Viele hydrothermale Lagerstätten der Region werden der triassischen (indosinischen) Vererzungsperiode zugeordnet, eine Korrelation von Fanjiabauzi mit anderen Lokalitäten und Vererzungstypen bekannter Bildungsalter erfordert weitere Untersuchungen. Die chemische Elementverteilung ausgewählter Talkproben spricht nicht für mehrere Generationen der Talkbildung.

Project summary

The chemical and structural analysis of the Aihai talc deposit confirmed the impression of the 2009 fieldwork. The talc shows exceptionally high quality and purity, which is almost unique worldwide. The Haicheng talc deposit is stated as the world's largest talc deposit by Chinese mining authorities. The chemical analysis of the talc samples collected during the 2010 field work shows very low grades of contamination with trace minerals like mica, also the values for trace elements embedded in the talc structure are very low especially for the grade 1 talc product. This causes the remarkably high grades of whiteness and the low LOI values for the grade 1 samples. The LOI is about 3 to 5 percent higher for grade 2 talc samples; the reason for this increase of volatile components is a higher content of carbonate minerals like magnesite and dolomite, which lose their CO₂ during heating. This higher carbonate content is also proved by higher CaO and MgO values for the average grade 2 talc. The contents of other trace elements like FeO and Al₂O₃ are also slightly higher in the average grade 2 talc, although the values in general are typically low, which can be expected for carbonate host talc deposits. These values are mostly controlled by mineral impurities, for example mica or other mineral components, which were mechanically integrated in the talc shear zones. The elements Co, Ni, Cr, Cu and W are throughout under the detection limit, this again proves the absence of ultramafic rocks during the primary talc formation. The only mafic components present at the Aihai talc mine are lamprophyre dykes which are younger than the talc formation and mostly do not influence the quality of the deposit. Only in some parts of the deposit, some dyke components are included into small talc bodies because of tectonic movement. This occurrence does not affect the quality of the mineable talc.

The host rock of the talc deposit consists mostly of magnesitic and dolomitic marble, the magnesite marble shows some interesting characteristics which allow to draw conclusions if major amounts of talc are present in the nearest environment. In general, the marble in the direct neighborhood of remarkable talc bodies shows a higher purity. There is less contamination with other mineral components like mica, although this pollution is also very minor for magnesite without talc in the nearest environment. This difference is proved by slightly lower Al and Sr values for the talc-

host magnesite samples. The values for trace elements included into the magnesite crystal lattice also show a decrease when a talc shear zone with a size relevant for production is close to the sampling spot. The values for Mn, Fe and Ca show the same trend, the reason for the higher Ca contents in non-talc magnesite most likely is caused by small amounts of dolomite admixed with the magnesite rock. Therefore, increasing dolomite contents could indicate the departure from the nearest deposit environment. In summary, the higher purity of talc-hosting magnesite in comparison to magnesite without talc in the direct neighborhood is evident and represents the influence of late hydrothermal activity, coherent with the actual talc formation in the older magnesite belt. The differences in the chemical composition could be helpful for the detection of mineable talc in the actual mining levels, although this can only be an additional support for traditional exploration and requires a constant sampling and testing procedure.

Another potential indicator for talc shear zones is the texture and coloration of the host rock. The magnesite at the borders of large talc bodies has a bright white coloration and a fine-grained, compact fabric. The magnesite occurring further away from the deposit borders has often a slightly grey coloration and a coarser grained fabric, dolomite occurs often away from the deposit borders whereas at the borders pure magnesite dominates. This correlates with the higher Ca and Fe content of the host rock samples, higher Ca values away from the deposit are caused by dolomite, higher Fe is likely to be caused by pyrite impurities which are common in dolomite but do not occur widespread in the pure magnesite.

The genetic processes involved in the deposition of massive Archean carbonate beds in the Eastern Liaoning Province are heavily discussed. Fluid inclusion chemism and isotopic composition of magnesite marble from Fanjiabauzi indicate that the carbonate beds were deposited in a lagoonal to shallow marine evaporitic environment, with significant freshwater dilution. Later hydrothermal and metamorphic processes modified fluid and mineral chemism as well as the isotopic composition of the host rock. This gives reason for different interpretations concerning the deposit formation and later development of the regional geology. By now, the age of deposit formation is not clearly defined and requires further investigation and correlation with data from other regional locations.

In contrast to the extraordinary good quality and purity of the high grade talc at the Aihai concession area, the structural situation due to the mining activity is more complicated. The past method of mining unfortunately caused the loss of valuable talc resources due to a comparatively low average recovery rate. This low recovery rate is caused by a lack of future-oriented mine planning as well as the use of inappropriate blasting techniques which destabilize the host rock due to extensive use of explosives. Because of the uncoordinated mining activities in three different underground mines, large parts of the deposit are lost for future production. Also the mining method itself destabilizes the overlying rock, the already tectonically weakened host rock reacts massively on the mining activity, this is documented by large sinkholes and tear-off edges which show the slope instability of large areas, especially above mine 6. Backfilling of empty tunnels with concrete would improve the situation, although the present damages are irreversible. For the safety of the workers and also the remaining resources, a detailed concept for future production should be worked out by mining engineers, better quality control and product reproducibility should be taken into account as well as a higher grade of process mechanization. An optimized process-chain from blasting to the sorting of different product qualities will increase the possible amount of production and reduces costs for explosives, blasting fines and unnecessary lost deposit parts. The basis for such a concept is the acquisition of more essential data concerning the deposit size, location and quality distribution. The 2011 drilling campaign will deliver this important deposit information and can be expected to be a great tool for future planning activities.

For the documentation of surface movements and potential mining-induced risks like sinkholes, a map of survey-points is necessary. Such points should be remeasured at least every two months to document possible rapid developments of slope instabilities. It seems that the slope destabilization in the whole concession area got worse between the 2009 and 2010 field work, although without a quantification by exact measurements, there is no possibility for a clear statement or a prognosis of further development in problematic zones. Especially if there is a plan for further open pit mining in the area of mine 6, there is a great potential for problems because of destabilization caused by past underground mining in the mines 6 and 1. In general, an actual surface map is missing. An adequate surface map is a basic requirement for the planning of extended waste dumps open pit operation etc.

Content

1	<i>Introduction</i>	1
2	<i>General Overview</i>	4
2.1	<i>Definition of Talc</i>	4
2.2	<i>Technical properties</i>	6
2.2.1	Ceramics	6
2.2.2	Coatings	6
2.2.3	Paper	6
2.2.4	Plastics.....	7
2.2.5	Cosmetics and Pharmaceuticals	7
2.3	<i>Types of talc deposits</i>	7
2.3.1	Ultramafic-hosted Talc Deposits	8
2.3.2	Carbonate-hosted Talc Deposits.....	8
2.4	<i>Worldwide distribution of talc producers and consumers</i>	10
2.5	<i>Chinese talc production – detailed review</i>	12
3	<i>Aihai Talc Deposit</i>	15
3.1	<i>Regional Geology</i>	15
3.2	<i>Local Situation</i>	20
3.3	<i>Types of talc mineralization</i>	27
3.3.1	Type 1	29
3.3.2	Type 2	31
3.3.3	Type 3	33
3.3.4	Type 4	35
3.4	<i>Chemical Analysis</i>	37
3.4.1	Methods and Equipment	37
3.4.2	Samples	38
3.4.3	Talc	40
3.4.4	Magnesite.....	45
3.5	<i>Tectonic Setting</i>	58
3.5.1	General Setting	59

3.5.2	Detailed Fault Systems	61
3.6	Geo-risks.....	63
4	Discussion.....	69
4.1	<i>Genetic aspects.....</i>	69
4.2	<i>Talc quality and exploration.....</i>	77
4.3	<i>Recommendations</i>	81
4.3.1	Mining and Geo-risks	81
4.3.2	Sorting.....	83
	References.....	86
5	Appendix	94
5.1	<i>Thin-Sections (see detailed description below)</i>	94
5.2	<i>Outcrops (see detailed description below).....</i>	99
5.3	<i>Mining subsidence damages (for detailed information see chapters “Geo-risks” above).....</i>	115
5.4	<i>Maps and Sections (provided by geological staff of Aihai Talc Company Ltd. (see references)).....</i>	117
5.5	<i>Mining levels (more detailed information retrievable from digital 3D deposit model (Misch & Pluch, 2009)).....</i>	129
5.5.1	Mine 1	129
5.5.2	Mine 4	136
5.5.3	Mine 6	138
5.6	Chemical Analysis.....	140
5.6.1	Talc main elements	140
5.6.2	Talc trace elements.....	140
5.6.3	Talc whiteness and yellowness index	141
5.6.4	Magnesite AAS	141
5.6.5	Magnesite whiteness and yellowness index.....	142
5.6.6	Main element content for selected samples from Aihai Magnesite....	142
5.6.7	Carbon and oxygen isotope distribution of selected magnesite samples from the Fanjiabauzi deposit	143
5.7	Structural Data.....	144

5.7.1	Mine 1	144
5.7.2	Mine 4	145
5.7.3	Mine 6	146
5.8	<i>Drillholes</i>	147

Figures

Figure 1: Geographical position of the Fanjiabauzi talc deposit near the village of Mafeng, Eastern Liaoning Province of China.....	1
Figure 2: Schematic crystal structure of 2:1 layer phyllosilikates (e.g. talc and pyrophyllite), the octrahedral cations are Mg for talc and Al for pyrophyllite, whereas the tetrahedral cations are Si for both minerals (http://wgharris.ifas.ufl.edu/SEED/). .	5
Figure 3: Typically talc has a massive habitus without visible crystals.	5
Figure 4: Development of mining production over the last three decades by regions (CPA: China, NAM: Northern America, WEU: Western Europe) (Weber et al, 2010).	10
Figure 5: Tectonic setting and location of main metallogenic provinces at the NCC (Zhai et al, 2004).	15
Figure 6: Position of Talc and Magnesite deposits in the north slope zone of the Eastern Liaoning paleorift environment (no. 12, red mark) (Chen et al, 2002).	16
Figure 7: Location of the Paleoproterozoic Jiao-Liao Belt which hosts the Liaohe-Group (Zhao et al 2001).	17
Figure 8: Detailed description of the Formations which represent the Early Proterozoic Liaohe-Group (Li et al 2004).....	18
Figure 9: Geological map of the Fanjiabauzi mining area (red outline shows the border of the Aihai concession area) after Wang et al, 2005.....	21
Figure 10: Pyrite-impurity in massive dolomite (height of picture equals 1,35mm)...	22
Figure 11: Coarsely grained, pinolitic magnesite (Height of picture equals 1,35mm).	23
Figure 12: Fine grained magnesite (Height of picture equals 1,35mm).	24
Figure 13: Outcrop of mafic dyke, picture from Aihai magnesite mine (0,5km NE of Village Qushugou).	25
Figure 14: Thin-section of mafic dyke (height of picture equals 1,35mm).....	25
Figure 15: Thin section of strongly tectonized, altered dyke (height of picture equals 1,35mm, crossed nicols).....	26
Figure 16: Silicified border between mafic dyke and surrounding magnesite.	27
Figure 17: Equidimensional talc body with zoned borders to the surrounding magnesite (type1).....	30

Figure 18: Thin section of fine grained, massive talc, height of picture equals 0.25mm (type 1).	31
Figure 19: Magnesite relicts in fine grained talc matrix; thin section of the border zone from a small talc body, height of picture equals 1.35mm (type1).....	31
Figure 20: Talc formation starts in weak-zones between large magnesite crystals; magnesite is replaced by talc along border zones, height of picture equals 1.35mm (type 2).	32
Figure 21: In zones where talc accumulates, magnesite crystals occur as small fragments with reaction fabrics, height of picture equals 1.35mm (type 2).	33
Figure 22: Type 2 represents the transition between Type 1 and 3.....	33
Figure 23: Coarsely grained magnesite with talc between magnesite crystals (type 3).	34
Figure 24: Coarsely grained magnesite, talc is embedded along the borders between large magnesite crystals; no further accumulation of talc, height of picture equals 1.35mm (type 3).	35
Figure 25: Fig: Talc formation along weak-zone between two magnesite crystals with sizes of several millimeters, height of picture equals 1.35mm (type 3).....	35
Figure 26: Talc accumulation in shear zone (type 4).	37
Figure 27: Schematic position of sampling spots at the Fanjiabauzi mining area.....	39
Figure 28: Schematic element distribution trend of magnesite samples in relation to distance from talc occurrence.....	48
Figure 29: General influencing factors leading to relatively lighter or heavier C (after Baiquan, 2011).	51
Figure 30: General influencing factors leading to lighter or heavier O (after Baiquan, 2011).	52
Figure 31: Cl/Br-Cl-Plot after McCaig et al, 2000. The dotted line represents the seawater evaporation line (after Fontes and Matray, 1993).....	55
Figure 32: Cl/Br-Na/Br plot after McCaig et al, 2000. Seawater evaporation line from Fontes and Matray, 1993.....	56
Figure 33: Na versus Cl, evaporation line from Fontes and Matray, 1993.....	56
Figure 34: K versus Cl, evaporation line from Fontes and Matray, 1993.	57
Figure 35: Br/Cl-I/Cl-plot after McCaig et al, 2000.	57
Figure 36: Ca-Mg-plot from Fanjiabauzi magnesite marble	58

Figure 37: Suspected position of the large fault zone which causes the complex tectonic setting in the Aihai mining area.	60
Figure 38: Change of dip direction from mine 1 over mine 6 to mine 4. The transition zone represents the change of dip direction of magnesite host rock, the position coincides with the estimated large fault zone in the area of mine 6.....	60
Figure 39: Pole point-plot of mine 1 fault-data.	61
Figure 40: Pole point-plot of the fault-data from mine 6.....	62
Figure 41: Pole point-plot of the fault-data from mine 4.....	63
Figure 42: Estimated position of mining induced mass movements.	64
Figure 43: Position of sinkholes (red circles) related to underground mining activity.	65
Figure 44: Estimated origin of sinkholes above mine 6.	65
Figure 45: Sinkholes above mine 6.	66
Figure 46: Destroyed buildings indicate underground movement.....	66
Figure 47: Deep mass movement documented in a closed tunnel in the area of mine 6.	68
Figure 48: Stromatolites found along the southern borders of the Fanjia Bauzi mining area.	70
Figure 49: thin-section of fine-grained magnesite, height of picture equals 1,35mm.	71
Figure 50: Estimated location of primary magnesite deposition in a high saline, shallow water environment (Warren, 2010).	71
Figure 51: $\delta^{18}\text{O}$ - $\delta^{13}\text{C}$ -plot for selected magnesite deposits (after Kralik et al, 1989; Schroll, 1997; Schroll et al, 1999). The red mark represents the samples from the Fanjia Bauzi deposit.....	73
Figure 52: Cl/Br-Cl-plot for different types of seawater modified after Foriel et al, 2004.....	76
Figure 53: Position of zones with reduced slope stability and sinkholes related to underground mining activity.....	82
Figure 54: Border zone off talc-magnesite-intergrowth. Height of picture equals 1,35mm.....	84

Tables

Table 1: Elevation of sampling spots.....	39
Table 2: Chemical analysis of main element contents for grade 1 talc samples.....	41
Table 3: Chemical analysis of main element contents for grade 2 talc samples.....	41
Table 4: Summary of main element contents for all analyzed talc samples.....	41
Table 5: Summary of trace element analysis for all grades of talc samples (part 1).	42
Table 6: Summary of trace element analysis for all grades of talc samples (part 2).	43
Table 7: Summary of trace element analysis for all grades of talc samples (part 3).	43
Table 8: Whiteness and yellowness index of pink talc.....	44
Table 9: Whiteness and yellowness index of white talc.....	44
Table 10: Whiteness and yellowness index of yellow talc.....	44
Table 11: Whiteness and yellowness index of grey talc.....	44
Table 12: Whiteness and yellowness index of weathered talc.....	44
Table 13: Whiteness and yellowness index of product D60 (mixture).....	45
Table 14: Summary of AAS Data from magnesite samples with talc in the nearest environment. Samples were taken at Fanjiabauzi talc deposit.....	47
Table 15: Summary of AAS Data from magnesite samples without talc in the nearest environment. Samples were taken both at Fanjiabauzi talc and Aihai magnesite (0.5km NE of Village Qushugou).....	48
Table 16: Whiteness and yellowness index of coarse magnesite without talc.....	49
Table 17: Whiteness and yellowness index of fine to medium grained magnesite with massive talc.....	49
Table 18: Whiteness and yellowness index of fine magnesite near talc shear bands.....	49
Table 19: C and O isotopic composition of magnesite marbles from the Haicheng talc deposit.....	53
Table 20: Comparison of main element contents for selected magnesite samples from Aihai Talc and Aihai Magnesite.....	80
Table 21: Main element contents of selected magnesite samples from the Qushugou magnesite deposit (Aihai Magnesite).....	80

1 Introduction

The Fanjiabauzi talc deposit is located near the village Mafeng in the Eastern Liaoning Province of China (Fig. 1). It is part of the eastern margin of the North China Craton (NCC), which hosts some of the world's largest talc and magnesite deposits. The Aihai Talc Company produces approximately 150.000 tons of ore per year from the Fanjiabauzi deposit; therefore, the deposit ranks under the top ten worldwide concerning the annual production rate.



Figure 1: Geographical position of the Fanjiabauzi talc deposit near the village of Mafeng, Eastern Liaoning Province of China.

The main aim of this report is the geological and structural characterization of the Fanjiabauzi talc deposit concerning different types and quality of ore, host rock and the surrounding environment. For a better understanding of the talc deposit, geochemical analysis and the investigation of structural relationships between ore and host rock is essential. The research project began in summer of 2009 with the first cooperation between Aihai Talc Company Ltd. and the Department of Applied Geosciences of the University of Leoben. In 2009, all available data from the Aihai deposit were combined with actually acquired structural data in a 3D-deposit model (Misch & Pluch, 2009). This model is very helpful for mine planning and quality

control, but it represents only the first step of the deposit characterization. The second step is the further analysis of the different deposit rocks and the surrounding environment, including chemical composition, structural properties and relationships between host rock and deposit material. Chemical properties and mineralogy of the ore have great influence on quality parameters, for example whiteness and loss on ignition. Therefore, understanding how chemical impurities influence certain quality parameters is not only theoretical knowledge but directly affects the quality of the end-product. Another important part of the deposit characterization is the understanding of talc genesis and the discrimination of different ore types. Understanding the mechanisms how talc accumulates in economic relevant amounts leads to more efficient mining and better predictability of new deposit parts. Also the geochemical analysis of the host rock plays an important role, often host rock properties change with the distance to the deposit material. This factor again can be useful for exploration and mine control. In summary, every kind of detailed information can be important for the understanding of the deposit, which is not only interesting from a theoretical point of view but also for economic interests like quality control, reserve estimation and further deposit exploration.

The project cooperation between Aihai Talc Company Ltd. and the Institute for Applied Geosciences of the University of Leoben began in July 2009. The time schedule of work done in the field at Fanjiabauzi as well as at the Institute of Applied Geosciences in Leoben, Austria, is listed below:

July 2009 - September 2009: Data acquisition and fieldwork at Fanjiabauzi Talc deposit, Eastern Liaoning Province of China. Implementation of 3D-deposit model with GEMCOM Surpac (Misch, 2009).

October 2009: Final report on deposit situation under consideration of geomechanic instabilities and recommendations for future mine planning (Misch & Pluch, 2009).

July 2010: Second field trip to Fanjiabauzi, geological and structural observation of the talc deposit, re-interpretation of information collected during the 2009 fieldtrip. Sampling for geochemical analysis and mineralogical characterization of ore and host rock.

September 2010: Poster-presentation of first results at PANGEO 2010 (University of Leoben) (Misch & Pluch, 2010).

September 2010 - June 2012: Analytical work at the Institute for Applied Geosciences, University of Leoben. Mineralogical and geochemical description of the deposit rocks, documentation and interpretation of mining induced geo-risks.

September 2012: Final report on deposit geology and recommendations for further mine planning and risk management.

2 General Overview

2.1 Definition of Talc

Talc is a member of the mineral group of silicates, more precise it is a phyllosilicate. Talc is a three-layer phyllosilicate with two tetraeder layers and one octaeder layer (2:1 structure) (Fig. 2). Talc has a similar crystal structure and properties like pyrophyllite and therefore many pyrophyllite deposits are erroneously counted as talc deposits in mining statistics (Prochaska 1988). In the octaeder positions of the crystal lattice, Mg can be substituted by other trace elements like Fe, Ni or Mn. This exchange of cations has influence on the coloration. Between the tetraeder and octaeder layers, there are only weak binding forces. This specific physical property is one important reason for many technical applications. Another criterion especially for the food and pharmaceutical industry is the chemical inactivity and resistivity of talc, the reason for this is the saturation of the talc layers with no empty positions in the structure (Prochaska 1988). Talc has ideal cation site occupancy in both tetraeder and octaeder layers and therefore the cation exchange capacity is remarkably low compared for example to clay minerals like bentonite. The chemical formula of talc is $Mg_3[Si_4O_{10}(OH)_2]$, therefore it can also be named as magnesia-silica-hydrate due to its chemical composition. Talc-crystals are members of the triclinic crystal-system; the hardness of talc is a standard value of the Mohs-hardness-scale and represents the hardness 1, which means talc can be scratched with the fingernail. This remarkably low hardness is one reason for the technical applications of talc. Another reason for the use of talc in the paper- and color-industry is the coloration; talc often has a bright white coloration. Other possible colors are pink, yellow, green and grey. The streak color of talc is white; talc is an opaque mineral with a greasy luster. The density of talc ranges between 2.58 and 2.83g/cm³, it has perfect cleavage along 001 crystal planes which causes the characteristic platy structure of the phyllosilicate minerals. Talc often has a massive habitus without visible crystals (Fig. 3); it feels slippery or greasy to the touch and can easily be pulverized by hand.

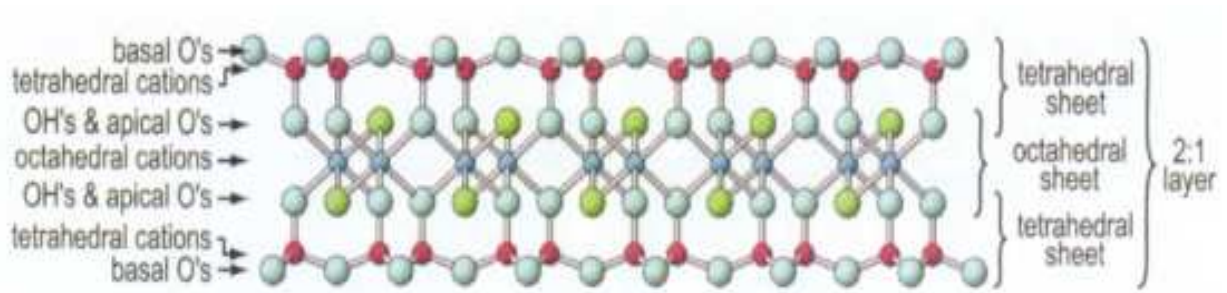


Figure 2: Schematic crystal structure of 2:1 layer phyllosilicates (e.g. talc and pyrophyllite), the octahedral cations are Mg for talc and Al for pyrophyllite, whereas the tetrahedral cations are Si for both minerals (<http://wgharris.ifas.ufl.edu/SEED/>).



Figure 3: Typically talc has a massive habitus without visible crystals.

Talc has a wide variety of technical applications. Great amounts of talc are used in the paper-, paintings- and plastics-industry as a filling material because of its high grade of whiteness and the easy processability due to the extraordinary low hardness. It is also used as a filler and lubricant for medicine products and in the food-industry because of its chemically inert behavior. Health risks are not very well documented, although excessive inhalation of talcum powder may cause symptoms similar to silicosis. Another problem is the use of fibrous talc which reacts similar to asbestos and is suspected to cause severe lung diseases. Therefore, fibrous talc is not allowed to be used in pharmaceutical industry. Talc can contain minor amounts of

asbestos, this value has to be monitored and considered for further processing if necessary.

2.2 *Technical properties*

In the following, the specific properties for talc in different industrial applications are described in detail (after Ciullo, 1996).

2.2.1 Ceramics

Talc used in ceramics industry has to match a variety of quality criteria:

- Low Ca- and Fe-content, low content of carbonate minerals
- Uniform fired shrinkage
- Uniform chemical composition
- Uniform particle size distribution
- Fine grained
- White firing

Talc is an important fluxing agent and helps to lower firing temperatures and to reduce firing times in the production of wall tiles and other ceramic products like electric insulators, etc.

2.2.2 Coatings

Talc primary acts as a TiO₂-extender for coatings. It also contributes to sheen control, suspension stability, chemical resistance, film integrity and weathering resistance of coating products. Whereas for architectural paintings, <325mesh talc is used, for most industrial paintings micronized talc is the common quality grade.

2.2.3 Paper

The most important quality criteria for applications in paper industry are brightness, purity and particle size of the talc product, platy talc mostly is preferred. Talc acts as a TiO₂ extender, improves the gloss, ink holdout, opacity and brightness of high quality papers. Talc also is used for the deinking of recycling paper. The most

important use of talc in the US paper industry is for pitch control, micronized, platy talc is the perfect match for this specific market.

2.2.4 Plastics

Talc is used to control the melt flow and to reduce the creep in molded parts. It reduces thermal stress and therefore improves the dimensional stability of parts. Talc also increases the heat deflection temperature. A very important application for talc in the plastics industry is as an additive for polypropylene products; talc increases the stiffness and reduces high temperature creeping. The main quality requirements for the use as a plastics additive are low moisture- and iron-contents. The importance of brightness depends on the further use of the raw product, for plastics used in the automotive industry, talc with perfect whiteness is more important than for low-cost applications.

2.2.5 Cosmetics and Pharmaceuticals

Talc used in the pharmaceutical industry has to meet the highest quality standards. High brightness and extraordinary pureness are basic requirements; the contents of chloride, iron, heavy metals, acid-soluble components and the loss on ignition have to be minor as well as the microbial contamination. In cosmetics, talc is used for makeup and dusting powders, whereas in Pharmaceuticals, talc acts as lubricant, filler and reinforcement for tablet coatings. Micronized, platy talc is the most common quality for those applications.

Additionally, talc has a variety of different other applications in smaller industrial segments, for example it is used as an anticaking agent for fertilizers or as additive for animal feed. The scope for new applications is not yet utilized. One major challenge in talc product preparation is the creation of powders with minimized and uniformly distributed particle sizes in the range of 10 to 30µm. Special grinding and sorting methods are still part of further development in the talc producing industry.

2.3 *Types of talc deposits*

There are several types of talc deposits documented from different geological and geochemical environments, but only two distinct types of talc deposits are important

from an economic point of view. The two important types of talc mineralizations are deposits with ultramafic source rocks and carbonate-hosted talc deposits. The most important factor for the formation of talc is the adequate supply of Mg- and SiO₂-rich fluids. Mg-providing minerals are mostly found in ultramafic rocks or Mg-rich carbonate rocks, whereas SiO₂ for example is delivered by felsic intrusions or sedimentary rocks under low-grade metamorphism (Chen et al, 2003). Another basic requirement for large-scale talc mineralization is the possibility of CO₂ removal and supply of H₂O (Prochaska, 1989). In general, talc formation requires open, fluid penetrable systems which are found when tectonic deformation took place. In jointed rocks, the local CO₂ partial pressure decreases and makes large-scale talc mineralization possible (Chen et al, 2003). Deformation also creates the necessary space for volume increase, which is necessary in the talc forming process. About 60% volume increase during talc mineralization is postulated (Chen et al, 2003).

2.3.1 Ultramafic-hosted Talc Deposits

This type of mineralization is very common in the Eastern Alps and also in the USA. Ultramafic rocks in the Eastern Alps often show minor amounts of talc, although economic deposit sizes are rare. In general, almost no large-scale deposits of this type exist (Gondim, 2004). Talc with ultramafic Mg-source characteristically shows high amounts of trace elements like Ni, Co etc. This allows a clear discrimination between talc associated to ultramafic rocks and carbonate-hosted talc. Unlike carbonate-hosted talc, the talc connected to ultramafic rocks can be emplaced directly within the magmatic rocks themselves but also occurs away from the source rock. Mg-rich fluids are likely to infiltrate other rock layers where the mineralization of talc takes place in an acidic environment (Prochaska 1988). This makes the exploration of the deposit genesis and the correlation of Mg-source and talc mineralization generally more difficult, for which reason trace element analysis is often the best way to prove the connection between source rock and actual deposit.

2.3.2 Carbonate-hosted Talc Deposits

In the case of carbonate hosted talc deposits, the most important factor for the talc genesis are high mineralized fluids with a high content of SiO₂. Brines can be crustal fluids, formation brines or ascending fluids associated to magmatic intrusions (Hecht et al, 1999). For example, felsic magmatic rocks deliver SiO₂ to Mg-rich wall rocks

like magnesite, or dolomite gets altered by Mg- and SiO₂-rich fluids (Chen et al, 2003). Another important factor is the temperature; talc formation takes place at temperatures of 200° to 300°C (Chen et al, 2003). These temperatures are reached in the surrounding area of felsic to mafic intrusions and during low grade metamorphism, for which reason carbonate-hosted talc deposits often occur in the nearest environment of felsic intrusions. Highly mineralized fluids often ascend along weak zones and are connected to extensional fault systems. These fluids are often derived from granitoid rocks but can also be reactivated seawater from buried sedimentary beds. The seawater alters siliceous, Mg-bearing carbonates and acts as a source for Si and Mg to form talc (Chen et al, 2003). Beside an active tectonic environment, heat transfer and element exchange are the two controlling factors of large scale talc mineralization in carbonate formations (Schandl et al, 2002). This type of mineralization is represented by most of the Asian talc deposits, including the Aihai talc deposit. Beside the large deposits in China, mineralizations of this type can be found in Spain, Italy, Austria, the French Pyrenees and the USA (Prochaska 1988). In general, talc deposits related to metasedimentary carbonate rocks are the most important type (Gondim, 2004). There are many advantages which make carbonate-host talc deposits attractive for economic use. The quality of the talc is often very high; especially the grade of whiteness is mostly higher compared to other types of talc. Another advantage is the absence of asbestos-minerals like tremolite. Asbestos minerals often cause problems at ultramafic deposits and increase processing costs because those harmful components have to be separated from the final product. Mechanical processing problems because of more resistible components, which remain in the final product, are minor compared to other talc deposits. The final product especially of European talc mines sometimes even is a mixture of talc and magnesite or dolomite.

The carbonate-hosted talc deposits have characteristic properties. The talc mineralizations often show remarkably low contents of trace elements like Ni, Co, Cr etc. (Prochaska 1988), the chemical analysis of ore from the Fanjiabauzi deposit also proves this general assumption. Another common notice is that carbonate-hosted talc is almost ever connected to strongly tectonized zones and the mineralization takes place in metamorphic terrain. This characteristic situation was also observed during the field work at the Fanjiabauzi mining area. Fluid inclusion analysis of brines from

the Trimouns talc deposit in the French Pyrenees shows high salinity (20-30% eq. wt% NaCl), intermediate temperature (320°C) and pressure of 2,5 kbar for the talc formation. It is remarkable that the actual mineralization process at Trimouns lasted for 16 million years under these conditions (Parseval et al, 2004).

2.4 Worldwide distribution of talc producers and consumers

In general, China plays a major role in the worldwide mining business (Fig. 4). The Chinese mining output increased rapidly over the last decade, whereas the western countries mostly had constant to slightly increasing output values (Weber et al, 2010). It is likely that this trend will continue in the future because of the high economic growth of China compared to the western countries and its high demands for raw materials which create an important domestic market.

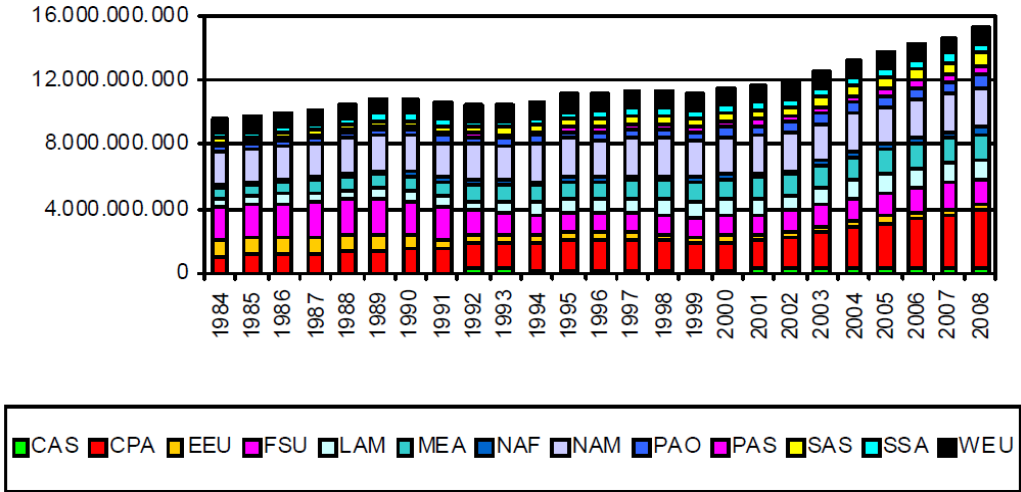


Figure 4: Development of mining production over the last three decades by regions (CPA: China, NAM: Northern America, WEU: Western Europe) (Weber et al, 2010).

The worldwide Talc production was 8.3 million tons in 2007, this value places Talc under the ten most important industrial minerals, according to the amount of mined raw material (Weber et al, 2009). The worldwide annual requirement for talc was comparatively constant over the last decade, the increase between 2003 and 2007 was only 8 percent, this difference is rather low compared to other industrial minerals like feldspar (44.5%) or Boron (19.8%) (Weber et al, 2009). After the economic crisis in 2008 and 2009, the talc production decreased slightly. The annual world production of 2010 was 7.5 million tons, which means a decrease of 9.6% between 2007 and 2010 (Weber et al, 2012). This trend will most probably invert in the future

because of the increased economic growth after a period of lower raw-material demands between 2008 and 2009. Compared to the most important mining products like Iron-ore, which had an annual mining rate of 1273 million tons in 2010 (Weber et al, 2012), talc seems to play a minor role in world mining business. Nevertheless, because of the high selling prices of talc compared to other mass products, the profit margin of talc producers is comparatively high. There are many important technical applications especially for talc powder with specific properties like high whiteness or electric inactivity. In the plastics industry, talc not only helps to reduce material costs as a filling material, it also improves the mechanical strength and resistance to corrosion of products (Gächter et al, 1989). Talc improves the adhesive power of paintings and reduces decomposition due to long storage. In paper industry, talc increases whiteness and gloss and plays an important role as a resin binder (Kittel, 1998). The lack of large deposits with good talc quality additionally raises the raw material price and makes talc mining more attractive from an economic point of view. The selling prices of talc products are relatively variable and heavily dependent on the quality, type and later application of the sold product. Lumps with whiteness of 90 achieve prices of 100 to 150 dollars per ton on the European market, whereas prices for high quality talc from China with whiteness above 94 used in paper industry can reach prices of 300 dollars per ton. Whiteness is important, but not the only factor which affects the value of talc products. Specific coloration, for example pink, often is more important than absolute whiteness. Particle properties like size, form and reactivity play a role as well as the content and type of admixed impurities. The main quality criteria for different industrial applications were described in detail above.

While the main talc producing countries were China, Japan and the USA between 1980 and 2000, other Asian countries like India and Korea increased their production over the last decade (Weber et al, 2011). In 2011, the talc production was mainly controlled by the three main talc producing countries China, India and Korea, although an exact breakdown of the production amounts from economic areas to single countries is difficult because statistic efforts mostly consider communities of states like the EU or the OECD countries. China had an annual production of 2.0 million tons in 2010, which means a share of 26.7% of the annual world production (Weber et al, 2012). There are some crucial points related to the definition of talc, in some statistics talcum means a mixture of talc and pyrophyllite and not pure talc from

a mineralogical point of view (Prochaska 1988). The large carbonate-hosted deposits in china show remarkably high qualities of pure talc, whereas the Japanese talcum is often a mixture of talc and pyrophyllite, which has similar properties as pure talc in terms of whiteness and processability (Prochaska 1988).

Altogether, the data has to be viewed critically because the accuracy is not always proved, especially for the information published by developing countries. The viability of the whole statistics is mainly affected by the quality of the raw data, which is provided by the different governmental mining authorities.

2.5 Chinese talc production – detailed review

Meanwhile, China is considered the world's leader of talc production (Agnihotri et al, 2003). Talc is mined mainly in three Chinese Provinces, the Liaoning, Shandong and Guangxi Province. It is estimated that those three Provinces alone produced about 500,000 tons of high-grade white talc. The major talc producing companies are listed below (after Mustansar et al, 2010):

1. Liaoning Aihai Talc Co. Ltd.
2. Haichen Beihai Minerals Co. Ltd.
3. Haichen Shuiquan Talc Mining Co. Ltd.
4. Haichen Pailou Talc Co. Ltd.
5. Shandong Pingdu Talc Co. Ltd.
6. Shandong Laizhou Talc Co. Ltd.
7. Guilin Guiguang Talc Development Co. Ltd.
8. Guangxi Longguang Talc Development Co. Ltd.
9. Guangxi Longsheng Huamei Talc Development Co. Ltd.

The nine listed companies account for almost 80 percent of the Chinese talc production and 95 percent of the country's talc export (Mustansar et al, 2010). Four reasons cause the remarkably low price of high-grade Chinese talc in comparison to other major producers of the same quality talc products (Zhuang, 2010):

1. Low labor costs
2. Low resource taxes

3. Almost no input for eco recovery
4. Good geographical conditions and low operating costs of the major production bases in coastal regions.

Large Chinese talc companies like Aihai are forming joint ventures with European trading partners like Imerys Talc (former Luzenac) to increase access to the important European market. The EU is the most important market for Chinese talc products worldwide. The export value of talc products from China amounted to approximately 72 Mio. USD in 2009, which means a share of 13 % of worldwide talc exports. In comparison, the import value was roughly 14.2 Mio. USD (Mustansar et al, 2010). Because of the large domestic demand for talc, the export rate shows a falling trend over the last years. The Chinese Government currently works on plans to regulate the rate of export for different industrial minerals to secure the fulfillment of domestic industrial demand. Existing export quotas and export restrictions as well as additional requirements for foreign companies especially apply to rare earth elements and metals like tungsten and molybdenum. The EU as one of the main importers of these materials brought in several charges at the WTO against the export restrictions set by the Chinese government so far. Nevertheless, China constantly widens the limitations to new resources like industrial minerals to take account to the rapidly growing domestic economy, ignoring adverse rulings of the WTO (European Commission Press Release, Ref. No. IP/12/239).

One problem that Chinese talc producers faced in the past was the possible occurrence of asbestos minerals in talc deposits (Zhuang, 2010). As the major importers of Chinese talc are located in the EU, European safety standards must be strictly adhered to. Most of the major talc companies have realized the problem and carried out detailed studies to prove that their talc is free of fibrous amphiboles. A first attempt to develop a fast and cheap testing procedure to determine the pollution of samples with asbestos minerals was carried out by (Hayashi et al, 1978). An energy dispersive spectrometer combined with a conventional transmissional microscope provided a rapid technique to determine semiquantitatively the content of fibrous amphiboles in thin sections. Today, the full impact of long-term exposure to asbestos minerals on health of workers and consumers is widely investigated. Only material from smaller, less controlled or illegal mines may be of doubtful quality. As long as the origin of talc is ensured by the providing company, asbestos minerals are only a

minor concern, as the pollution with problematic asbestos contents is only reported from deposits with almost no economic relevance and is not evident for the deposits in Eastern Liaoning (Zhuang, 2010). Strict testing procedures and a low threshold value for carcinogenic minerals is essential to constantly prove the innocuousness of Chinese talc.

3 Aihai Talc Deposit

3.1 Regional Geology

The Liaoning Province is part of the eastern margin of the North China Craton (NCC) which is located east of the Tancheng-Lujiang deep-fault (Fig. 5). It is part of the Liaoning-Jilin Continental Massif which consists of thick sedimentary formations with an Archean to Proterozoic crystalline basement (Zhao, 2001). Large metallogenic systems were formed in the Mesozoic due to different thermal events after plate reactivation in a large scale. In the eastern Liaoning Province, the Mg-rich metallogenic system shows major talc-, magnesite- and boron-deposits as well as different other Mg-rich minerals like serpentine (Zhai et al, 2004). Regional metamorphism of greenschist to amphibolite-facies took place during several orogenic periods from the Precambrian to the Mesozoic (Zhai et al, 2004).

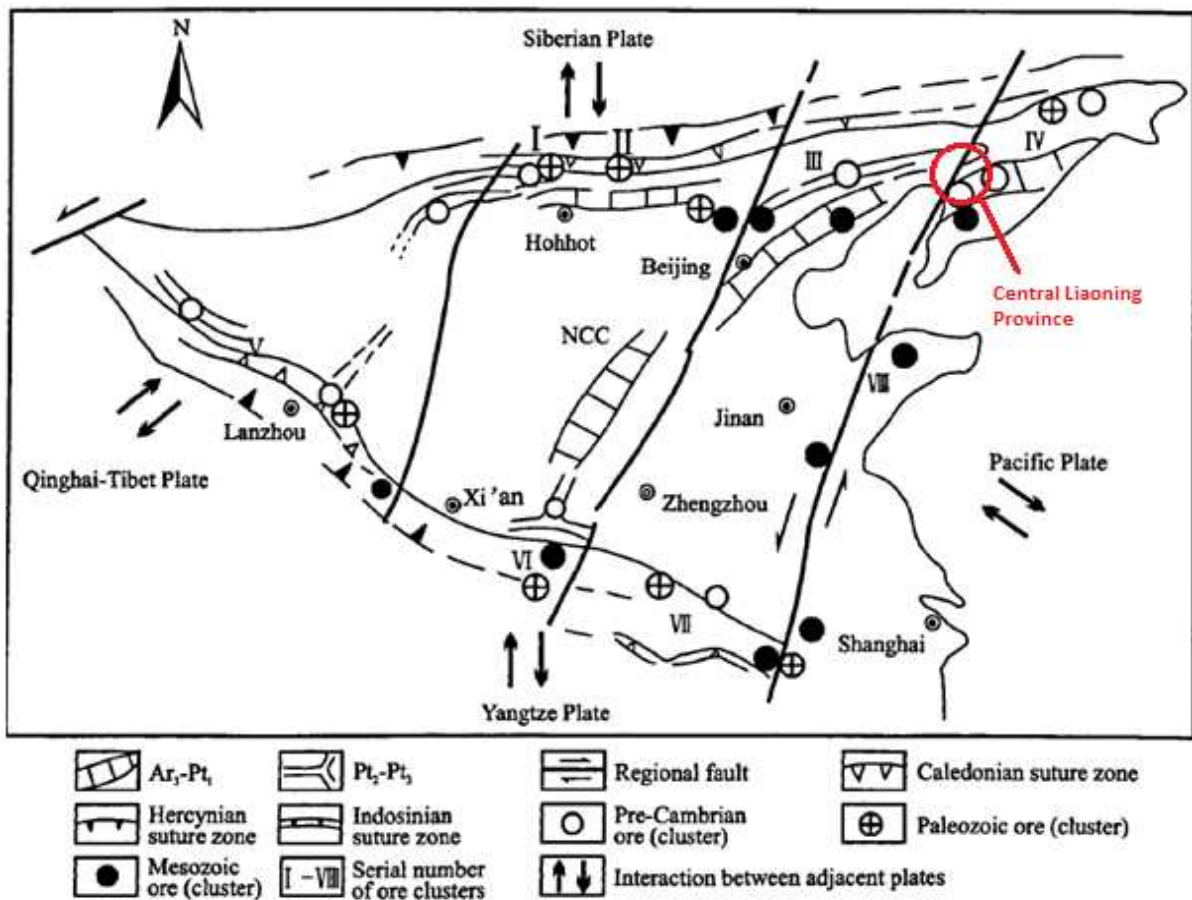


Figure 5: Tectonic setting and location of main metallogenic provinces at the NCC (Zhai et al, 2004).

The paleorift environment in the Eastern Liaoning Area can be divided into three different facies zones, which are named the north slope zone, inner depression zone and the south shallow zone (Chen et al, 2002). Those three zones show distinct rock assemblages and mineral deposits. The major talc and magnesite deposits are located in the north slope zone which extends from Yingkou in the West over Caohekou, Huanren and Qinghe to Linjiang in the East (Chen et al, 2002) (Fig. 6).

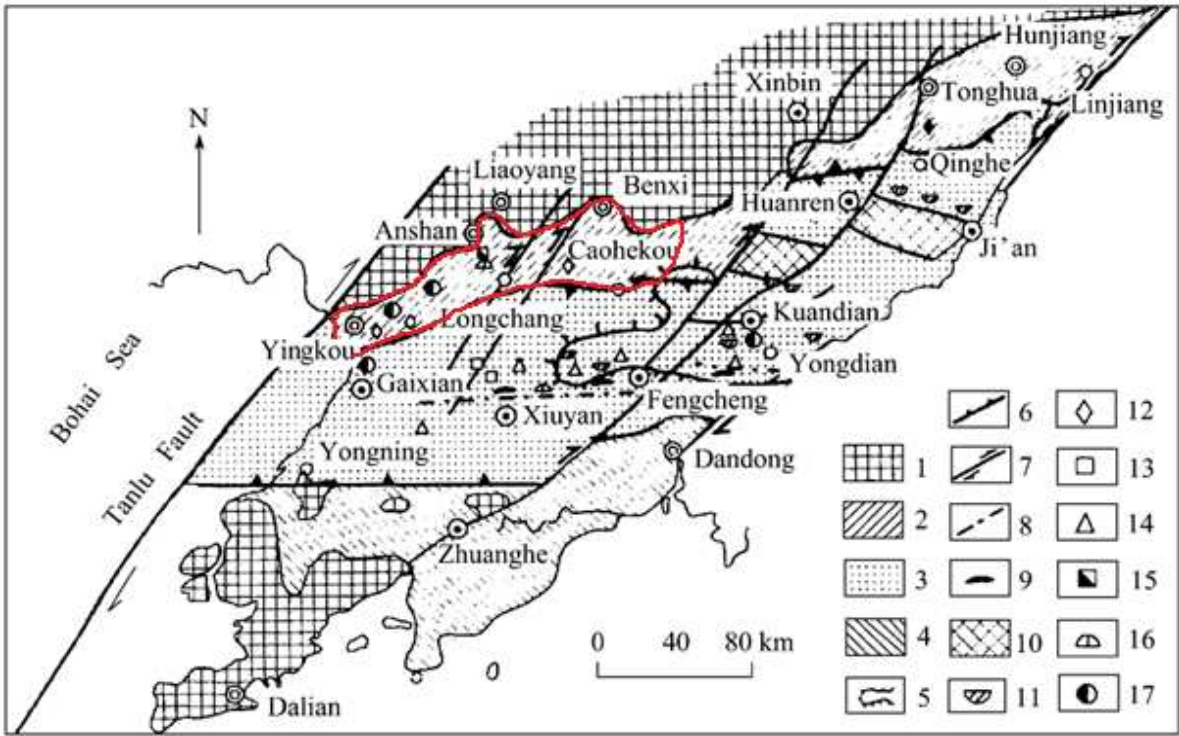


Figure 6: Position of Talc and Magnesite deposits in the north slope zone of the Eastern Liaoning paleorift environment (no. 12, red mark) (Chen et al, 2002).

The geological situation in the surrounding area of the Aihai talc deposit is mainly dominated by early Proterozoic carbonate rocks. The talc deposit is embedded in Mg-rich carbonates of the early Proterozoic Dashiqiao Formation. The Dashiqiao Formation is located in the eastern Liaoning Province of China and is part of the Liaohe Group which is hosted by the Jiao-Liao belt (Fig. 7). The Jiao-Liao belt represents a closed intra-continental rift system at the eastern continental border of the North China Craton (Lu et al, 2008). The East-North-East trending belt of the Liaohe Group extends over a wide area from Haicheng over Dashiqiao and Fengcheng to Hunjiang, which represents the northeastern border.

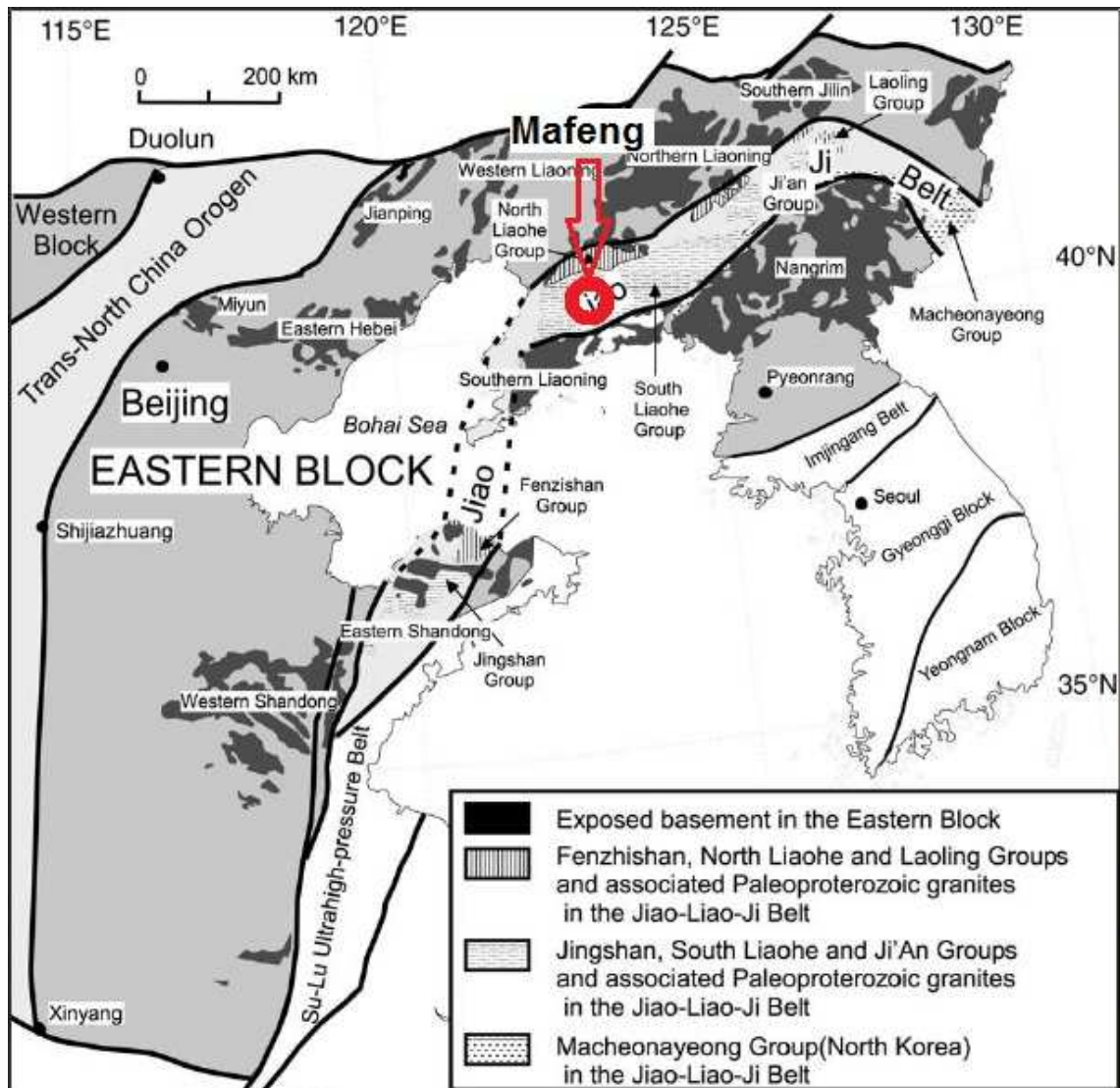


Figure 7: Location of the Paleoproterozoic Jiao-Liao Belt which hosts the Liaohe-Group (Zhao et al 2001).

Four different formations represent the Liaohe Group (Fig. 8). The base is the so called Langzishan Formation; overlaid by the Li'eryu/Gaojiayu Formation. The Li'eryu Formation hosts local important boron deposits (Jiang et al, 2004). The third formation of the tectonic group is the Dashiqiao Formation; it contains dolomitic marbles intercalated with minor carbonaceous slates, micaschists and magnesite. The massive, Mg-rich carbonatic rocks of the Dashiqiao Formation host the Aihai talc and magnesite deposits. The formation on top of the Liaohe Group is the Gaixian Formation.

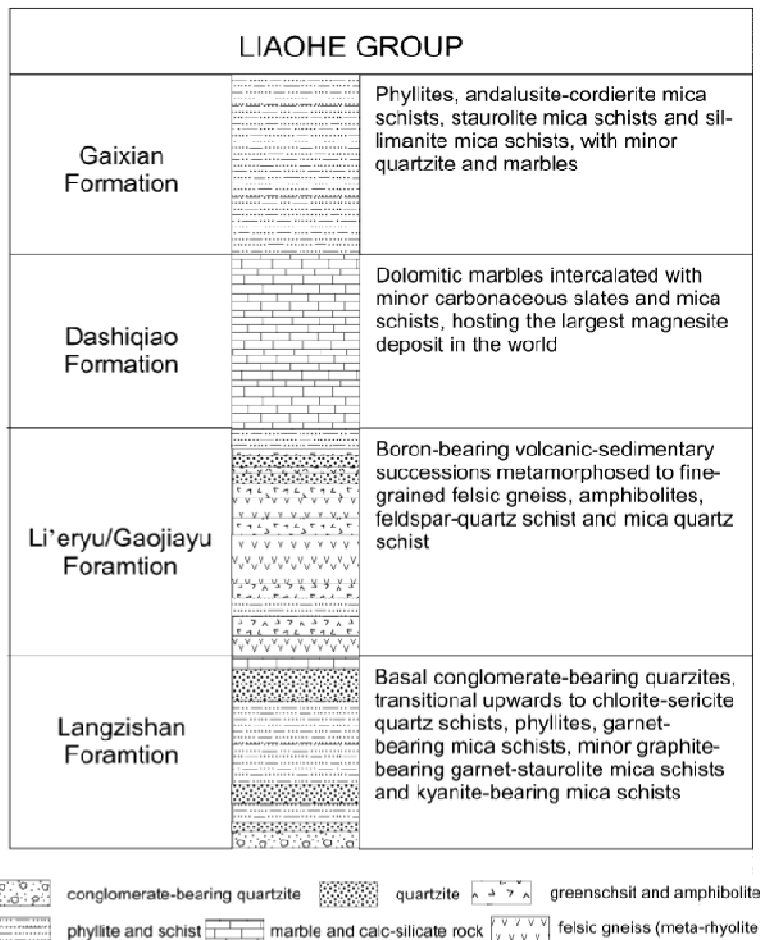


Figure 8: Detailed description of the Formations which represent the Early Proterozoic Liaohe-Group (Li et al 2004).

The Dashiqiao Formation is the most important part of the Liaohe Group from the economic point of view. It is subdivided into four sedimentary environments. The formation hosts large magnesite and talc deposits of excellent quality (Haicheng-Dashiqiao talc and magnesite ore belt) as well as serpentine jade deposits (Chen & Cai, 2000). The magnesite was deposited in a natural sedimentary environment. In the early Proterozoic, a platform facies was present. The environment contained lagoons on the continental margins. When the climate changed to dry conditions, the seawater of the lagoons evaporated quickly and due to low water depths, the salinity in these areas increased rapidly. This situation caused the formation of massive layers of dolomite and later magnesite (Chen et al 2002). The Haicheng-Dashiqiao talc and magnesite ore belt is a roughly E-W trending belt that extends over approximately 100km with an average width of 4km. The super-large magnesite deposits located along this belt range from 200 to 2700m in length and reach thicknesses of 30 to 300m (Jiang et al, 2004). The whole Dashiqiao Formation varies

greatly in thickness. The maximum thickness postulated is 3600m, whereas the average strata thickness of carbonate beds from the Dashiqiao Formation at the north flank of the Yingluo-Caohekou-Taipingsao synclinorium is 1700m (Jiang et al, 2004).

The sedimentary formation of the massive magnesite layers was under critical view for a long time. Different genetic models were discussed, including the secondary recrystallisation of other carbonates like dolomite to magnesite under conditions with high Mg-supply from the environment. One argument against magnesite formation primary from seawater pools is the fact that the salinity and Mg-content of modern oceans is not sufficient for the process of magnesite precipitation (Jiang et al, 2004). In contrast to this, research concerning Early Proterozoic sedimentary environments shows evidence that the seawater composition of ancient oceans is not comparable to modern seawater (Chen et al, 2003). In comparison, ancient seawater was enriched in Mg and depleted in O_2 , moreover, the CO_2 partial pressure of the Proterozoic atmosphere was significantly higher (Tu, 1996). Under these conditions, after a first step of Dolomite + Calcite precipitation and further Mg-enrichment, primary magnesite precipitation is possible. Isotopic composition of C and O from magnesite and lying dolomite of the Dashiqiao Formation confirm that the stratified carbonate beds have the same genetic origin (Chen et al, 2003). The controversy around the genesis of magnesite deposits is not only a regional problem. A similar discussion is reported from the alpine magnesite deposit of Breitenau (Austria), where the more traditional thesis of syngenetic-sedimentary origin faces strong opposition (Gallhofer, 2010). Modern research favors an epigenetic-metasomatic model for the formation of magnesite deposits of the greywacke zone (Azim Zadeh, 2009). Although the deposits of the greywacke zone have different characteristics in comparison to the deposits of the Haicheng-Dashigiao-belt, the circumstances show the difficulty of discrimination between primary magnesite formation in a marine sedimentary environment with high Mg-supply and later, hydrothermal alteration of dolomitic rocks. Furthermore, later metamorphic processes like recrystallisation and redolomitization often obscure sedimentary and diagenetic features important for genetic conclusions.

After the sedimentary accumulation of massive carbonate layers, large-scale regional metamorphism took place in the Liaohe area. This metamorphism also caused the formation of the economically valuable talc deposits. The peak of the regional metamorphosis is still not well defined, only post peak cooling ages of 1,869 +/- 7 Ma (Yin & Nie 1996) allow the rough assumption that the peak was in the late early Proterozoic. The metamorphism was caused by the so called Lueliang event, which also stopped the rifting of the Liaodong rift System (Chen et al 2002). During the peak of the regional metamorphism, SiO₂-enriched fluids with high salinity intruded into the tectonically weakened, Mg-rich carbonate rocks and formed large amounts of talc, which later were further accumulated mechanically by tectonic movements.

Due to crust thinning, lamprophyre dyke swarms intruded into the massive carbonate layers in the late Jurassic (155Ma) (Jiang et al 2005). Talc formation in relation to the younger magmatic process was not found, although the existence of quartz in the border zone between dyke and surrounding magnesite suggests that the fluids connected to the intrusion were enriched in Si. Possible detaining factors for talc mineralization are insufficient heat flow or fluid migration, as reported from other deposits like the Eastern Alpine deposit in Lassing, Austria (Prochaska, 1989).

3.2 Local Situation

The geological map below (Fig. 9) shows the geology of the Fanjiabauzi mining area.

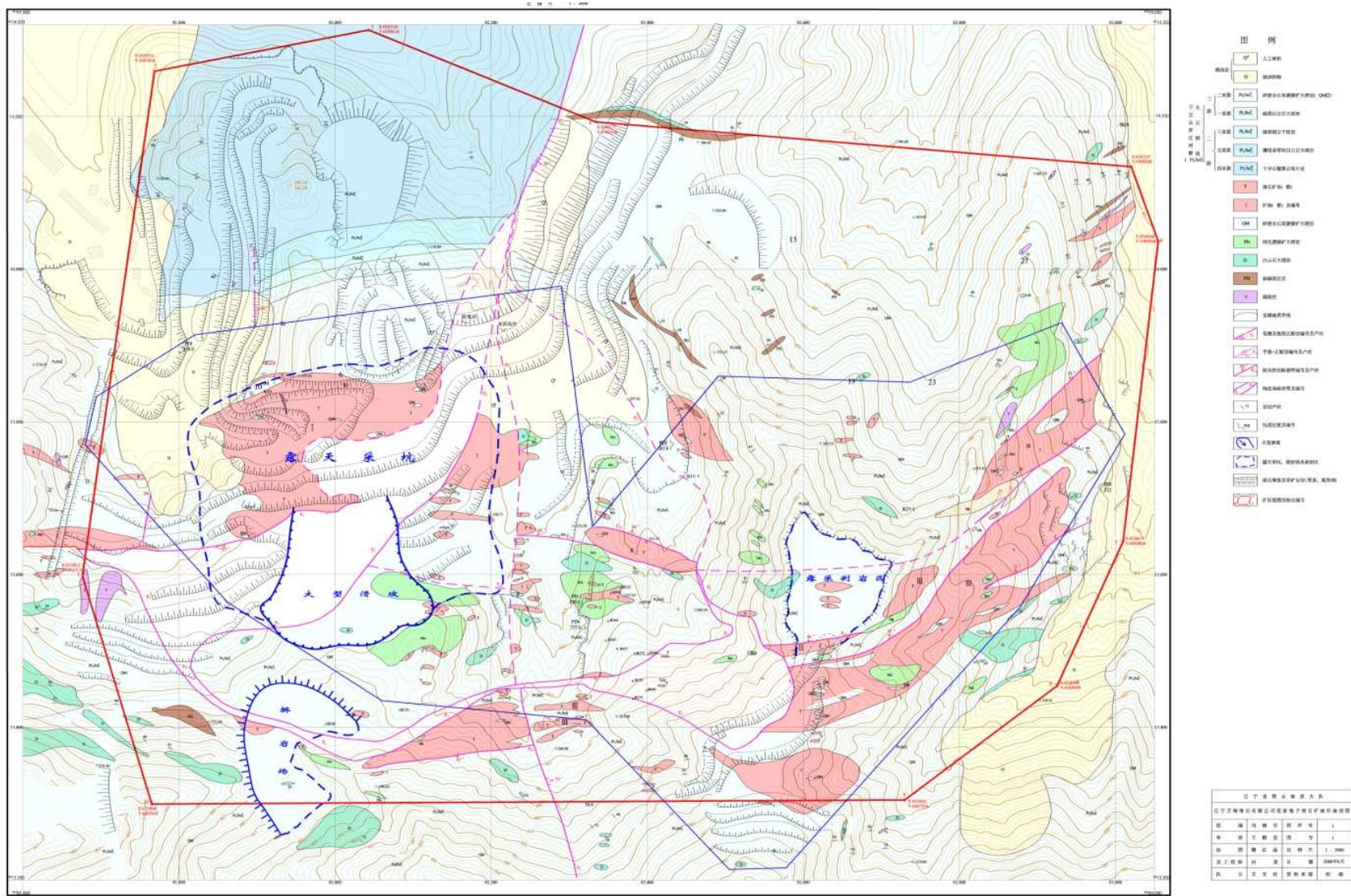


Figure 9: Geological map of the Fanjiabauzi mining area (red outline shows the border of the Aihai concession area) after Wang et al, 2005.

The local geology at the Fanjiabauzi mining area is dominated by massive low grade (greenschist to lower-amphibolite facies) meta-carbonate layers, which are part of the Dashiqiao Formation (Li et al, 2004). These layers are mostly magnesite, dolomite occurs in minor amounts. The borders between dolomite and magnesite are not clear; dolomite is sporadically intermeshed with magnesite. This makes it very difficult to discriminate exactly dolomite and magnesite in the field. Dolomite often shows a fine-grained texture and a light grey color. Pyrite is a common impurity of carbonate minerals, it is also found in the dolomite at Fanjiabauzi mining area but only infrequently in magnesite (Fig. 10). Quartz-rich veins in the massive carbonates document the migration of fluids enriched in SiO_2 . Those fluids were essential for the formation of talc. Whereas dolomite mostly has a massive habitus, magnesite shows different grain-sizes and textures depending on the location.

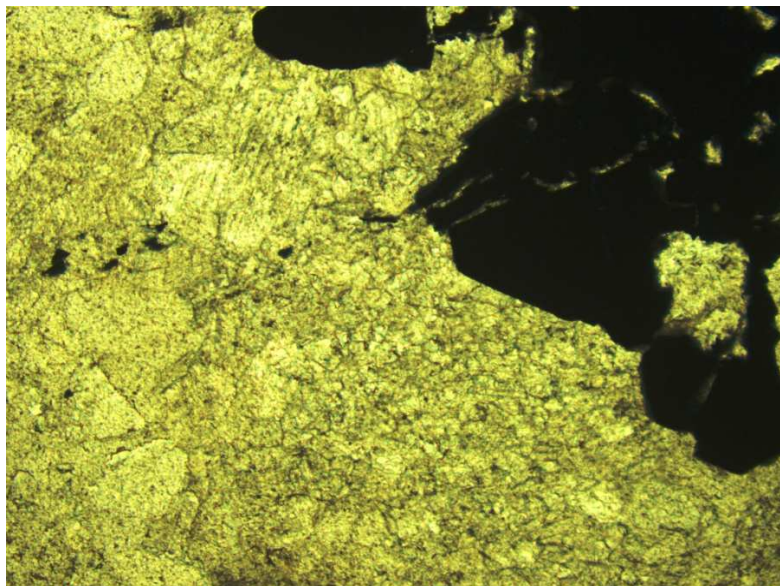


Figure 10: Pyrite-impurity in massive dolomite (height of picture equals 1,35mm).

The magnesite grain sizes range from $10\mu\text{m}$ up to several centimeters, different types of magnesite occur, ranging between two “end-members”:

- Pinolitic magnesite with grains from millimeters to several centimeters in size
- Finely grained, compact magnesite with grain-sizes between $10\mu\text{m}$ and $50\mu\text{m}$

The pinolitic magnesite has a light grey to grey coloration, the coloration changes over yellow (coarse grained magnesite) to white (medium to fine grained magnesite). The coarse grained magnesite sometimes has talc in the intergranular space; the talc shows a grey coloration. Isolated talc bodies of sizes from several centimeters to

0.5m are related to the compact, medium grained white magnesite, this type of talc occurrence mostly shows a light pink coloration and has a massive habitus without visible crystals. The main deposit consists of talc shear bands with thicknesses between 0.5m and several meters. The talc from these shear bands has a variety of different colorations from white, light grey, light green and yellow to pink which is most common for the high quality product. The different colorations are a result of slight differences in the mineral chemistry. There are few studies on the influence of mineral chemistry on coloration of talc so far, as well as on the general mechanisms of cation exchange and substitution in the talc structure (Wilamowski et al, 2004). The shear talc is finely grained and laminated, single talc crystals are not visible. The magnesite which hosts the primary deposit is mostly compact and medium to fine grained with a bright white coloration. Impurities like pyrite are rare in this type of magnesite, if pyrite occurs it is finely crystalline which means that no processing problems due to degradation of whiteness occur. Figures 11 and 12 show the difference between coarsely grained pinolitic and finely grained magnesite in the microscopic scale.

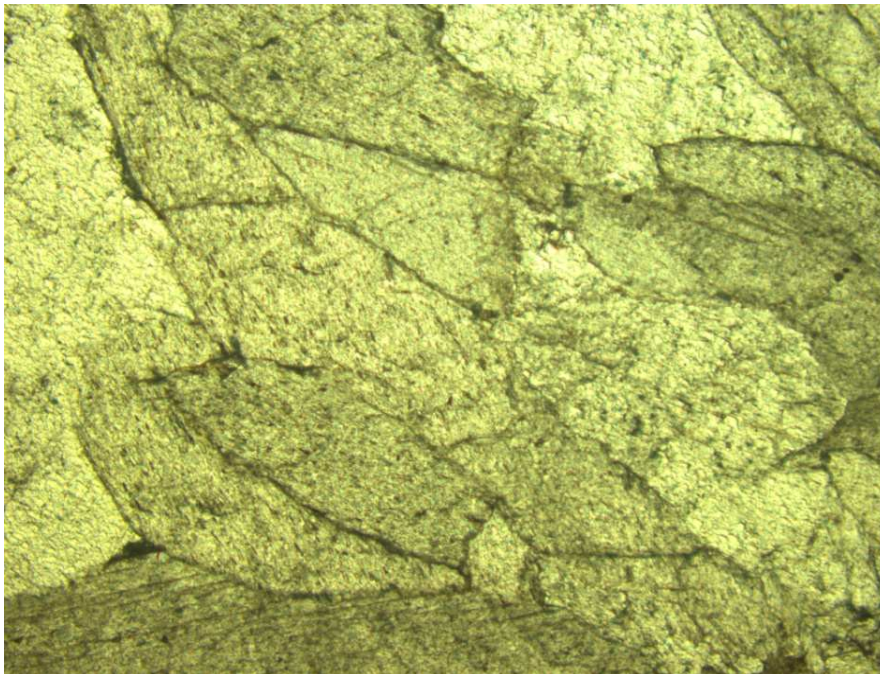


Figure 11: Coarsely grained, pinolitic magnesite (Height of picture equals 1,35mm).



Figure 12: Fine grained magnesite (Height of picture equals 1,35mm).

The greenschists which crop out in the northwestern part of the Fanjiabauzi area are presumed to be part of the deposit basement. The contact between greenschist and magnesite dips sharply to the south in the western part of the deposit; the magnesite which hosts the talc shear bands also dips to the south. Whereas there are many other magnesite deposits to the south of the Fanjiabauzi area, other deposits in the north are non-existing. The geographical position of the schists as well as the high garnet content leads to the assumption that the greenschists are part of the Langzishan or Gaojiayu formation which underlie the Dashiqiao formation and overlie the late archean Anshan complex (Li et al, 2004). So far, garnet bearing mica-schists are only documented from the Langzishan formation of the Liaohe group (Li et al, 2004). Garnet shows single crystals up to two centimeters in diameter. Mafic components are chlorite and pyroxenes as well as epidote.

The Lamprophyr dykes which crosscut through the massive carbonates and the talc shear bands range between several tens of centimeters and several meters in width (Fig. 13). The intrusion of the mafic dykes most likely was caused by a period of late Mesozoic crust extension in an intracontinental rift event (Liu et al, 2009). The dykes are fine to medium crystalline; plagioclase and chlorite are the dominant minerals whereas pyrite, titanite and tourmaline occur in minor amounts. Other mafic components like pyroxenes and amphiboles are rare and mostly only found as altered relicts. The dykes often are strongly tectonized and hydrothermally

transformed. Those altered dykes show high amounts of quartz and sericite. The fine grained mica is a common alteration product of plagioclase feldspars. In the altered dykes, albite is almost completely transformed into fine grained mica, only few relicts can be found. Undisturbed dykes show characteristic tabular albite crystals and acicular chlorite crystals with a non-directional fabric (Fig. 14).



Figure 13: Outcrop of mafic dyke, picture from Aihai magnesite mine (0,5km NE of Village Qushugou).

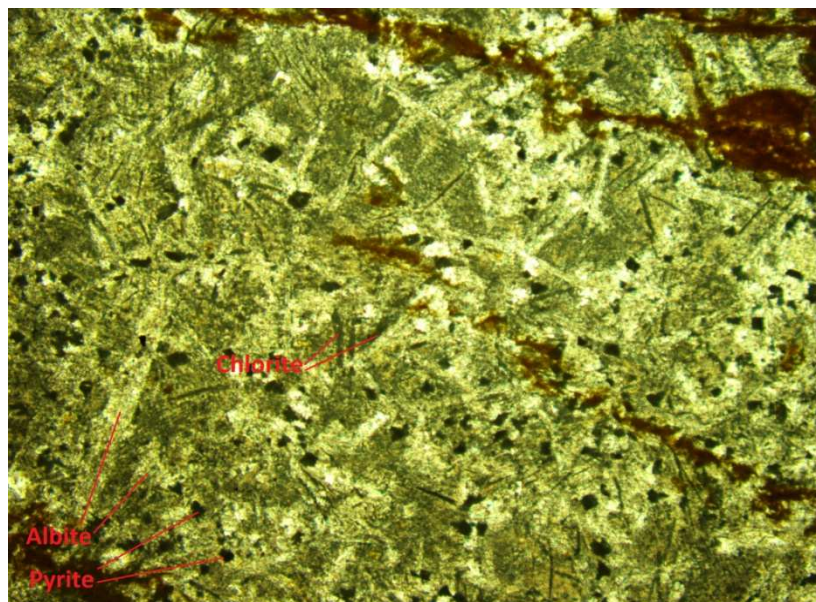


Figure 14: Thin-section of mafic dyke (height of picture equals 1,35mm).

Crenulation cleavage was observed in several thin-sections (Fig. 15). This type of cleavage suggests tectonic stress in more than one direction, causing a complex

foliation. Those rocks show relicts of primary dyke components like chlorite and pyroxenes in a fine grained, secondary formed mica matrix. Former Iron-rich components like pyrite often are transformed to alteration products like limonite. Intensive hydrothermal interaction leads to remarkable amounts of fine grained quartz enriched between mica shear bands. Those high quartz contents are rather uncommon for former mafic dykes and show the availability of SiO_2 enriched fluids in the deposit environment. This is also documented by the silicified borders between altered mafic dykes and the surrounding meta-carbonate rocks (Fig. 16).

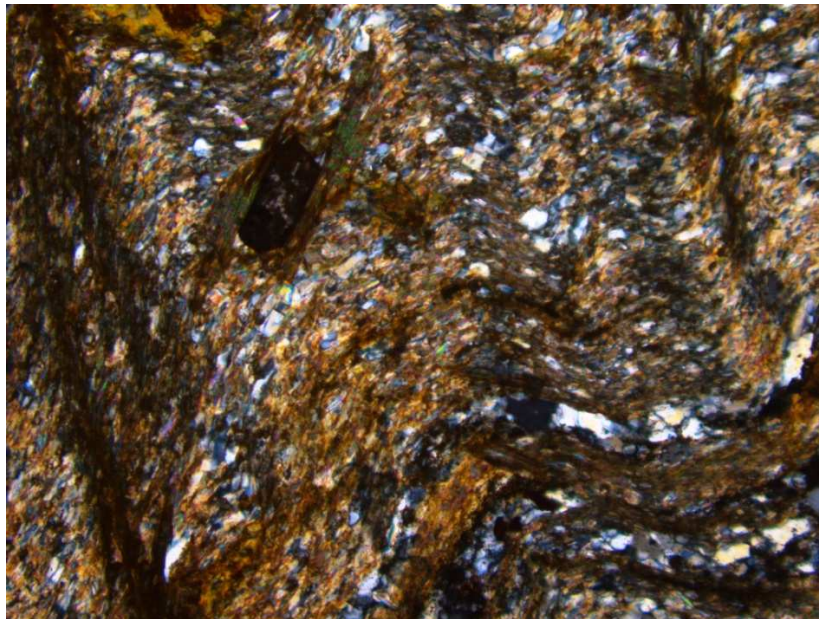


Figure 15: Thin section of strongly tectonized, altered dyke (height of picture equals 1,35mm, crossed nicols).



Figure 16: Silicified border between mafic dyke and surrounding magnesite.

It is questionable why the young dyke intrusions did not lead to talc mineralization, because SiO_2 -enriched fluids are documented. Wallrock alteration is limited to the nearest environment of the dykes (approx. 1m); a silicified border zone represents the transition to the surrounding meta-carbonates. Fieldwork shows no talc formation connected to the young dyke intrusions, although minor talc was found admixed into the border zone between dyke and surrounding rocks. Dykes preferably intruded along weak zones, which are mostly talc bearing. Therefore, talc was remobilized mechanically and incorporated into the silicified border zones. The talc forming reaction requires medium temperature (200-400°C) as well as an open fluid system. Whereas sufficient heat flow was most likely present during dyke intrusion, the compact wall rock may have prevented the necessary fluid flow and therefore the talc forming reaction could not take place. A comparable situation was reported from the Austrian talc deposit of Lassing (Prochaska, 1989). Tectonic deformation seems to be a key factor, controlling whether mineralization of talc takes place or not.

3.3 Types of talc mineralization

The genesis of talc and magnesite along the Haicheng-Dashiqiao-belt is strongly discussed. It is clear that talc and magnesite represent two distinct genetic steps. The

Mg-rich carbonate rocks were deposited in an Early Proterozoic marine environment. Afterwards, several metamorphic deformation events led to low grade meta-carbonates and to high-quality magnesite deposits. The age of talc mineralization is not well determined, but clearly younger than the deposition of the magnesite host rock. Talc was preferably formed in strongly tectonized zones, where fluid migration was possible. Afterwards, talc was mechanically enriched in shear zones up to several meters thickness and the actually mined deposit was formed. Genetically, mafic dyke intrusions mark the latest event in the deposit history, although the intrusions seem to have no major influence on the deposit quality.

Four different types of magnesite-talc intergrowths were documented at various outcrops in the Fanjiabauzi mining area (description and pictures of different types presented in chapters 3.3.1-3.3.4).

- Relatively small talc accumulations in fine grained magnesite, size of the talc aggregations between one and eight centimeters in diameter; mostly not influenced by tectonic stress (type 1).
- Coarse grained magnesite with larger talc aggregations and talc embedded into the magnesite structure (type 2). This type represents the change from type 1 to type 3 in the field.
- Coarse grained magnesite with talc embedded in the magnesite structure (type 3). No talc accumulation, therefore no larger talc aggregations in these areas.
- Talc accumulations in large shear zones, thickness of shear bands up to one meter and above – actually mined ore (type 4).

These different types may be representatives of earlier and later stages of mechanical talc accumulation, or otherwise they could originate from two or more distinct talc generations. Due to the comparable trace element composition of the talc samples and the surrounding magnesite, it is more likely that the talc was formed in one genetic step and after that, some areas were involved in more intense tectonic relocation, where talc acted as a weak compound and accumulated in shear zones

because of its specific mechanical properties. The sizes of these zones vary from several centimeters to meters in length and from centimeters up to one meter in thickness. They appear like classic shear bands with a characteristic habitus. The different colorations of the embedded talc occur at all four types of magnesite-talc compounds, this may also be a sign that the colorations are influenced by slightly different fluid compositions at different parts of the deposit but not by different genetic origins.

In the following, the four types of talc-magnesite intergrowths are further described with reference to their macroscopic occurrence in the field as well as to their microscopic characteristics.

3.3.1 Type 1

This type seems to be an early form of the occurring talc. Tectonic stress did not affect the small talc bodies; therefore they have a massive habitus and show no signs of tectonic elongation or shear induced structures such as schistosity. The boundaries between talc and magnesite are irregular; also some zoned transitions between massive talc and fine grained magnesite were observed (Fig. 17). This also strengthens the conclusion that this form of talc appearance is part of the primary talc formation without further material transport or major change of chemical composition. At some points, talc layers surrounding small talc bodies in several centimeters range were found. These layers show the same coloration like the enclosed talc bodies and represent the latest stages of chemical talc formation. The interruption of the talc genesis most likely was caused by the changed chemistry of the fluid which infiltrated the host rock.

The talc bodies are mostly equidimensional to slightly elongated, the elongation caused most likely in the early stage fluid transport along weak zones in the magnesite, not in later deformation. Therefore there are no sharp edges or crossings in the talc structures, which would appear in areas with a lot of tectonic stress. The talc often has a light pink to white coloration, but also yellow or light green coloration was observed in some areas.

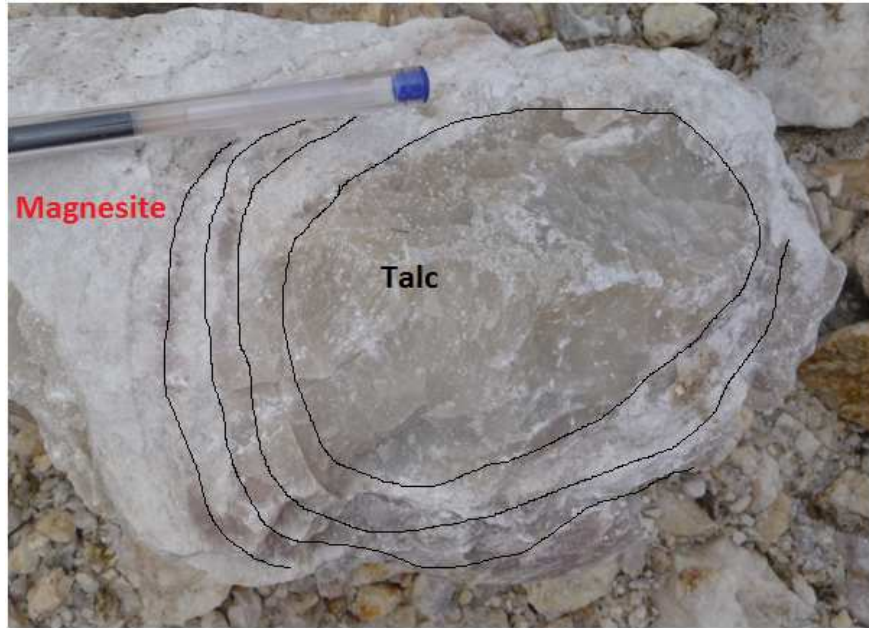


Figure 17: Equidimensional talc body with zoned borders to the surrounding magnesite (type1).

The microscopic analysis of type 1 samples shows fine grained talc with a non-directional fabric (Fig. 18). Some relicts of magnesite were found incorporated into the talc matrix. The abundance of magnesite relicts is much higher in marginal zones of talc bodies than in central parts (Fig. 19). Also the grain size of the magnesite relicts decreases to the core of talc bodies; this is sign for the advanced chemical transformation from magnesite to talc. Another sign for this is also that there are no isolated coarse relicts of magnesite, there are only zones were the magnesite was protected from the transformation into talc. In these zones, the old magnesite texture seems to be originally conserved. This indicates that there was no major mechanical accumulation of talc, otherwise the talc would show shear bands and the magnesite relicts would be elongated and not in their original position.

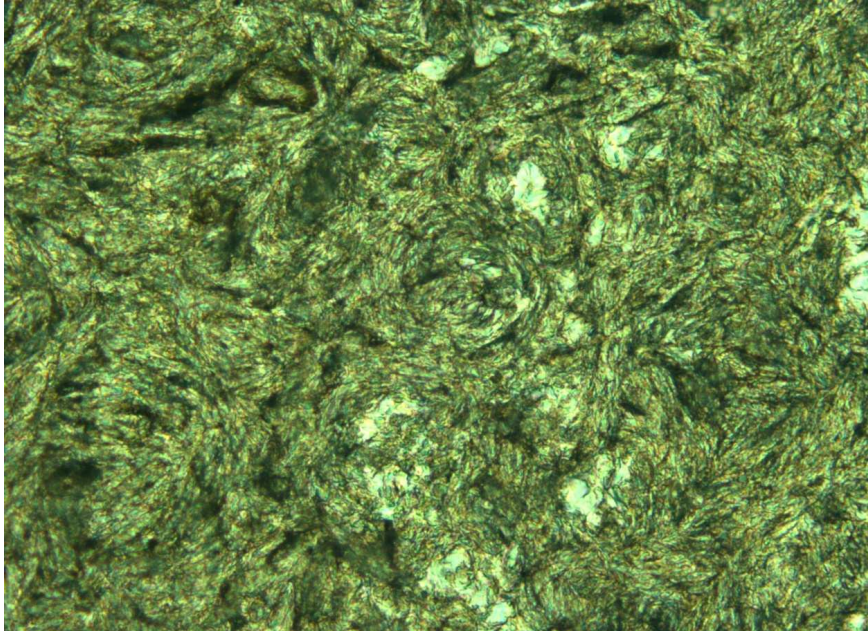


Figure 18: Thin section of fine grained, massive talc, height of picture equals 0.25mm (type 1).

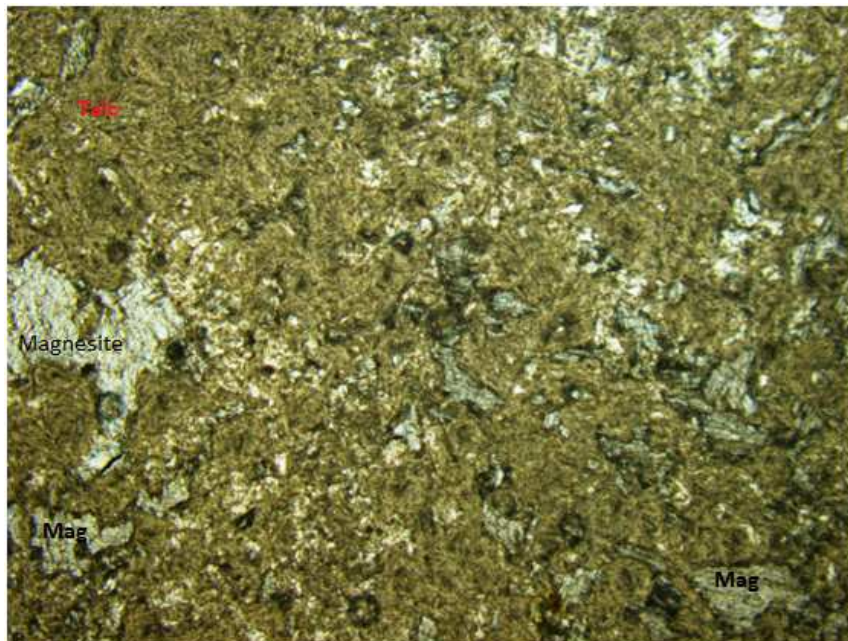


Figure 19: Magnesite relicts in fine grained talc matrix; thin section of the border zone from a small talc body, height of picture equals 1.35mm (type1).

3.3.2 Type 2

Type 2 shows a coarse grained fabric and talc is embedded in between magnesite grains but also shows some accumulated bodies which are relatively pure. Typically, talc formation starts in weak zones like micro joints or crystal boundaries (Fig. 20). Talc accumulation bodies contain small amounts of magnesite, mostly as fragments of sizes between 30 and 50 μ m. The fragments show reaction fabrics at the grain

boundaries (Fig. 21) where magnesite is replaced by talc. In areas with minor talc, the magnesite grain sizes range between 300 and 700 μm , whereas the magnesite gets more fine grained, where more talc was formed (grain sizes between 50 and 100 μm). This indicates that also a magnesite recrystallization took place at the spots where talc was primarily formed. The texture of the magnesite is non-directional, large grains mostly have equidimensional shapes, smaller fragments are equidimensional to slightly elongated but show no shear marks. Figure 22 shows a representative sample of ore type 2.

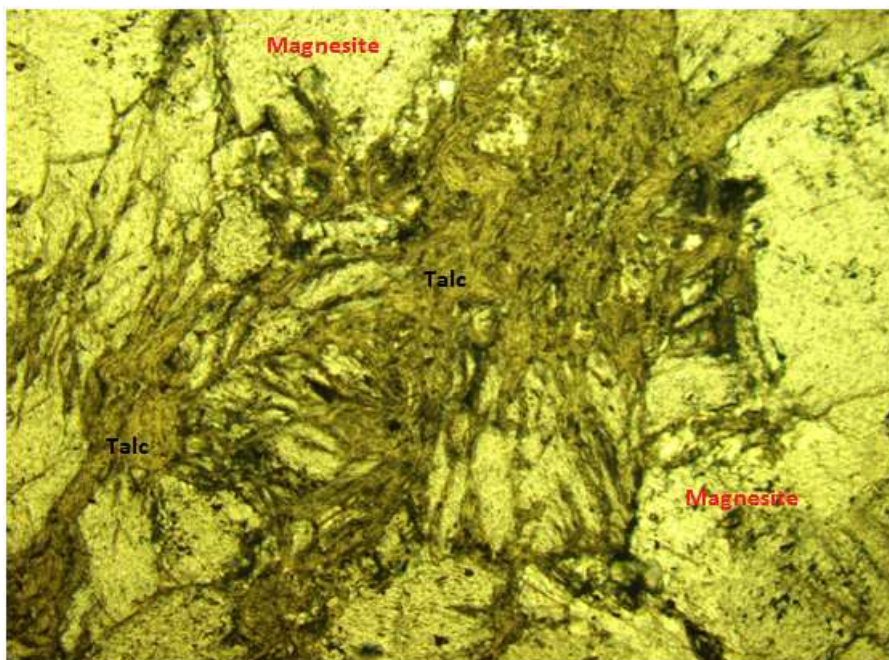


Figure 20: Talc formation starts in weak-zones between large magnesite crystals; magnesite is replaced by talc along border zones, height of picture equals 1.35mm (type 2).

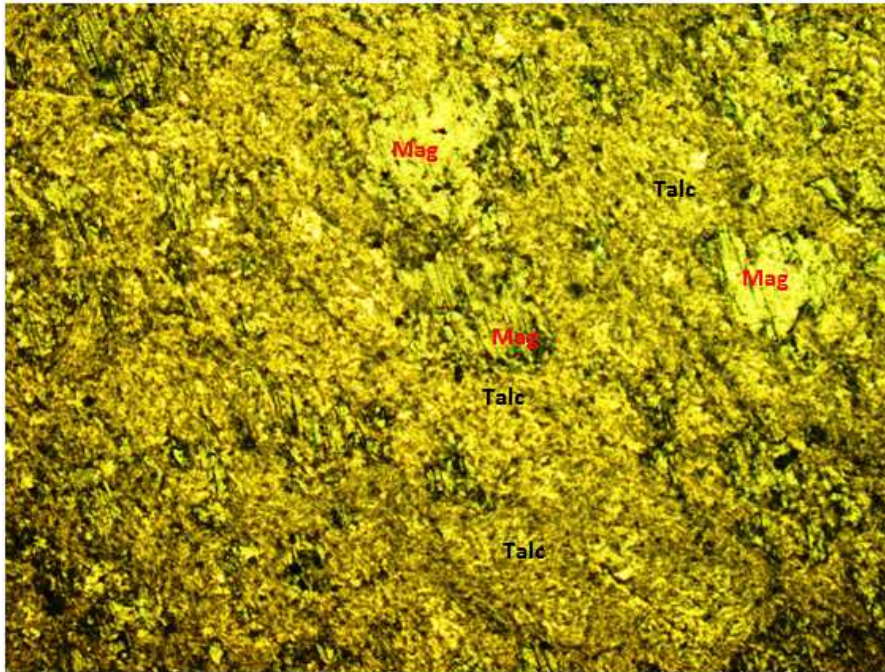


Figure 21: In zones where talc accumulates, magnesite crystals occur as small fragments with reaction fabrics, height of picture equals 1.35mm (type 2).



Figure 22: Type 2 represents the transition between Type 1 and 3.

3.3.3 Type 3

Type 3 shows an especially coarse fabric, the magnesite crystals have sizes up to 5 millimeters, sometimes there are pinolitic crystals with sizes up to 5 centimeters in length and one centimeter in width. The texture of the magnesite is mostly non-directional. The large magnesite grains are equidimensional to slightly elongated.

Type 3 shows less talc than type 1 and there are no larger amounts of talc accumulated in the magnesite structure at all. But this type of magnesite-talc intergrowth shows some interesting characteristics for the general understanding of the talc formation in the magnesite structure. Due to the coarse grains, there seems to be a good possibility for fluids to infiltrate the rock. Therefore talc was formed in the intergranular space between the large magnesite crystals (Fig. 23). There was no mechanical accumulation of talc in these areas; the undisturbed texture of the rock still exists. The original boundaries between talc and magnesite are often well preserved and can be microscopically examined. The talc formation starts at the crystal-boundaries and infiltrates the crystals along weak zones like microjoints and cleavage planes (Fig. 24 and 25). The transformation from magnesite to talc is mostly incomplete, completely transformed crystals show the original grain shape and size. Type 3 represents an early state of the deposit history and therefore is not relevant for exploration, it can be estimated that areas of very coarse magnesite are not likely to carry large amounts of talc. It can be observed that a coarse to fine change in the magnesite fabric takes place with increasing talc content and increasing accumulation of distinct talc bodies. Type 2 connects Type 1 and Type 3 and can be interpreted as smooth transition between the two other types.



Figure 23: Coarsely grained magnesite with talc between magnesite crystals (type 3).

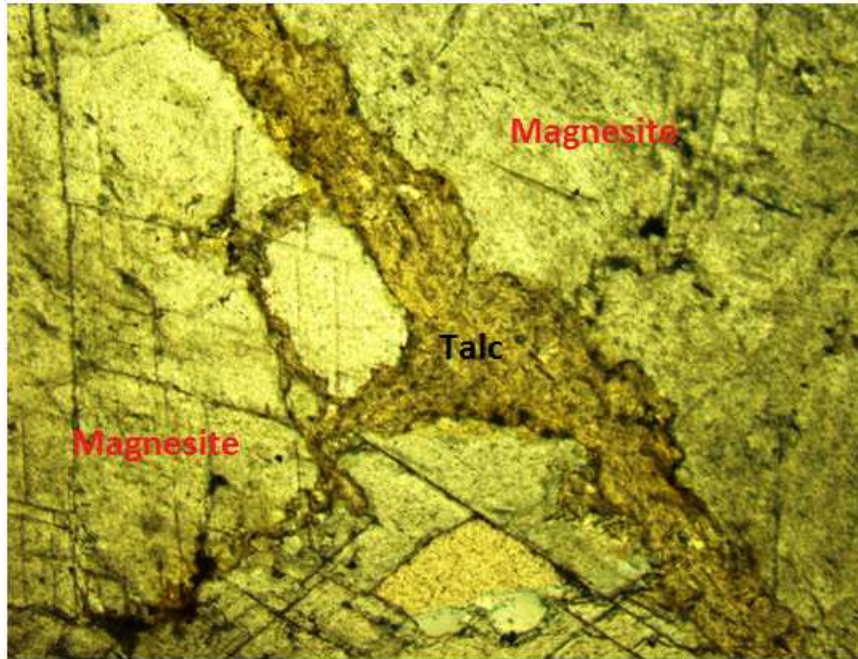


Figure 24: Coarsely grained magnesite, talc is embedded along the borders between large magnesite crystals; no further accumulation of talc, height of picture equals 1.35mm (type 3).

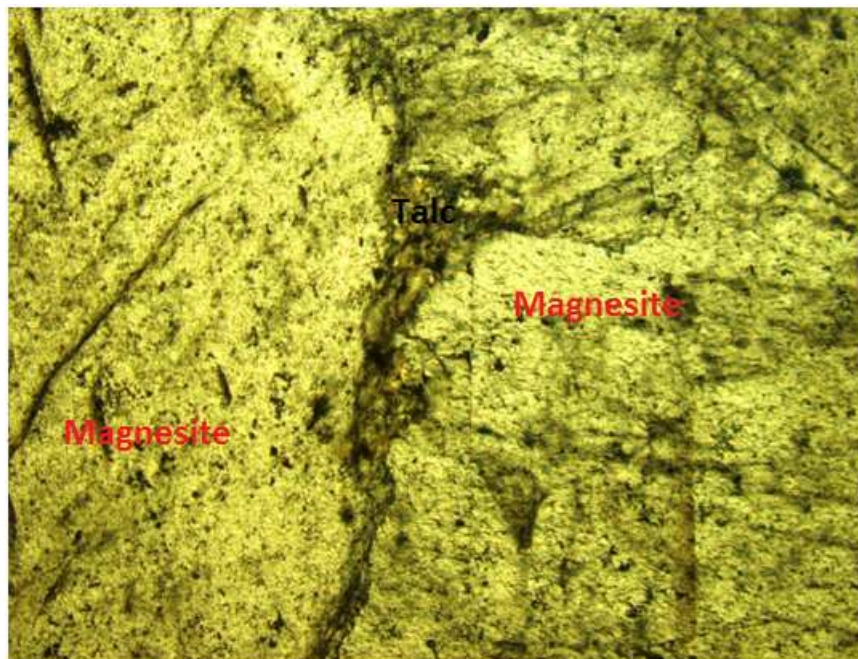


Figure 25: Fig: Talc formation along weak-zone between two magnesite crystals with sizes of several millimeters, height of picture equals 1.35mm (type 3).

3.3.4 Type 4

Type 4 represents the classic talc ore in the Fanjiabauzi mining area. Talc occurs mostly in shear zones (Fig. 26). The shear bands range between centimeters up to

several meters in length and centimeters up to 1-2 meters in width. Mechanical talc accumulation dominates, there seems to be no dissolution or chemical exchange between talc and magnesite in this stage, this is proven by chemical analysis of talc and magnesite samples from the actual mining area. Talc coloration is mostly white and light pink, yellow and green colors are rare. The best talc qualities are mostly light pink to white and have low LOI and MgO values. Lower qualities include more magnesite, dolomite and dyke components and therefore have often darker colors (grey) and higher LOI values. The talc in shear bands is laminated and very fine grained, in pure zones there is almost no magnesite embedded into the talc matrix. In smaller shear zones, massive talc bodies included into the shear bands can be found. These massive bodies represent the primary form of talc as described above (type 1). These bodies are weak zones in the rock structure and acted as starting points for the tectonic movements which formed the deposit. There are no significant chemical differences between massive talc and laminated talc in shear zones, this proves the thesis that the deposit formation was only mechanically induced and not supported by chemical solution processes or a second step of talc genesis by fluid transport. At some spots, isolated massive talc bodies with shear marks can be observed; these bodies are sometimes elongated or split up and pulled apart characteristically. In a larger scale, this process leads to the formation of the typical talc enrichments in elongated shear bands, where talc from different weak zones joins together in large laminated lenses. These lenses act as sliding planes and cause further accumulation. Finally these processes trigger the almost pure talc bodies with sizes in the range of meters, which easily can be mined.

The magnesite at the borders of large talc accumulation zones is mostly fine grained and compact with bright white coloration. Further away of the deposit borders, magnesite is coarse grained and sometimes has a more grey habitus. It seems that the recrystallisation process that leads to massive, very pure magnesite in the areas where talc is concentrated is not an early diagenetic process, but is associated to the later talc mineralization. The genetic process leading to this dependence is difficult to prove, but again, the phenomenon of finely crystalline surrounding rocks in the nearest deposit environment is also described from other talc deposits like Lassing, Austria (Prochaska, 1989). In Lassing, coarsely grained meta-carbonates are

dominant in the surroundings of the deposit, but the actual, dolomitic host rock is exceptionally pure and shows an average grain size of 0,1mm (Prochaska, 1989).

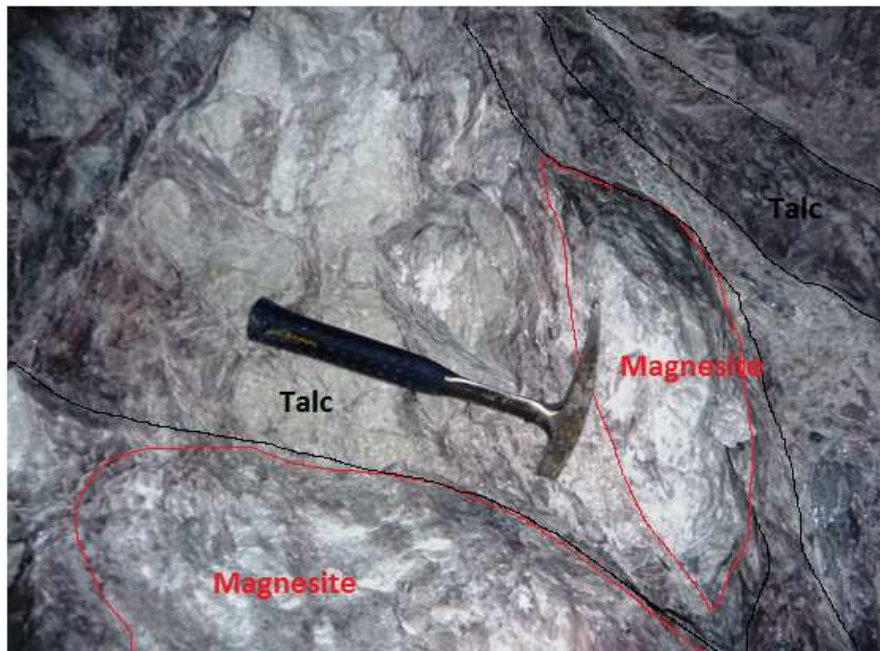


Figure 26: Talc accumulation in shear zone (type 4).

3.4 Chemical Analysis

3.4.1 Methods and Equipment

Microscopic analysis of thin sections was done with an Olympus BX 60 transition microscope. Olympus objectives with 10x and 50x optical enlargement were used, for the creation of detail pictures, an additional Jenoptik ProgRes CF scanner was implemented. Talc samples were ground below 200 mesh and analyzed by Actlabs Ltd., Canada. The techniques used are ICP-OES (Inductively coupled plasma optical emission spectrometry) for main elements like Si, Mg, Ca, etc., and ICP-MS (Inductively coupled plasma mass spectrometry) for trace elements like Cr, Co or Ni and rare earth elements. Magnesite samples were also ground below 200 mesh and analyzed using Atomic Absorption Spectroscopy at the AAS-laboratory of the Department of Applied Geosciences, University of Leoben. The elements analyzed are Fe, Mn, Ni, Ca, Sr and Al. Whiteness and yellowness index of talc and magnesite samples were determined using a Datacolor Elrepho 3000 Series device, the samples were ground to 200 mesh and measured as powder pills. Crush and leach samples were ground by hand in an agate mortar, leached with distilled water and

centrifuged. Afterwards, the aqueous solution without the solid fraction was used for the analysis. The quantifiable elements for fluid inclusions from carbonate samples are the monovalent cations Na and K as well as the anions F, Br, Cl, I, NO₃ and SO₄ (Prochaska, 1999). The most abundant divalent cations Mg, Ca and Fe cannot be determined quantitatively because pore fluid and host rock are in permanent contact. Stable isotope composition of carbonate rocks (C and O isotopes) is an important indicator for the paleofacies at the time of deposition. C and O isotopes from magnesite powder samples were measured using standard stable isotopic methods in the isotopic laboratory of the Department of Applied Geosciences at the University of Leoben. Values reported are in the conventional delta notation with respect to the widely used international artificial standard Vienna Pee Dee Belemnite (VPDB) composed after the natural standard of a belemnite from the Pee Dee Formation.

3.4.2 Samples

The position of the analyzed samples in the field is shown in the schematic map below (Fig. 27). The coordinates have to be correlated with the corresponding elevation in Table 1. Samples were taken as grab samples in the field, washed and air dried afterwards to prevent contamination with powder traces from other locations. For main and trace element assay of talc and magnesite, weathered parts of the rock samples were removed and only fresh cut surfaces were taken into account. To ensure proper results, samples were crushed, the fraction <2mm was sieved and inhomogenities from weathering or trace minerals like pyrite were removed per hand in a second step. Afterwards, samples were ground to 200 mesh for further processing. For the C and O isotopic composition of magnesite, samples of 1mg were taken out of fresh cut surfaces with a diamond drill to ensure representative results. Whiteness and yellowness of talc was determined from bulk samples taken from the processing plant as well as from samples directly taken from the underground mines. These samples were not especially prepared but directly ground and measured, to reproduce the conditions of the real product after mining best possible.

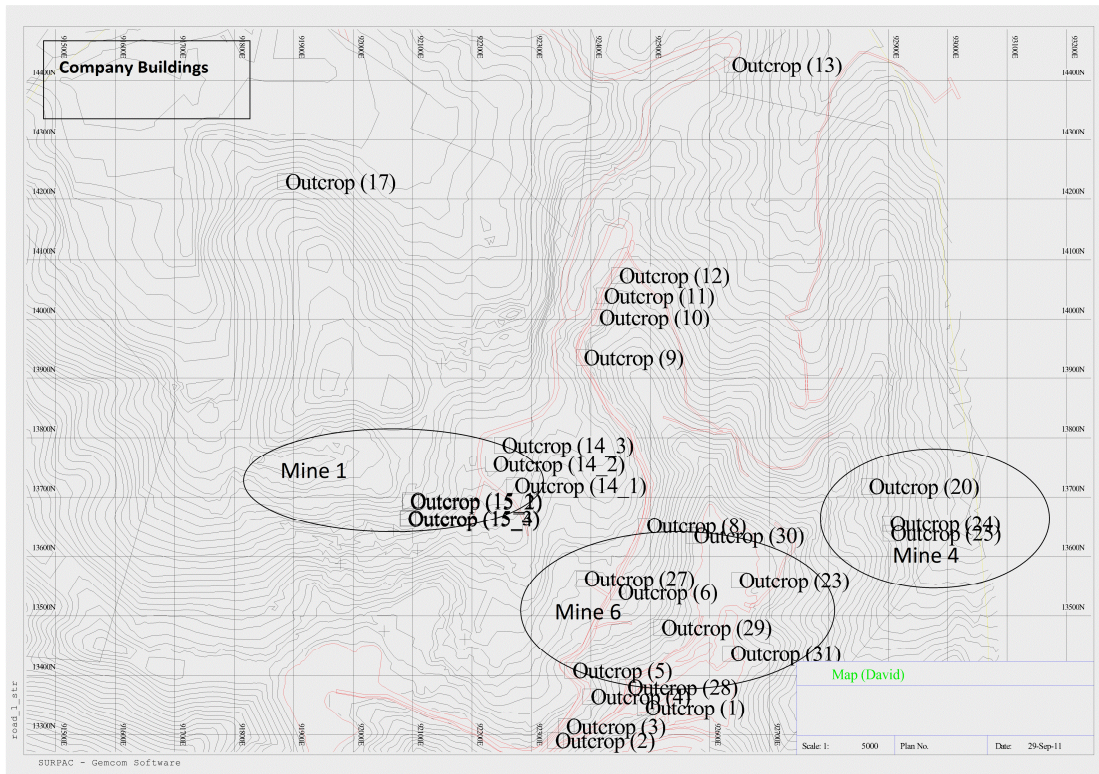


Figure 27: Schematic position of sampling spots at the Fanjiabauzi mining area.

Outcrop No.	elevation [m]	comment
1	surface	
2	surface	
3	surface	
4	surface	
5	surface	
6	surface	
8	surface	
9	surface	
10	surface	
11	surface	
12	surface	
13	surface	
14	90	
15	84	
17	surface	
18_1	mine 6, grade 1 grey	samples from processing
18_2	mine 4, D60	samples from processing
18_3	mine 6, grade 1 white-yellow	samples from processing
19	mine 3	samples from mine 3 (outside of Fanjiabauzi area)
20	187	
23	176	
24	176	
25	170	
26	surface	
27	222	
28	222	
29	222	
30	222	
31	230	

Table 1: Elevation of sampling spots.

The exact positions of sampling spots in the actual underground mining levels can be found in detailed maps which are attached to the appendix.

3.4.3 Talc

3.4.3.1 Main elements

The mined talc is divided into three different grades; grade 1 represents the highest quality of talc products. In the following, only grade 1 and grade 2 will be further investigated, because grade 3 talc has no commercial relevance. The SiO₂ content of grade 1 talc ranges between 61.5% and 62.5%, the SiO₂ content of grade 2 talc is significantly lower and lies between 56% and 58%. The lower values for grade 2 talc are caused by the higher magnesite content; therefore the talc/magnesite ratio of the sample is crucial for this parameter. Fe₂O₃ averages at 0.103% for grade 1 and at 0.203% for grade 2. The iron-oxide content is also related to the magnesite/talc-ratio, magnesite integrates iron cations to its structure, therefore the higher magnesite content of grade 2 talc causes higher iron-oxide values in the samples. Other possible iron-oxide sources are dyke components which have high iron contents. Examples for such minerals in the lamprophyric dykes are pyroxenes, amphiboles and Fe-rich mica (biotite). The average MgO content of grade 1 samples is 31.4% whereas in comparison the average MgO content of grade 2 samples is significantly higher with 33.2%. This value is also linked to the higher average magnesite concentration in grade 2 talc samples; an exact determination of the magnesia-source is difficult because almost all involved minerals include magnesia-cations into their structure. The CaO content of grade 1 talc averages at 0.18%, the average CaO of grade 2 talc is significantly higher and ranges at 0.41%. The CaO source which leads to the higher CaO contents of grade 2 talc is most likely fine distributed dolomite which is embedded in the mined shear bands. Dolomite layers were found widely spread in the whole underground mining area. At last, the most relevant value for the quality of the final product is the LOI (loss on ignition). This is also the value with the most apparent difference between the analyzed grade 1 and grade 2 samples. In comparison, the average LOI of grade 1 talc is 4.85% whereas the average LOI of grade 2 talc doubles this value and ranges at 10.4%. This large difference affects the quality of the end-product; it affects further processing and deteriorates the ratio raw material to useable product. Major reasons for the higher

LOI values of the lower talc-qualities are most likely the higher values of carbonate minerals like magnesite and dolomite, which react at higher temperatures and lose their CO₂. Minor influence may be attributed to the loss of crystal-water of mica-minerals which are main components of the lamprophyric dykes. Tables 2-4 show the results of FUS-ICP measurements carried out on the different types of talc samples.

Analyte	SiO ₂	Al ₂ O ₃	Fe ₂ O ₃ (T)	MnO	MgO	CaO	Na ₂ O	K ₂ O	TiO ₂	P ₂ O ₅	LOI	Total
Unit	%	%	%	%	%	%	%	%	%	%	%	%
Detect Limit	0.01	0.01	0.01	0.001	0.01	0.01	0.01	0.01	0.001	0.01		0.01
Method	FUS-ICP	FUS-ICP	FUS-ICP	FUS-ICP	FUS-ICP	FUS-ICP	FUS-ICP	FUS-ICP	FUS-ICP	FUS-ICP	FUS-ICP	FUS-ICP
15_1	62.3	0.02	0.05	< 0.001	31.43	0.15	< 0.01	< 0.01	< 0.001	0.13	4.8	98.87
18_1	62.6	0.04	0.1	< 0.001	31.89	0.12	< 0.01	< 0.01	< 0.001	0.11	4.83	99.68
18_2	62.23	0.09	0.12	< 0.001	31.67	0.35	< 0.01	< 0.01	0.002	0.06	4.97	99.5
18_3	61.47	0.03	0.17	< 0.001	31.3	0.19	< 0.01	< 0.01	< 0.001	0.17	4.8	98.12
23_1	62.46	0.03	0.11	< 0.001	31.01	0.22	< 0.01	< 0.01	< 0.001	0.12	4.97	98.92
29_1	62.24	0.06	0.09	< 0.001	31.25	0.08	< 0.01	< 0.01	< 0.001	0.05	4.89	98.65
30_1	62.52	0.06	0.08	< 0.001	31.15	0.15	< 0.01	< 0.01	0.001	0.08	4.72	98.78

Table 2: Chemical analysis of main element contents for grade 1 talc samples.

Analyte	SiO ₂	Al ₂ O ₃	Fe ₂ O ₃ (T)	MnO	MgO	CaO	Na ₂ O	K ₂ O	TiO ₂	P ₂ O ₅	LOI	Total
Unit	%	%	%	%	%	%	%	%	%	%	%	%
Detect Limit	0.01	0.01	0.01	0.001	0.01	0.01	0.01	0.01	0.001	0.01		0.01
Method	FUS-ICP	FUS-ICP	FUS-ICP	FUS-ICP	FUS-ICP	FUS-ICP	FUS-ICP	FUS-ICP	FUS-ICP	FUS-ICP	FUS-ICP	FUS-ICP
14_1	55,65	0,08	0,09	< 0.001	32,89	0,24	< 0.01	< 0.01	0,002	0,1	9,69	98,76
14_2	57,99	0,04	0,06	< 0.001	32,64	0,2	< 0.01	< 0.01	< 0.001	0,13	7,75	98,8
20_1	57,23	0,04	0,11	< 0.001	32,08	0,99	< 0.01	< 0.01	< 0.001	0,08	8,09	98,63
28_1	34,93	13,28	0,63	< 0.001	35,33	0,19	< 0.01	< 0.01	0,421	0,06	16,15	> 101,0

Table 3: Chemical analysis of main element contents for grade 2 talc samples.

Analyte	SiO ₂	Al ₂ O ₃	Fe ₂ O ₃ (T)	MnO	MgO	CaO	Na ₂ O	K ₂ O	TiO ₂	P ₂ O ₅	LOI	Total
Unit	%	%	%	%	%	%	%	%	%	%	%	%
Detect Limit	0.01	0.01	0.01	0.001	0.01	0.01	0.01	0.01	0.001	0.01		0.01
Method	FUS-ICP	FUS-ICP	FUS-ICP	FUS-ICP	FUS-ICP	FUS-ICP	FUS-ICP	FUS-ICP	FUS-ICP	FUS-ICP	FUS-ICP	FUS-ICP
4_1	63.27	0.04	0.25	< 0.001	30.51	0.06	< 0.01	< 0.01	< 0.001	0.05	4.67	98.84
5_1	42.06	0.05	0.35	0.006	35.73	0.16	< 0.01	< 0.01	< 0.001	0.07	20.71	99.15
1_4	50.78	0.04	0.19	< 0.001	33.83	0.08	< 0.01	< 0.01	< 0.001	< 0.01	13.82	98.76
14_1	55.65	0.08	0.09	< 0.001	32.89	0.24	< 0.01	< 0.01	0.002	0.1	9.69	98.76
14_2	57.99	0.04	0.06	< 0.001	32.64	0.2	< 0.01	< 0.01	< 0.001	0.13	7.75	98.8
15_1	62.3	0.02	0.05	< 0.001	31.43	0.15	< 0.01	< 0.01	< 0.001	0.13	4.8	98.87
15_3	57.22	0.03	0.07	< 0.001	32.9	0.13	< 0.01	< 0.01	< 0.001	0.07	8.71	99.14
18_1	62.6	0.04	0.1	< 0.001	31.89	0.12	< 0.01	< 0.01	< 0.001	0.11	4.83	99.68
18_2	62.23	0.09	0.12	< 0.001	31.67	0.35	< 0.01	< 0.01	0.002	0.06	4.97	99.5
18_3	61.47	0.03	0.17	< 0.001	31.3	0.19	< 0.01	< 0.01	< 0.001	0.17	4.8	98.12
19_1	61.95	0.04	0.22	< 0.001	31.6	0.01	< 0.01	< 0.01	< 0.001	< 0.01	4.96	98.77
19_2	63.26	0.03	0.2	< 0.001	32.2	0.02	< 0.01	< 0.01	< 0.001	< 0.01	4.87	100.6
19_4	43.68	< 0.01	0.18	< 0.001	35.61	0.08	< 0.01	< 0.01	< 0.001	< 0.01	19.2	98.78
20_1	57.23	0.04	0.11	< 0.001	32.08	0.99	< 0.01	< 0.01	< 0.001	0.08	8.09	98.63
23_1	62.46	0.03	0.11	< 0.001	31.01	0.22	< 0.01	< 0.01	< 0.001	0.12	4.97	98.92
26_1	61.6	0.02	0.19	< 0.001	31.88	0.19	< 0.01	< 0.01	< 0.001	0.12	5.63	99.62
26_2	62.89	0.01	0.31	< 0.001	31.56	0.02	< 0.01	< 0.01	< 0.001	< 0.01	4.63	99.4
28_1	34.93	13.28	0.63	< 0.001	35.33	0.19	< 0.01	< 0.01	0.421	0.06	16.15	> 101.0
29_1	62.24	0.06	0.09	< 0.001	31.25	0.08	< 0.01	< 0.01	< 0.001	0.05	4.89	98.65
30_1	62.52	0.06	0.08	< 0.001	31.15	0.15	< 0.01	< 0.01	0.001	0.08	4.72	98.78
31_1	62.17	0.05	0.18	< 0.001	31.38	0.03	< 0.01	< 0.01	< 0.001	< 0.01	4.72	98.53

Table 4: Summary of main element contents for all analyzed talc samples.

3.4.3.2 Trace Elements

The values of Cr, Ni and Zn are below 20ppm, the contents of Co mostly below 1ppm. The low values for those elements are characteristically for Carbonate-bound talc deposits and therefore expected. Higher values would indicate the influence of

fluids, derived from mafic to ultramafic rocks, on the talc genesis, which clearly can be eliminated. The only mafic rocks in the deposit surroundings are the lamprophyre dykes which are younger than the talc genesis and therefore may only cause higher trace element contents due to contamination of the talc samples. The average Ba/Sr-ratio is at least 2 for the collected talc samples, this ratio is strongly connected to the origin of the deposit forming fluids. Trapped marine fluids and marine species tend to have extremely low Ba/Sa-ratios in comparison to terrestrial fluids and species with terrestrial habitats (Burton et al., 1990).

Rare earth element values are mostly under the detection limit and therefore not useful for further characterization of the deposit formation or discrimination of different ore qualities. Tables 5-7 show trace element contents of talc samples from all grades.

Analyte Symbol	Sc	Be	V	Ba	Sr	Y	Zr	Cr	Co	Ni	Cu	Zn	Ga	Ge
Unit Symbol	ppm	ppm	ppm	ppm	ppm	ppm	ppm	ppm	ppm	ppm	ppm	ppm	ppm	ppm
Detection Limit	1	1	5	3	2	2	4	20	1	20	10	30	1	1
Analysis Method	FUS-ICP	FUS-ICP	FUS-ICP	FUS-ICP	FUS-ICP	FUS-ICP	FUS-ICP	FUS-MS	FUS-MS	FUS-MS	FUS-MS	FUS-MS	FUS-MS	FUS-MS
4_1	<1	<1	5	5	<2	<2	6	<20	<1	<20	<10	<30	<1	<1
5_1	<1	<1	6	4	<2	2	5	<20	<1	<20	<10	<30	<1	<1
1_4	<1	<1	5	5	<2	<2	4	<20	<1	<20	<10	<30	<1	<1
14_1	<1	<1	5	5	<2	<2	6	<20	<1	<20	<10	<30	<1	<1
14_2	<1	<1	<5	4	<2	<2	4	<20	<1	<20	<10	<30	<1	<1
15_1	<1	<1	8	4	<2	<2	5	<20	<1	<20	<10	<30	<1	<1
15_3	<1	<1	<5	4	<2	<2	5	<20	<1	<20	<10	<30	<1	<1
18_1	<1	<1	6	4	<2	<2	<4	<20	2	<20	<10	<30	1	<1
18_2	<1	<1	<5	5	10	<2	7	<20	<1	<20	<10	<30	<1	<1
18_3	<1	<1	6	4	<2	<2	6	<20	<1	<20	<10	<30	<1	2
19_1	<1	<1	6	4	<2	<2	5	<20	<1	30	<10	<30	<1	<1
19_2	<1	<1	<5	4	<2	<2	26	<20	<1	20	<10	<30	<1	<1
19_4	<1	<1	<5	4	<2	<2	5	<20	<1	<20	<10	<30	3	<1
20_1	<1	<1	<5	4	<2	<2	7	<20	<1	<20	<10	<30	<1	<1
23_1	<1	<1	<5	4	<2	<2	5	<20	<1	<20	<10	<30	<1	<1
26_1	<1	<1	<5	4	<2	<2	6	<20	3	<20	<10	<30	1	1
26_2	<1	<1	<5	4	<2	<2	5	<20	2	<20	<10	<30	3	<1
28_1	5	<1	58	5	<2	3	187	60	3	<20	<10	<30	15	<1
29_1	<1	<1	5	4	<2	<2	10	<20	<1	<20	<10	<30	<1	<1
30_1	<1	<1	<5	4	<2	<2	5	<20	<1	<20	<10	<30	<1	<1
31_1	<1	<1	<5	4	<2	<2	<4	<20	1	<20	<10	<30	<1	<1

Table 5: Summary of trace element analysis for all grades of talc samples (part 1).

Analyte Symbol	As	Rb	Nb	Mo	Ag	In	Sn	Sb	Cs	La	Ce	Pr	Nd	Sm
Unit Symbol	ppm	ppm	ppm	ppm	ppm	ppm	ppm	ppm	ppm	ppm	ppm	ppm	ppm	ppm
Detection Limit	5	2	1	2	0.5	0.2	1	0.5	0.5	0.1	0.1	0.05	0.1	0.1
Analysis Method	FUS-MS	FUS-MS	FUS-MS	FUS-MS	FUS-MS	FUS-MS	FUS-MS	FUS-MS	FUS-MS	FUS-MS	FUS-MS	FUS-MS	FUS-MS	FUS-MS
4_1	< 5	< 2	< 1	< 2	< 0.5	< 0.2	< 1	< 0.5	< 0.5	< 0.1	< 0.1	< 0.05	< 0.1	< 0.1
5_1	< 5	< 2	< 1	< 2	< 0.5	< 0.2	< 1	< 0.5	< 0.5	0.1	0.4	0.06	0.3	< 0.1
1_4	< 5	< 2	< 1	< 2	< 0.5	< 0.2	< 1	< 0.5	< 0.5	0.1	0.2	< 0.05	0.2	< 0.1
14_1	< 5	< 2	< 1	< 2	< 0.5	< 0.2	< 1	< 0.5	< 0.5	< 0.1	0.3	0.05	0.1	< 0.1
14_2	< 5	< 2	< 1	< 2	< 0.5	< 0.2	< 1	< 0.5	< 0.5	0.1	0.3	< 0.05	0.1	< 0.1
15_1	< 5	< 2	< 1	< 2	< 0.5	< 0.2	< 1	< 0.5	< 0.5	< 0.1	0.1	< 0.05	< 0.1	< 0.1
15_3	< 5	< 2	< 1	< 2	< 0.5	< 0.2	< 1	< 0.5	< 0.5	< 0.1	0.3	< 0.05	< 0.1	< 0.1
18_1	< 5	< 2	< 1	< 2	< 0.5	< 0.2	< 1	< 0.5	< 0.5	< 0.1	< 0.1	< 0.05	< 0.1	< 0.1
18_2	< 5	< 2	< 1	< 2	< 0.5	< 0.2	< 1	< 0.5	< 0.5	0.1	0.3	< 0.05	0.2	< 0.1
18_3	< 5	< 2	< 1	< 2	< 0.5	< 0.2	< 1	0.5	< 0.5	< 0.1	< 0.1	< 0.05	< 0.1	< 0.1
19_1	< 5	< 2	< 1	< 2	< 0.5	< 0.2	< 1	< 0.5	< 0.5	< 0.1	< 0.1	< 0.05	< 0.1	< 0.1
19_2	< 5	< 2	< 1	< 2	< 0.5	< 0.2	< 1	< 0.5	< 0.5	< 0.1	0.2	< 0.05	< 0.1	< 0.1
19_4	< 5	< 2	< 1	< 2	< 0.5	< 0.2	< 1	< 0.5	< 0.5	0.1	0.4	0.07	0.4	0.1
20_1	< 5	< 2	< 1	< 2	< 0.5	< 0.2	< 1	< 0.5	< 0.5	0.1	0.3	< 0.05	0.1	< 0.1
23_1	< 5	< 2	< 1	< 2	< 0.5	< 0.2	< 1	< 0.5	< 0.5	0.2	0.5	0.07	0.3	< 0.1
26_1	< 5	< 2	< 1	< 2	< 0.5	< 0.2	< 1	< 0.5	< 0.5	0.1	0.3	0.05	0.3	< 0.1
26_2	< 5	< 2	< 1	< 2	< 0.5	< 0.2	< 1	< 0.5	< 0.5	< 0.1	0.2	< 0.05	< 0.1	< 0.1
28_1	< 5	< 2	8	< 2	< 0.5	< 0.2	2	< 0.5	0.6	0.3	0.8	0.14	0.6	0.2
29_1	< 5	< 2	< 1	< 2	< 0.5	< 0.2	< 1	< 0.5	< 0.5	< 0.1	< 0.1	< 0.05	< 0.1	< 0.1
30_1	< 5	< 2	< 1	< 2	< 0.5	< 0.2	< 1	< 0.5	< 0.5	< 0.1	< 0.1	< 0.05	< 0.1	< 0.1
31_1	< 5	< 2	< 1	< 2	< 0.5	< 0.2	< 1	< 0.5	< 0.5	< 0.1	< 0.1	< 0.05	< 0.1	< 0.1

Table 6: Summary of trace element analysis for all grades of talc samples (part 2).

Analyte Symbol	Eu	Gd	Tb	Dy	Ho	Er	Tm	Yb	Lu	Hf	Ta
Unit Symbol	ppm	ppm	ppm	ppm	ppm	ppm	ppm	ppm	ppm	ppm	ppm
Detection Limit	0.05	0.1	0.1	0.1	0.1	0.1	0.05	0.1	0.04	0.2	0.1
Analysis Method	FUS-MS	FUS-MS	FUS-MS	FUS-MS	FUS-MS	FUS-MS	FUS-MS	FUS-MS	FUS-MS	FUS-MS	FUS-MS
4_1	< 0.05	< 0.1	< 0.1	< 0.1	< 0.1	< 0.1	< 0.05	< 0.1	< 0.04	< 0.2	< 0.1
5_1	< 0.05	< 0.1	< 0.1	< 0.1	< 0.1	< 0.1	< 0.05	< 0.1	< 0.04	< 0.2	< 0.1
1_4	< 0.05	< 0.1	< 0.1	< 0.1	< 0.1	< 0.1	< 0.05	< 0.1	< 0.04	< 0.2	< 0.1
14_1	< 0.05	< 0.1	< 0.1	< 0.1	< 0.1	< 0.1	< 0.05	< 0.1	< 0.04	< 0.2	< 0.1
14_2	< 0.05	< 0.1	< 0.1	< 0.1	< 0.1	< 0.1	< 0.05	< 0.1	< 0.04	< 0.2	< 0.1
15_1	< 0.05	< 0.1	< 0.1	< 0.1	< 0.1	< 0.1	< 0.05	< 0.1	< 0.04	< 0.2	< 0.1
15_3	< 0.05	< 0.1	< 0.1	< 0.1	< 0.1	< 0.1	< 0.05	< 0.1	< 0.04	< 0.2	< 0.1
18_1	< 0.05	< 0.1	< 0.1	< 0.1	< 0.1	< 0.1	< 0.05	< 0.1	< 0.04	< 0.2	0.1
18_2	< 0.05	< 0.1	< 0.1	< 0.1	< 0.1	< 0.1	< 0.05	< 0.1	< 0.04	< 0.2	< 0.1
18_3	< 0.05	< 0.1	< 0.1	< 0.1	< 0.1	< 0.1	< 0.05	< 0.1	< 0.04	< 0.2	< 0.1
19_1	< 0.05	< 0.1	< 0.1	< 0.1	< 0.1	< 0.1	< 0.05	< 0.1	< 0.04	< 0.2	< 0.1
19_2	< 0.05	< 0.1	< 0.1	< 0.1	< 0.1	< 0.1	< 0.05	< 0.1	< 0.04	< 0.2	< 0.1
19_4	< 0.05	0.2	< 0.1	0.2	< 0.1	< 0.1	< 0.05	< 0.1	< 0.04	< 0.2	< 0.1
20_1	< 0.05	< 0.1	< 0.1	< 0.1	< 0.1	< 0.1	< 0.05	< 0.1	< 0.04	< 0.2	< 0.1
23_1	< 0.05	< 0.1	< 0.1	< 0.1	< 0.1	< 0.1	< 0.05	< 0.1	< 0.04	< 0.2	< 0.1
26_1	< 0.05	< 0.1	< 0.1	< 0.1	< 0.1	< 0.1	< 0.05	< 0.1	< 0.04	< 0.2	< 0.1
26_2	< 0.05	< 0.1	< 0.1	< 0.1	< 0.1	< 0.1	< 0.05	< 0.1	< 0.04	< 0.2	< 0.1
28_1	0.06	0.3	< 0.1	0.4	< 0.1	0.4	0.07	0.6	0.11	4.4	0.8
29_1	< 0.05	< 0.1	< 0.1	< 0.1	< 0.1	< 0.1	< 0.05	< 0.1	< 0.04	< 0.2	< 0.1
30_1	< 0.05	< 0.1	< 0.1	< 0.1	< 0.1	< 0.1	< 0.05	< 0.1	< 0.04	< 0.2	< 0.1
31_1	< 0.05	< 0.1	< 0.1	< 0.1	< 0.1	< 0.1	< 0.05	< 0.1	< 0.04	< 0.2	< 0.1

Table 7: Summary of trace element analysis for all grades of talc samples (part 3).

3.4.3.3 Whiteness and yellowness index

The whiteness and yellowness indices of talc samples from different grades were determined. The values for whiteness and yellowness index correlate with the color of the analyzed talc sample (Tables 8-13). Pink and white talc variations show high values for whiteness and low yellow indices, whereas the whiteness of grey talc strongly depends on the intensity of the grey coloration. Light grey talc also shows good values for whiteness, whereas grey to dark grey talc has an average whiteness of 88 and yellowness of 1.9. In comparison, the average whiteness of pink talc is 93.4 with an average yellowness index of 1.8 and the measured whiteness of white talc is 92.1 with a remarkably low yellowness of 0.96. Yellow talc samples reached the

highest measured whiteness values with 95.0; the yellowness of 2.4 is predictably higher than for white and pink talc. Weathered talc from the open pit operation shows light to dark brown coloration. The weathered samples show an average whiteness of 92.9 but significantly elevated values for yellowness. The average yellowness index of the weathered surface samples is 3.4 (Tables 8-13 show whiteness and yellowness indices for distinct talc colors). The selling product D60, which is a mixture of yellow, pink and grey talc, shows a relatively high whiteness value and at the same time low yellowness.

sample no.	color (rock)	whiteness	yellowness index
14_2	pink	92,75	1,58
15_1	pink	94,49	2,06
15_3	pink	92,91	1,87

Table 8: Whiteness and yellowness index of pink talc.

sample no.	color (rock)	whiteness	yellowness index
31_1	white	92,13	0,96

Table 9: Whiteness and yellowness index of white talc.

sample no.	color (rock)	whiteness	yellowness index
18_3	yellow	95,00	2,42

Table 10: Whiteness and yellowness index of yellow talc.

sample no.	color (rock)	whiteness	yellowness index
18_1	grey	86,70	0,74
29_1	grey	92,35	2,41
30_1	grey-brown	89,86	2,45

Table 11: Whiteness and yellowness index of grey talc.

sample no.	color (rock)	whiteness	yellowness index
4_1	yellow-light brown	95,12	2,63
19_1	brown-grey	92,37	3,21
19_2	yellow-light brown	93,50	3,21
26_1	brown	90,60	4,52

Table 12: Whiteness and yellowness index of weathered talc.

sample no.	color (rock)	whiteness	yellowness index
D60	mix yellow, pink, grey	91,39	1,22

Table 13: Whiteness and yellowness index of product D60 (mixture).

3.4.4 Magnesite

The types of magnesite present at the mining area were described above. They show great differences in their fabric, average grain size and talc content. The chemical analysis of different magnesite samples aims to display dependences between chemical composition of magnesite and presence of major amounts of talc in the surrounding area. Significant differences between talc-neighbor magnesite and magnesite without talc in the direct environment could help to find new spots with high potential talc content. The samples were taken from the underground mine as well as from the new and old open pit area. There were also some samples taken from the Mafeng magnesite mine, these samples were added to the group of magnesite samples without talc in the direct environment. The chemical analysis includes the contents of Fe, Mn, Ni, Ca, Sr, Al. The analyzing method was Atom Absorption Spectroscopy, done at the laboratory site of the Department of Applied Geosciences at the University of Leoben. This method is relatively cheap and easy to use. The biggest advantage is the possibility to detect small amounts of elements which are incorporated into the magnesite structure. This allows the characterization of certain parameters which may help to predict the presence of remarkable amounts of talc in the neighborhood of the sample.

The average content of Al for samples without talc in the surrounding area is 0.093%, the average content of samples with nearby talc is 0.07%. There is a slight difference, but it has to be mentioned that neither talc nor magnesite incorporate Al into their crystal structure, therefore the value for Al represents only impurities in the rock samples and not differences in the mineral chemistry. Nevertheless the amount of admixed mineral compounds in the magnesite host rock could also be an indicator for the distance to possible talc locations. For sure the significance of this assumption has to be proved by other parameters.

The Sr contents of both magnesite sample groups are extremely low and mostly below the detection limit of 0.01%. At least for the group of magnesite without talc in

the environment there were some detectable amounts of Sr in few samples, but not enough to make a clear conclusion whether there is a coherence between talc presence and Sr content or not. Most likely the small amounts of Sr are part of the mineral impurities described above.

For all samples of both groups, Ni values were throughout below the detection limit. This does not help in terms of ore characterization, but the remarkably low Ni contents show the absence of mafic and ultramafic rocks as origin for deposit forming fluids during the talc genesis. The values correlate with the results for the analyzed talc samples presented above.

Mn shows a significant difference between the two test groups, with higher values for the non-talc magnesite samples. The average value for non-talc magnesite lies at 0.012%, the average for talc-host magnesite is 0.0086%. Mn is a common impurity for magnesite, but not for talc. Nevertheless, the difference is likely to represent an actual difference between the two magnesite compositions, because the amount of incorporated talc in the samples of talc-host magnesite is minor and therefore can be neglected.

The average value for Fe ranges at 0.23% for non-talc magnesite and at 0.18% for talc-host magnesite. Fe is incorporated into the talc structure as well as into the magnesite structure; therefore the difference between the two groups is most likely not caused in the possible talc contamination of the talc-host magnesite.

The amounts of Ca show the most remarkable difference between the two test groups. The average Ca content for non-talc magnesite samples is 3.26% whereas the average Ca content of talc-host magnesite is only 0.45%. This difference seems to be a clear indicator for the discrimination of the two sample groups, but it has to be mentioned that most of the Ca is not incorporated into the magnesite structure but shows the presence of significant amounts of dolomite in the sampled rocks. It is almost impossible to differentiate between pure magnesite and zones of magnesite/dolomite mélange in the field, therefore the samples with extraordinary high Ca contents are likely to represent such mixed rock environments. Nevertheless it has to be noticed that there seems to be no dolomite present at the host rock near to the talc deposit borders, presence of dolomite indicates that no larger amounts of

talc can be expected in the nearest (range of meters) environment of the sample area.

The main conclusion of the chemical analysis of magnesite samples in talc-host and talc-free zones is that there is a tendency to higher amounts of trace elements (Mn, Sr) in zones where no talc is expected (Tables 14-15). Also the contents of Fe and Ca are higher for non-talc magnesite, probably due to higher dolomite content. All measured element contents show the same trend, the average values for non-talc magnesite are without exceptions higher than those for talc-host magnesite samples. At the same time the talc-host magnesite shows a more compact structure with a lower average grain size and a bright white coloration, whereas the non-talc magnesite is coarser grained in average and sometimes shows grey or yellowish coloration. Dolomite occurrence seems to be widespread throughout the mining area, but gets rare in the nearest talc deposit environment. The sum of incorporated trace elements could be a possible indicator for spots with higher talc potential, although single element values can be influenced by different impurities and sampling errors and therefore should not be overrated.

Sampling Area	Sample No.	results [%]	Fe	Mn	Ni	Ca	Sr	Al
Aihai Talc	15_2		0,0977	0,0063	<0,00001	0,5337	<0,000001	0,0834
Aihai Talc	15_4		0,1349	0,0073	<0,00001	0,6965	<0,000001	0,0848
Aihai Talc	1_3		0,2407	0,0106	<0,00001	0,3146	<0,000001	0,0430
Aihai Talc	20_2		0,2128	0,0122	<0,00001	0,2961	<0,000001	0,0921
Aihai Talc	26_3		0,2061	0,0068	<0,00001	0,3894	<0,000001	0,0457
		Σ	0,1785	0,0086	<0,00001	0,4461	<0,000001	0,0698

Table 14: Summary of AAS Data from magnesite samples with talc in the nearest environment. Samples were taken at Fanjiabauzi talc deposit.

Sampling Area	Sample No.	results [%]	Fe	Mn	Ni	Ca	Sr	Al
Aihai Magnesite	20_1		0,0128	0,0022	0,0016	21,9659	0,0014	0,0411
Aihai Magnesite	13_2		0,0493	0,0027	<0,00001	0,6009	0,0005	0,0791
Aihai Magnesite	19_2		0,2605	0,0175	<0,00001	0,4385	<0,000001	0,0383
Aihai Magnesite	13_1		0,1748	0,0080	<0,00001	0,7989	0,0007	0,3795
Aihai Magnesite	15_1		0,1229	0,0060	<0,00001	0,4586	<0,000001	0,0427
Aihai Magnesite	15_2		0,1448	0,0093	<0,00001	0,5637	<0,000001	0,0343
Aihai Magnesite	21_2		0,1001	0,0051	<0,00001	5,3370	0,0003	0,0548
Aihai Magnesite	16_2		0,0905	0,0051	<0,00001	0,8009	<0,000001	0,0561
Aihai Magnesite	8_9		0,7064	0,0319	<0,00001	0,4904	0,0002	0,0715
Aihai Magnesite	8_10		1,1121	0,0480	<0,00001	6,8081	0,0041	0,3531
Aihai Magnesite	8_4		0,0956	0,0039	<0,00001	0,3943	0,0002	0,0592
Aihai Magnesite	8_8		0,0814	0,0040	<0,00001	1,2624	0,0003	0,0941
Aihai Talc	11_3		0,3424	0,0200	<0,00001	0,5550	<0,000001	0,0581
Aihai Talc	14_3		0,1931	0,0100	<0,00001	0,6944	0,0002	0,0604
Aihai Talc	7_1		0,1016	0,0061	<0,00001	0,8575	<0,000001	0,0363
Aihai Talc	11_2		0,1962	0,0099	<0,00001	0,9091	<0,000001	0,0638
Aihai Talc	16_1		0,1646	0,0093	<0,00001	0,8897	0,0001	0,0987
Aihai Talc	10_1		0,2630	0,0134	<0,00001	0,9222	<0,000001	0,0922
Aihai Talc	33_1		0,1331	0,0197	<0,00001	17,3677	0,0024	0,0458
		Σ	0,2287	0,0122	0,0001	3,2692	0,0005	0,0926

Table 15: Summary of AAS Data from magnesite samples without talc in the nearest environment. Samples were taken both at Fanjiabauzi talc and Aihai magnesite (0.5km NE of Village Qushugou).

Figure 28 shows the schematic trend of element distribution from three magnesite samples taken at mining level 84m of mine 1 (sampling spots 15_2, 15_4, 16_1). The tendency to higher purity of magnesite approaching the talc mineralization is obvious, although it has to be mentioned that element contents from one randomly chosen sampling location cannot be assumed as representative.

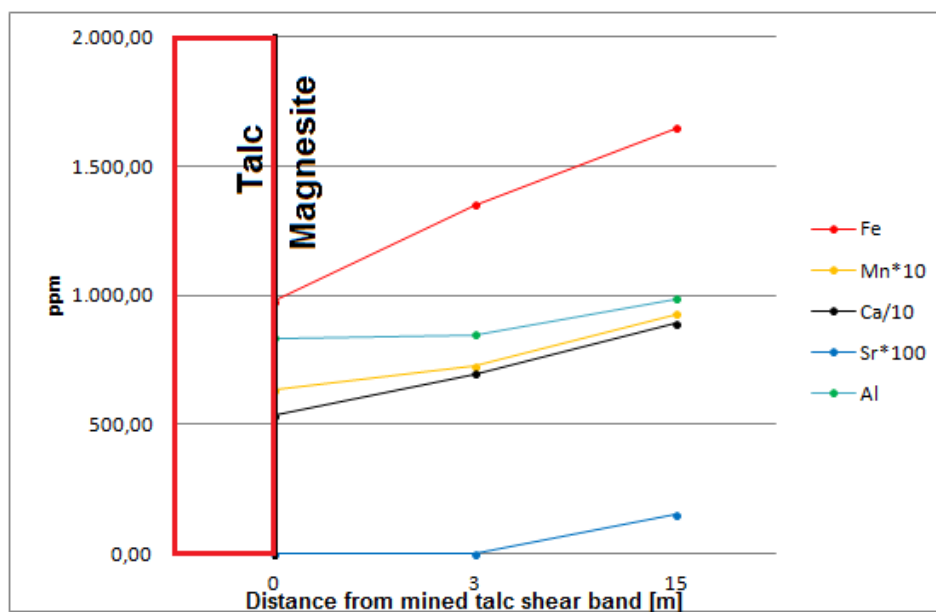


Figure 28: Schematic element distribution trend of magnesite samples in relation to distance from talc occurrence.

3.4.4.1 Whiteness and yellowness index

The whiteness of magnesite correlates with the grain size, fine grained magnesite samples show an average whiteness of 92.6 whereas coarse grained samples range at 89.4 for average whiteness. There is also a correlation between talc content of the magnesite and whiteness, magnesite from talc rich zones is not only more pure chemically, but also the whiteness increases. The average yellowness index for coarse magnesite without talc in the nearest environment is 4.5, the average value for intermediate to fine grained magnesite with small to medium, massive talc bodies is 2.3, whereas the yellowness index for fine grained magnesite near large talc shear bands averages at 1.7. Tables 16-18 show the trend of whiteness and yellowness depending on talc content and texture of the sampled rocks.

sample no.	structure	whiteness	yellowness index
10_1	coarse, no talc	88,36	3,19
11_2	coarse, no talc	91,15	4,24
11_3	coarse, no talc	88,63	6,08

Table 16: Whiteness and yellowness index of coarse magnesite without talc.

sample no.	structure	whiteness	yellowness index
1_3	fine, massive talc (surface)	92,74	2,02
7_1	fine, massive talc (surface)	91,87	2,18
26_3	fine, massive talc (surface)	93,25	2,77

Table 17: Whiteness and yellowness index of fine to medium grained magnesite with massive talc.

sample no.	structure	whiteness	yellowness index
14_3	fine, shearzone talc	90,58	1,86
15_2	fine, shearzone talc	94,31	1,45
15_4	fine, shearzone talc	92,59	1,80
20_2	fine, shearzone talc	93,09	1,55
33_1	fine, shearzone talc	92,57	1,59

Table 18: Whiteness and yellowness index of fine magnesite near talc shear bands.

3.4.4.2 Oxygen and carbon isotopes

Stable isotope analysis of carbonate rocks is very useful for the determination of depositional or diagenetic environments. Especially the carbon isotope ratios of

marine carbonate rocks are extremely useful for the reconstruction of ancient environmental changes (Baiquan, 2011). Oxygen isotopic composition is strongly dependent on temperature; therefore the ratio is used to estimate diagenetic processes and the ancient seawater temperature during carbonate formation. The $\delta^{18}\text{O}$ of carbonate rocks is controlled mainly by the $\delta^{18}\text{O}_w$ of the surrounding seawater (Veizer and Hoefs, 1976).

Table 19 shows the isotopic composition of Fanjiabauzi magnesite samples. The normal marine range for $\delta^{13}\text{C}(\text{PDB})$ is between 0.3 and 3.5‰. These values can be found in finely grained magnesite deposited in sedimentary playa and sabkha environments. A recent example for this is Coorong Laguna near Adelaide (Australia). Ancient examples for magnesite formed in marine evaporitic processes are the Adelaide Syncline and Barton Farm (Schroll, 2002). The influence of non-marine solutions causes the trend to lighter carbon (Kralik et al, 1989). For example, the Sebkh el Mela magnesites from Tunisia have an average $\delta^{13}\text{C}(\text{PDB})$ value of -3‰ (Kralik et al, 1989). Magnesites from the Fanjiabauzi talc deposit range between marine and non-marine $\delta^{13}\text{C}$ values, this indicates that after the primary sedimentary formation of the magnesite in an evaporitic environment, a secondary change of the isotopic composition occurred due to hydrothermal processes. The $\delta^{13}\text{C}$ values of Proterozoic magnesite rocks are typically extraordinary high (7-12‰) (Melezhik et al, 2001). The average value for the analyzed samples from the Fanjiabauzi area is significantly lower than expected (0.4‰). This indicates major changes in the primary composition during the metamorphic history of the carbonate beds in this area. The influence of meteoric water on hydrothermal processes during the deposit formation also leads to a relatively lighter isotopic signature of carbon. The $\delta^{18}\text{O}$ value strongly depends on the grade of metamorphism (Schroll, 2002). The samples from the Aihai talc deposit show remarkably light oxygen compared to other locations related to marine evaporitic playa or sabkha environments. Samples related to talc shear bands show a tendency to lighter oxygen compared to relatively undisturbed locations.

Detailed investigation on C and O stable isotopic composition of Precambrian carbonates from different locations showed some general trends leading to heavier or lighter C or O (Fig. 29 and 30 after Baiquan, 2011). It is clear that multiple environmental changes, water influx from different sources, temperature changes

Sample No.	d18O/16O VPDB	d13C/12C VPDB
20_2	-16,51237	0,78137
16_1	-17,42927	0,88037
11_2	-17,37147	0,44317
1_3	-16,10627	0,11797
33_1	-17,94047	0,26187
10_1	-17,80427	0,77007
15_4	-17,47447	0,39717
14_3	-16,54597	0,39307
15_2	-17,39417	0,74577
7_1	-18,26997	-0,05573
11_3	-16,72967	0,70487
26_3	-16,46447	-0,35743
11_2	-17,11257	0,05707
20_2	-16,88047	0,63027
16_1	-17,76857	0,81237
1_3	-16,16667	0,11757
33_1	-17,98217	0,27387
10_1	-17,60487	0,87577
15_4	-17,34167	0,40857
14_3	-16,84587	0,60017
26_3	-16,34887	-0,61133
15_2	-17,26387	0,46517
11_3	-16,81627	0,69357
average	-17,13803087	0,408939565

Table 19: C and O isotopic composition of magnesite marbles from the Haicheng talc deposit.

3.4.4.3 Crush and Leach

Crush and Leach Analysis is a controversially discussed method. It is easy to perform as it requires almost no sample preparation. Silicate or carbonate samples are crushed per hand and afterwards fluid inclusions are leached out of the rock material and analyzed geochemically. The most important disadvantage of the method is the obvious mixture of different fluid inclusions from the individual mineral phases. Therefore, crush and leach analysis is mostly representative for undisturbed, tectonically unaffected areas with homogeneous character. Obviously, this is not the case for the Fanjiabauzi area, as different orogenic phases overprinted the former shallow marine environment and changed the geochemical signature of the rocks. Nevertheless, as the method is cheap and easy to handle, Crush and Leach Analysis can provide an overview about the geochemical signature of the deposit forming

fluids and also can be useful for the comparison between different locations. For this task, Crush and Leach data from different regional deposits would be required for comparison. With this information, trends in the element distribution of formation fluids could be derived and errors caused by multiple orogenic overprint or inhomogeneous samples could be balanced. As there are no former studies on fluid inclusions of whole rock samples available for Liaoning magnesite, the Crush and Leach data acquired in this study cannot be used to gain information about genetic questions concerning age and environment of the talc formation. Nevertheless, the values can be compared to trace element distributions of fluid inclusions from other locations to estimate the environment present at the time when the massive carbonate beds were deposited in the Liaoning Province. A good indicator for the origin of salinar brines included into the carbonate beds are absolute values of halogenes and halogene-ratios. By far the most important sources for halogenes in the Earth's crust are evaporites and seawater (Wilkinson, 2001). J, Cl, F and Br are incompatible elements, which means that they are almost not included into mineral-fluid-exchange reactions of typical rock-forming minerals and therefore concentrations are mostly uninfluenced by later metamorphic processes. Generally, brines can have four different origins:

- Magmatic fluids related to granitic or granodioritic intrusions (Bodnar, 1995)
- Concentration of seawater by evaporation or precipitation of salts („evaporitic (connate) brines“, Carpenter, 1978)
- Dissolution of halite and other salts („diagenetic brines“, Carpenter, 1978)
- Concentration by removal of water during water-consuming metamorphic reactions (Bennett and Barker, 1992)

The different brines have different compositional „fingerprints“. The halogene and alkali contents are plotted as range boxes when the single values are irregularly distributed. Typical values for seawater, average crust and different types of Triassic and Cretaceous carbonates and carbonate-rich phyllites from different locations at the French Pyreneas after McCaig et al., 2000 and Fontes and Matray, 1993 (Fig. 31-35).

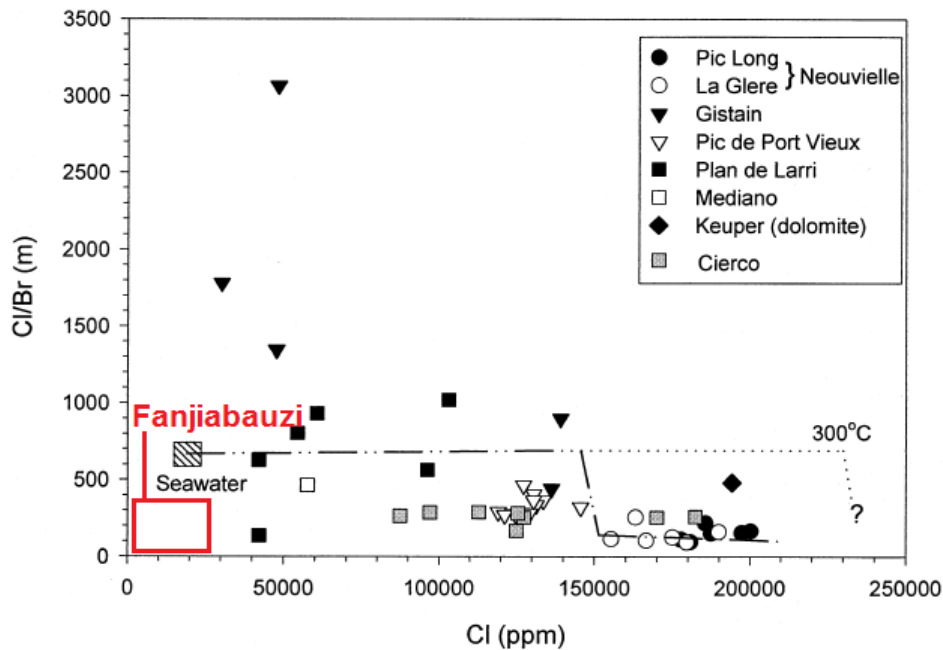


Figure 31: Cl/Br-Cl-Plot after McCaig et al, 2000. The dotted line represents the seawater evaporation line (after Fontes and Matray, 1993).

High absolute Cl-contents and high Cl/Br-ratios occur when dissolution of halite is an important factor in brine composition. The Cl-concentration is below seawater average for the fluid inclusions from Fanjabauzi magnesite marble, with an average of 8,860ppm. Single values spread from 550ppm in a silicified shear zone to 27,700ppm in homogeneous magnesite. Typical seawater averages around 20,000ppm Cl (McCaig et al., 2000). The balance between Cl + Na and Br is controlled by evaporation. When evaporation of seawater takes place, Na and Cl precipitate as halite. Br is incorporated in the precipitates only in minor amounts, which means that the residual fluid is relatively enriched in Br and gets depleted in Cl and Na (“halite-precipitation”). The reverse of this process occurs when Cl and Na are relatively enriched due to solution of evaporates by migration of fluids in upper parts of the crust (“halite-solution”). The system Na-Cl-Br is well discovered because it allows conclusions how paleo-fluids gain their specific salinity (Prochaska, 1999).

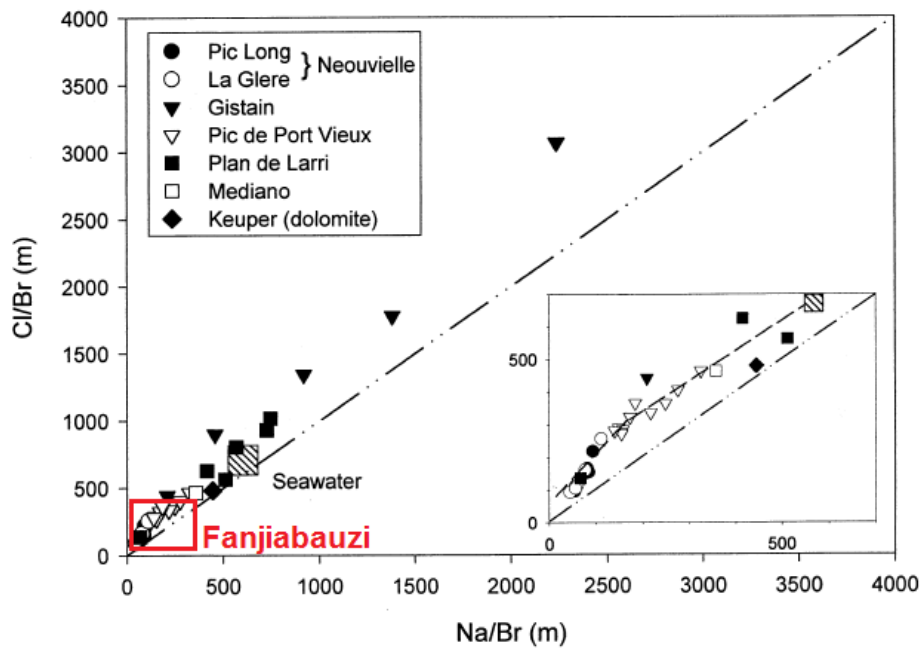


Figure 32: Cl/Br-Na/Br plot after McCaig et al, 2000. Seawater evaporation line from Fontes and Matray, 1993.

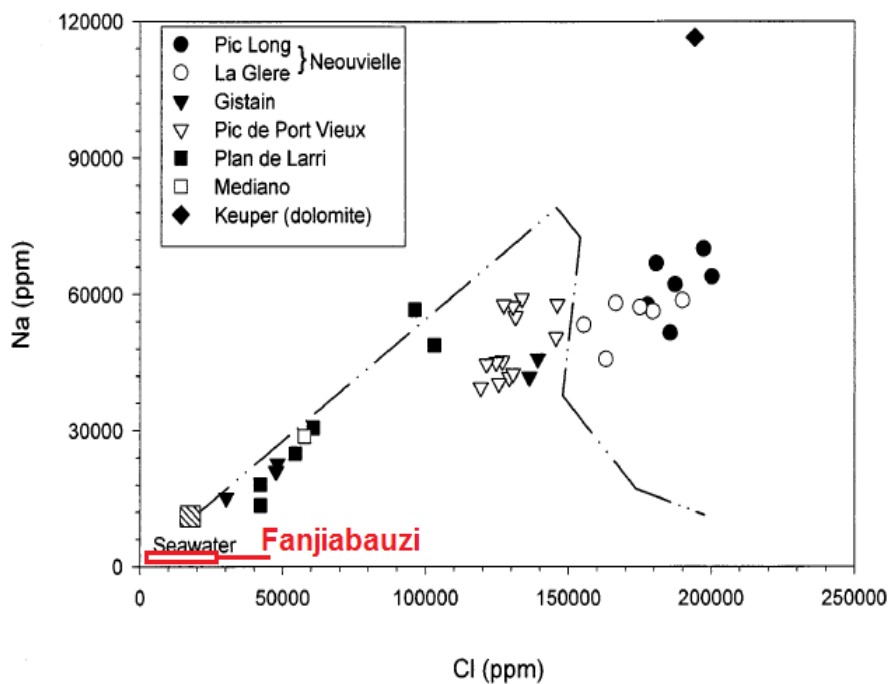


Figure 33: Na versus Cl, evaporation line from Fontes and Matray, 1993.

The average ratio between Cl/Br and Na/Br fits into the typical evaporation line after Fontes and Matray, 1993. Nevertheless, the fluid inclusions from Fanjiabauzi magnesite marble are depleted in Cl and Na, compared to recent average seawater. Especially the absolute values for Na-content are consistently low.

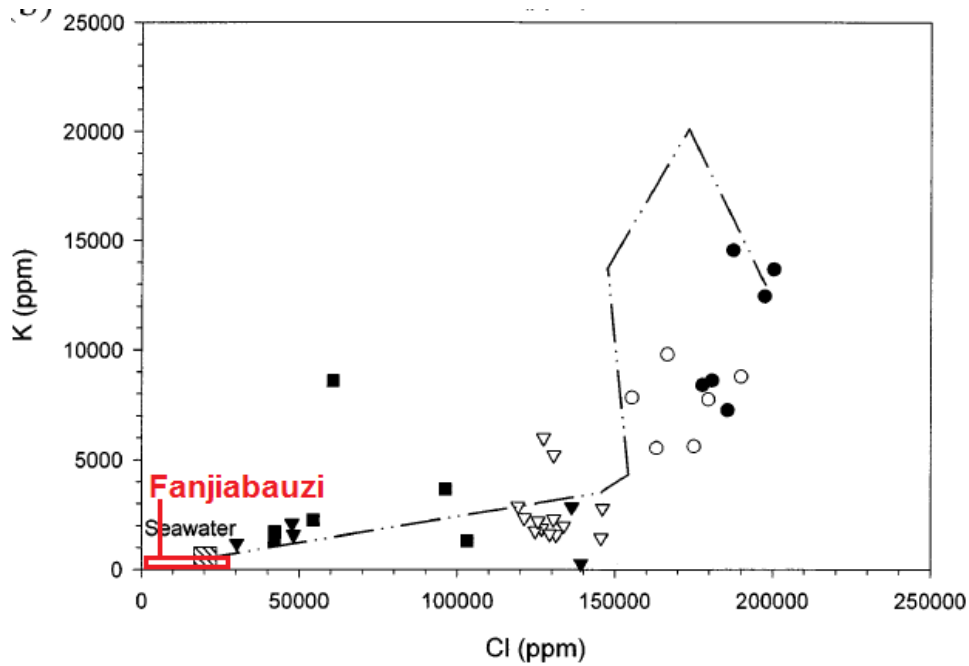


Figure 34: K versus Cl, evaporation line from Fontes and Matray, 1993.

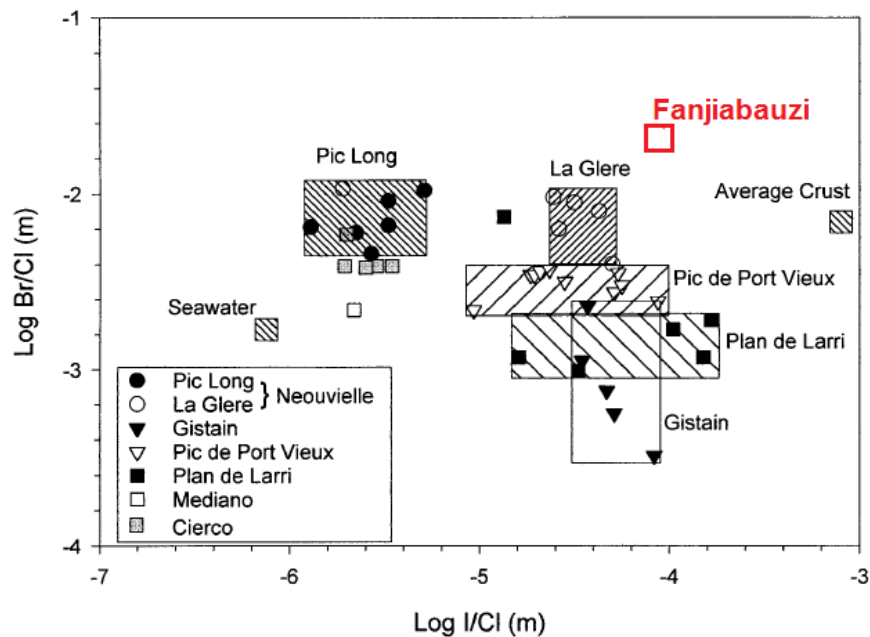


Figure 35: Br/Cl-I/Cl-plot after McCaig et al, 2000.

K contents from Fanjiabauzi marble fluid inclusions are slightly below the range of recent seawater and far below juvenile waters. The ratio of I/Cl is higher than expected for seawater influence, because the salinity is generally low due to dilution. The absolute values for I range consistently under 1ppm, with an average of 0.36ppm. The elevated I/Cl-ratio relative to seawater is therefore caused by low Cl,

not by high I content. Li ranges between 1.48 and 0.03ppm, with an average of 0.4ppm. Recent seawater average for Li is around 0.17ppm.

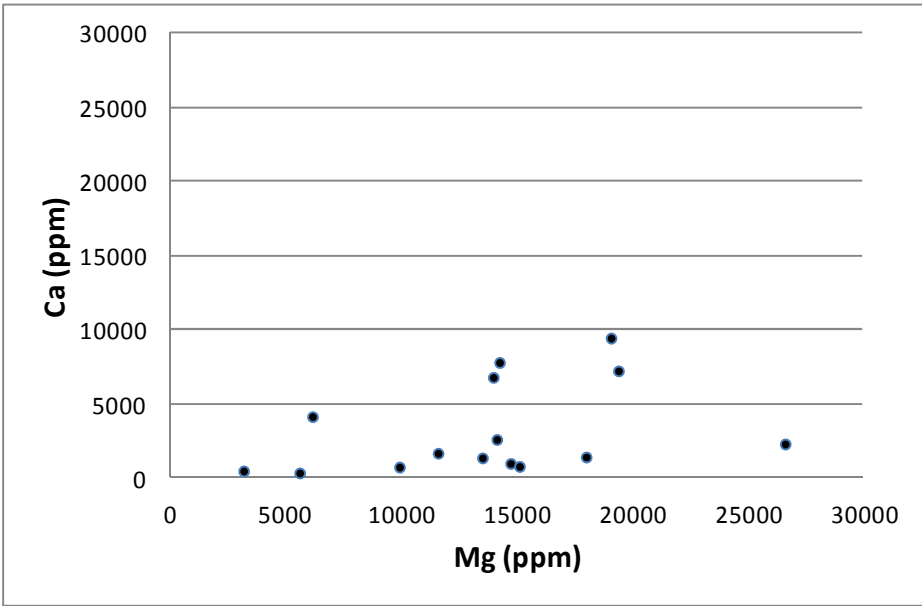


Figure 36: Ca-Mg-plot from Fanjiabauzi magnesite marble

The most important factor for talc mineralization is the sufficient Mg supply. Mg is by far the most present element in fluid inclusions from Fanjiabauzi magnesite marble, with an average content of 13,700ppm. Normal brines have Ca/Mg ratios above 1, meaning that Ca is more often the dominant element in fluid inclusions (McCaig et al, 2000). The average ratio is 0.237 for samples from Fanjiabauzi, therefore average Mg is more than four times elevated in comparison to Ca (Fig. 36).

3.5 Tectonic Setting

The following data was acquired during two stays at the Aihai talc mine. These data sets include open pit and underground data points from the mines 1, 4 and 6. For a better understanding of the tectonic setting, both data sets were joined together and evaluated as a single data group. This reduces the chance of false interpretations due to lack of representative data. A main reason for the analysis of tectonic fault data is the understanding of the deposit geometry which is essential for future mine planning and actual mine control. The past tectonic events are also essential for the deposit generation and the accumulation of talc in the high quality and purity which exists at the Aihai mining area. Therefore, tectonic data acquisition and interpretation is basis for an entire deposit overview. In large parts, the new data points approve

the collected underground mine data of 2009 and their interpretation. The general assumptions were underpinned by the new tectonic information from the open pit area.

3.5.1 General Setting

A large fault zone divides the mining area in two main parts (Fig. 37). The fault zone crosses the underground mine 6 and causes a complex tectonic setting with different dip directions in large parts of the deposit. In large scale, the dip direction changes from S in mine 1 to N in mine 4. This large fault zone changed the tectonic environment of the talc deposit but is not relevant for the talc genesis. It is younger than the faults which indicate the talc accumulating movement that was essential for the high quality and amount of mineable talc in large shear bands. Beside the large shear zone between mine 1 and mine 4, there are two main fault systems which occur at the whole concession area. The first, older fault system consists of N and S dipping normal faults. This fault system probably is part of the deposit generation and caused the mechanical accumulation of talc in high quality grades. The faults are often filled with talc and are connected to the large shear bands which form the deposit bodies. The second main fault system consists mainly of N-S striking strike-slip faults and is clearly related to the large shear zone between the eastern and the western part of the mining area. It indicates a relative movement between mine 1 and mine 4 and causes a complex tectonic environment in mine 6. The faults of the younger system mostly occur in the area of mine 6 and only have few influence on the tectonic setting at the mines 1 and 4, except the change of dip direction from N to S (Fig. 37). The younger faults are not filled with talc in a large scale; this proves the thesis that there is no connection between those faults and the deposit formation. Sometimes there is talc included into the faults together with dyke material; the result is a dark grey fault material with high talc content.

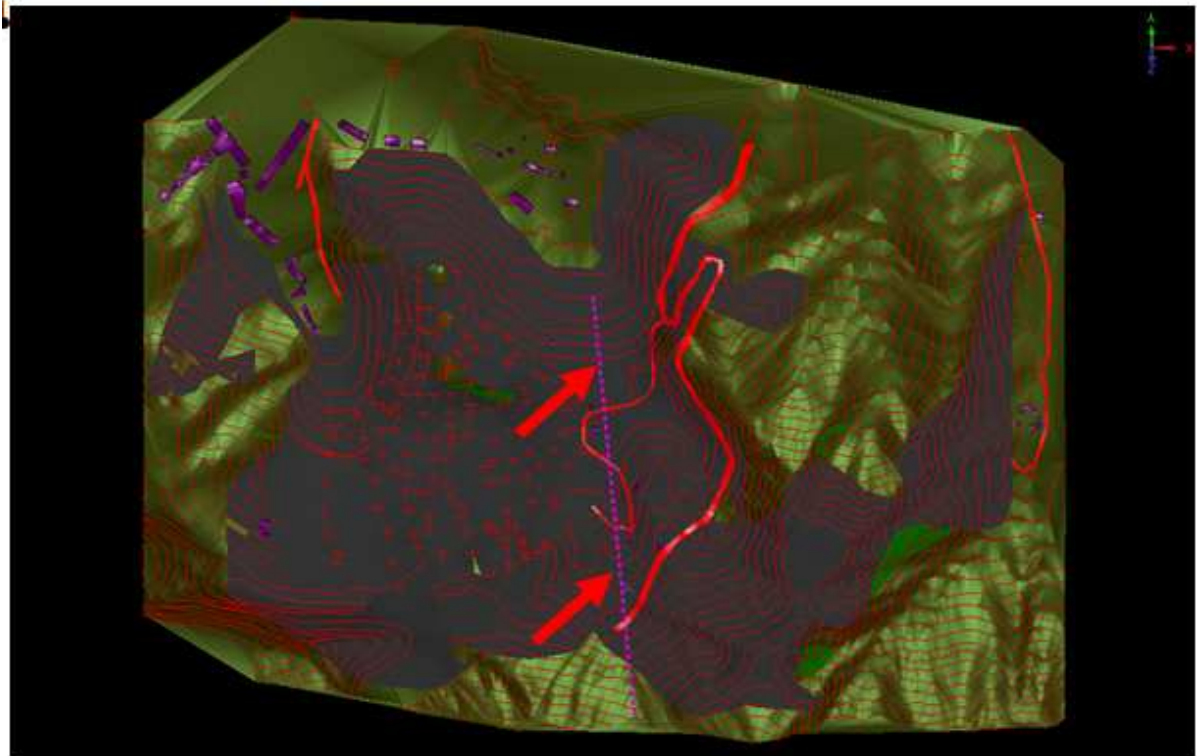


Figure 37: Suspected position of the large fault zone which causes the complex tectonic setting in the Aihai mining area.

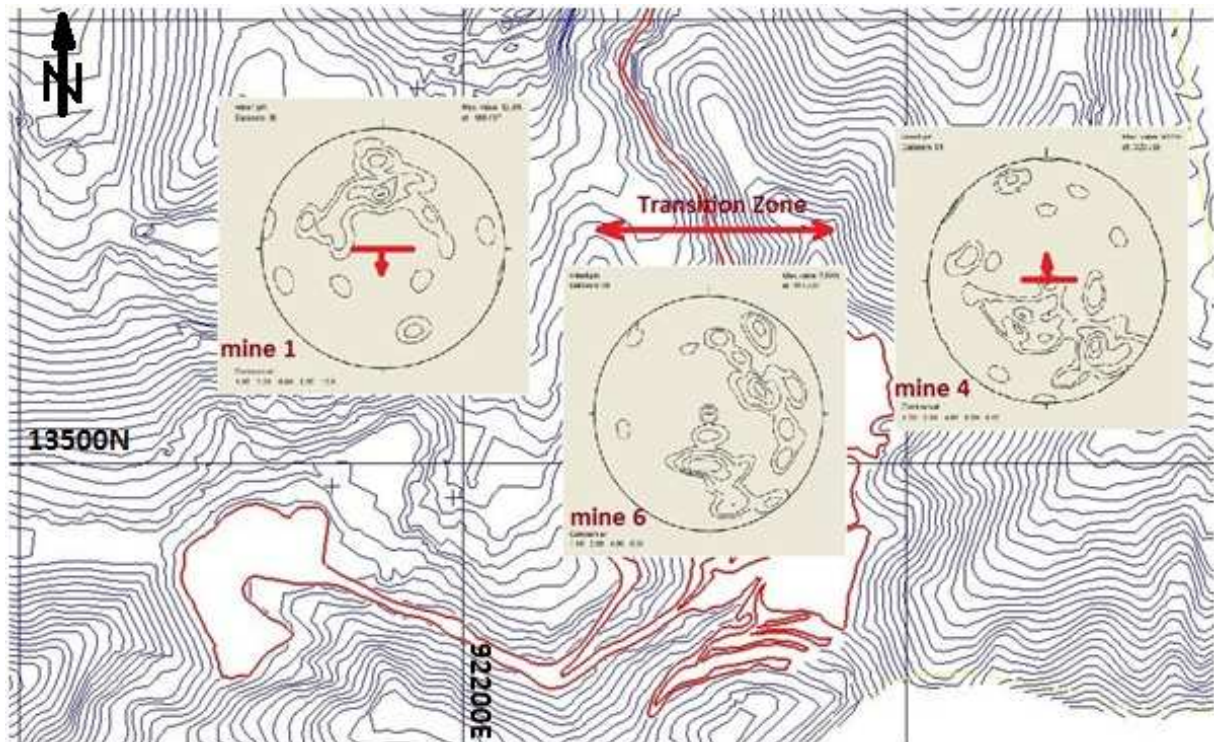


Figure 38: Change of dip direction from mine 1 over mine 6 to mine 4. The transition zone represents the change of dip direction of magnesite host rock, the position coincides with the estimated large fault zone in the area of mine 6.

3.5.2 Detailed Fault Systems

The following contour-plots represent the fault data of the three underground mines (Fig. 39-41). The data-set of every mine is plotted separately to show the tendency of dip change within the Aihai concession area.

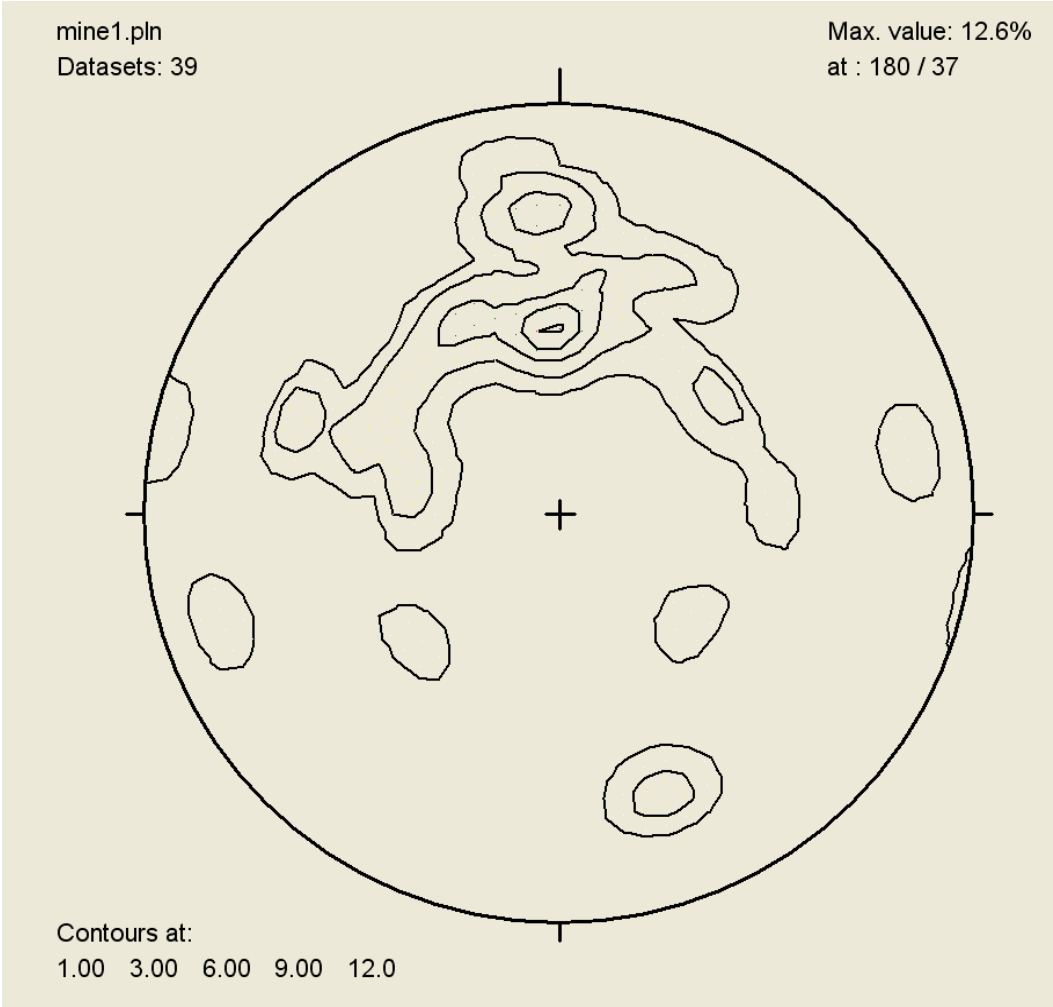


Figure 39: Pole point-plot of mine 1 fault-data.

The contour-plot of the fault data acquired from mine 1 shows a clear maximum at a dip direction of 160 to 200 degrees. This dip direction represents the old system of normal faults. This system is likely to coincide with the deposit formation, which is proved by the talc-filling of some faults. The younger N-S striking fault system is present only in minor quantity.

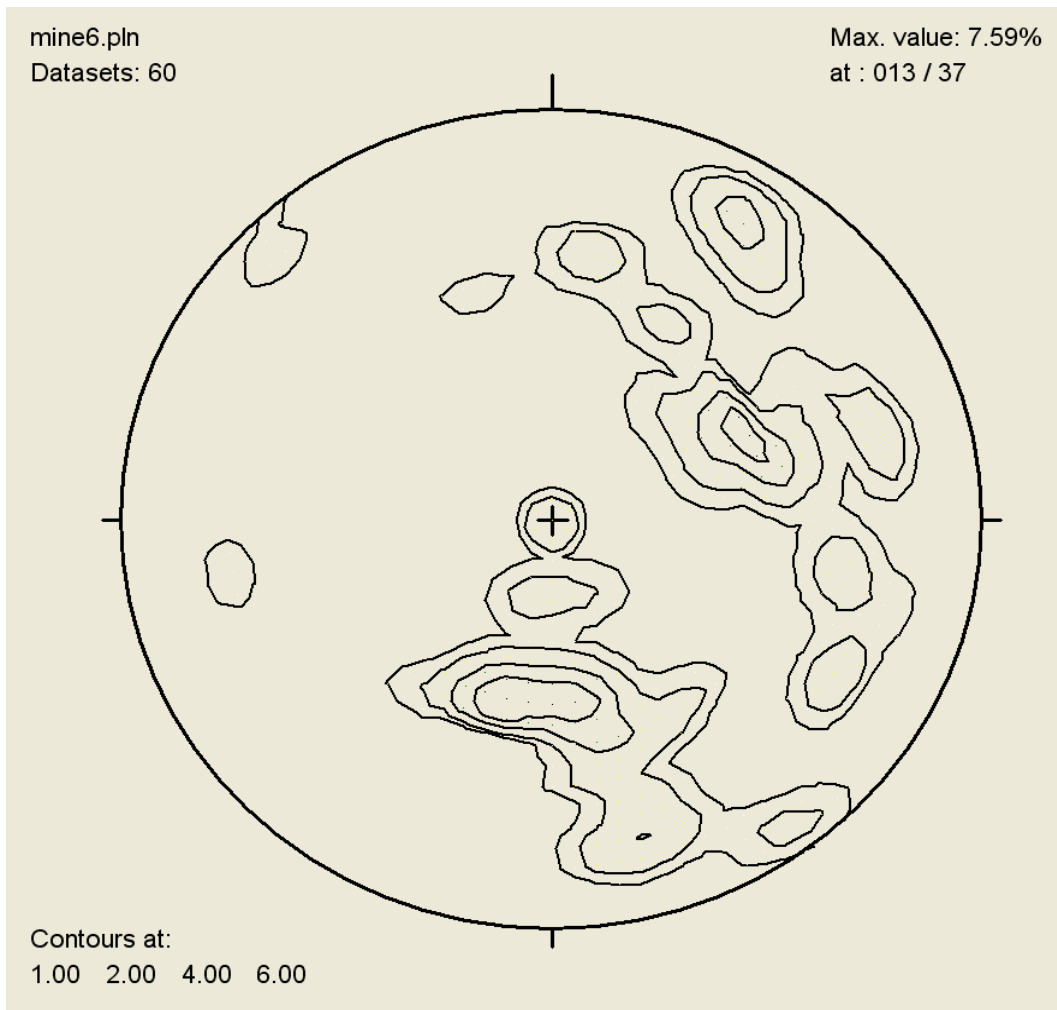


Figure 40: Pole point-plot of the fault-data from mine 6.

The fault-data of mine 6 mainly shows two distinct maxima which represent the older E-W striking normal fault system and the younger N-S striking strike-slip faults connected to a large shear zone which crosses the area of mine 6.

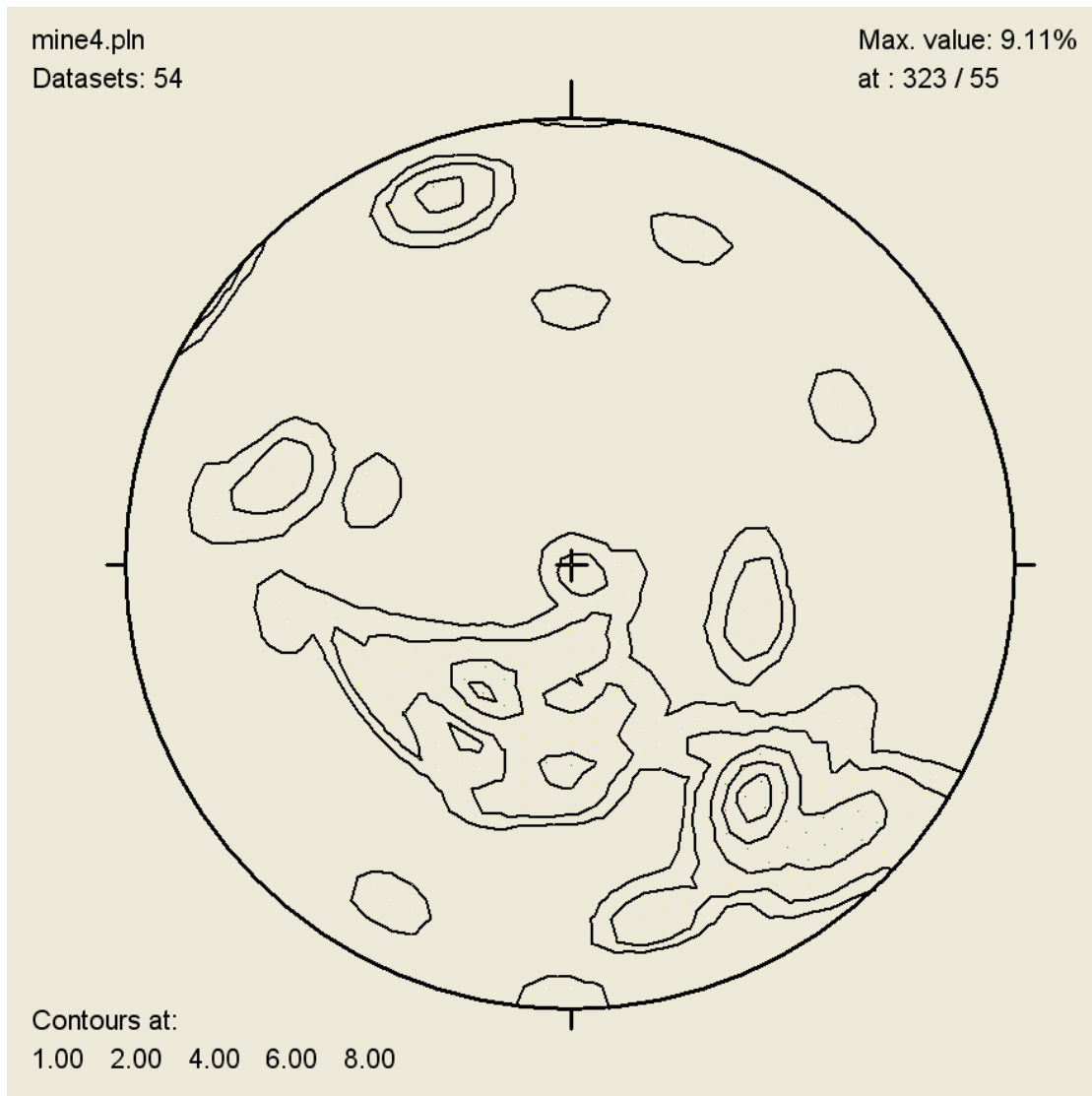


Figure 41: Pole point-plot of the fault-data from mine 4.

Comparable to mine 1, in mine 4 the older E-W striking system of normal faults is dominant. The main difference is the changed dip direction from mainly S in mine 1 to N in mine 4. The change is visible in mine 6 but not evident in mine 4. The dip direction is not as uniform as in mine 1, few N-S striking strike-slip faults represent the younger movement described above.

3.6 Geo-risks

Throughout the mining area, large zones with visible mass movement were recorded (Fig. 42). Especially in the surface area above mine 6 and mine 1, large tear-off edges were detected. The displacement at these edges ranges between 10 centimeters and several meters; this situation means a great risk for landslides especially in times with high precipitation rates and during freeze-thaw-changes. In

NE China, the monsoon climate is characterized by warm-humid conditions in summer with high precipitation of 1000-1100mm for the months Juli and August. Winters are cold and dry with strong ground frost and average temperatures of only -16°C (December-February).

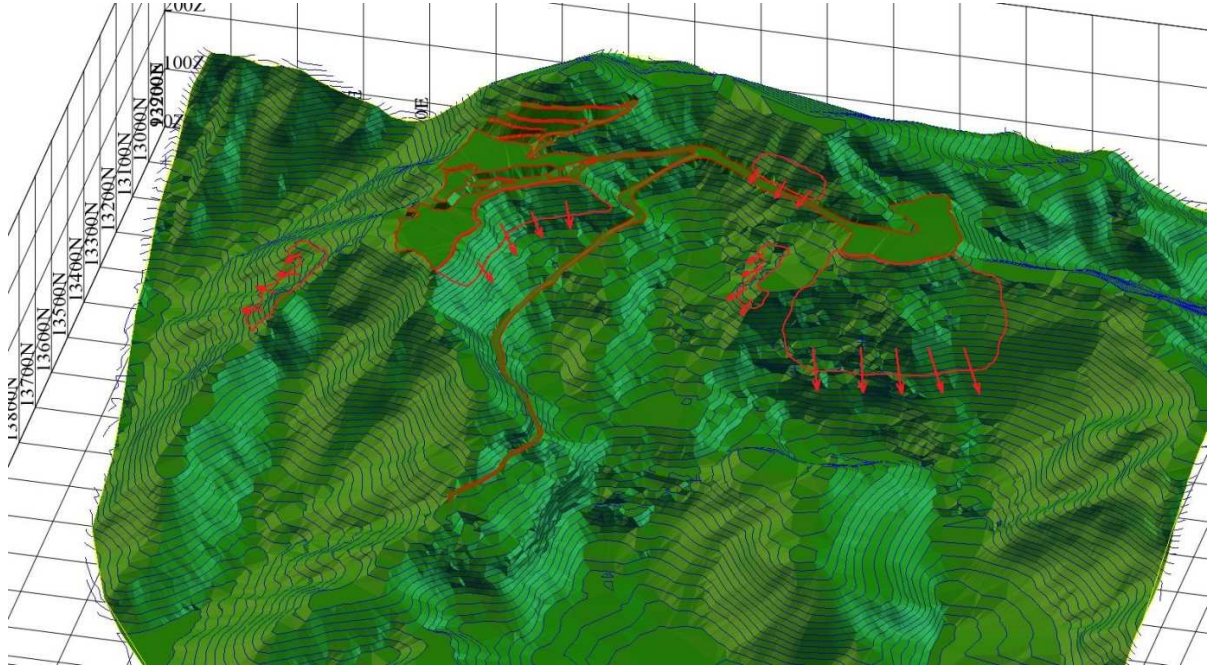


Figure 42: Estimated position of mining induced mass movements.

In the surface area above mine 6, massive sinkholes occur widespread (Fig. 43). The average diameter of the sinkholes is about 8 to 10 meters, with an average depth of 5 to 10 meters. The rapid increase of visible sinkholes on the surface is an indicator for mining-induced mass movements, which lead to a pressure-release in the rock. When the rock mass collapses into the empty space created by old underground tunnels, the movement continues to the surface and shows as sinkholes or tear-off edges. In zones where the rock is massively destabilized, further underground production is impossible. Figure 44 displays the modeled origin of sinkholes above mine 6. Again, mass movements are triggered by climatic factors like intense rain during summer monsoon and destabilization of former frozen soil during thaw period.

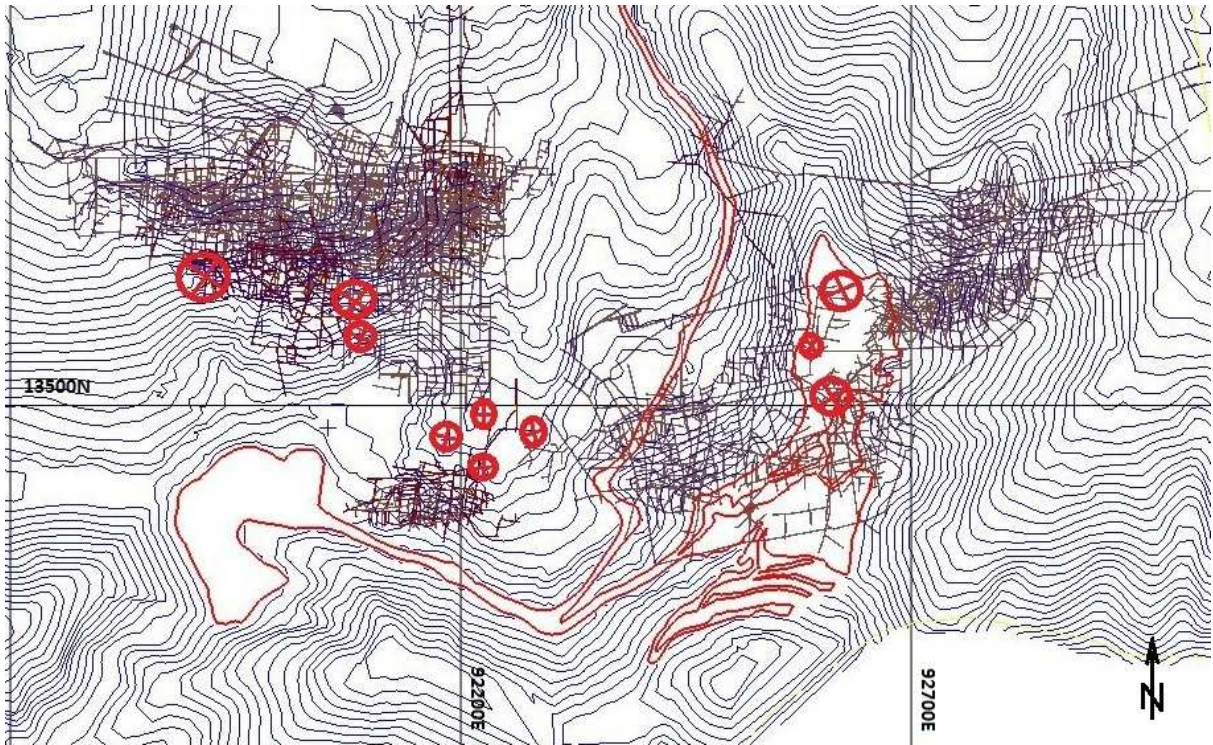


Figure 43: Position of sinkholes (red circles) related to underground mining activity.

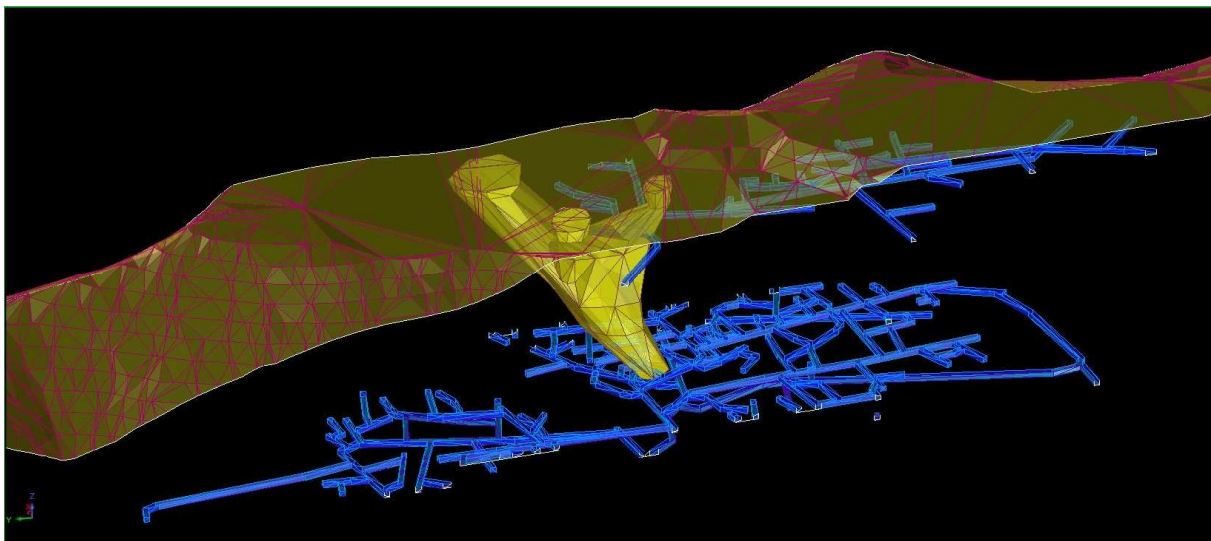


Figure 44: Estimated origin of sinkholes above mine 6.

Although no surface measurements have been made to quantify this impression, it seems that the situation got worse between the fieldwork summer 2009 and the work in 2010 (Fig. 45). This rapid increase of potential endangered zones should be taken seriously and considered in future mine planning, especially in terms of further surface mining activities. The unstable situation is also documented in many destroyed old buildings above the actual underground mines, massive stress cracks

can be found in almost every building (Fig. 46). The most alarming sign for the dangerous state of the slope stability in some areas was a deep-going landslide discovered in an old tunnel of mine 6. The slide goes several tens of meters underground and extends over a large area, an exact statement about the extension is difficult because of the limited accessibility of the old tunnel system were the slide was documented at first. The sliding surface shows a zone of several meters thickness with massively disturbed rock material (Fig. 47).



Figure 45: Sinkholes above mine 6.



Figure 46: Destroyed buildings indicate underground movement.

The white colored cataclastic material consists of magnesite and talc and acts as a lubricant for the mass movement. Another important factor is the fluid transport from the surface along of sliding planes like this, a great danger originates in times with great amounts of precipitation, because the meteoric water can easily intrude to deeper regions and cause further destabilization. On the surface especially in the area where the large weak zone is located underground, a lot of tear-off edges were documented also. It has to be mentioned that the landslide is older than the present mining activity, but there is a possible risk of reactivation of the deep going sliding wedge due to underground or open pit mining activities. Especially in the area above mine 6 were the most signs for slope instabilities occur on the surface, surveying of defined measurement points would be a very important improvement for the safety situation. Although the analysis of structural data from mine 1 and mine 6 suggests a large fault zone in the area between those two underground mines, the exact position of this zone is not clear defined because there are no visible outcrops of the fault material. Due to the lack of information in terms of the stability situation at this fault area and its exact position, new mining activity especially near the postulated weak-zone has to be monitored intensively concerning effects to the slope stability. Destabilization may also show in form of increasing surface movement or decreased rock stability at the nearest underground mines.



Figure 47: Deep mass movement documented in a closed tunnel in the area of mine 6.

4 Discussion

4.1 Genetic aspects

The talc at the Fanjiabauzi area was formed in a typical geologic environment, which is often involved in hydrothermal-metasomatic mineralization processes over the whole Chinese continent. The geological history of the Chinese craton is dominated by many phases of continental extension and collision. Recent research on the regional epochs of deposit formation shows that extensional environments by far have the highest importance for deposit formation on the North China Craton (NCC), whereas compressive tectonic regimes produced minor ore deposits. Statistics show that 1,294 of 1,573 investigated ore deposits (82.3%) are connected to regional or local extension, only 123 deposits (7.8%) occur in a compressive tectonic environment (Wan, 2010). This assumption differs from the traditional opinion published by most of the Chinese researchers that the majority of important mineralizations in China are connected to collision zones and the main ore-forming epochs are related to regional orogenic events. It is also contrary to the thesis that the scale of deposits is directly related to the intensity of collision in the orogenic period (Qiu, 2002).

The massive magnesite layers which host the Eastern Liaoning talc deposits show thicknesses of several hundred meters. They have a special status, as they are believed to be primary formed in a Precambrian lagoon or near shore marine environment (Schmidt, 1984; Fountain, 1992), whereas the most common magnesite forming process is of epigenetic metasomatic or replacement type (Dill, 2010). Still, the genetic question for the large magnesite occurrences in the Haicheng-Dashiqiao magnesite belt is not clearly answered. Nevertheless, some evidence was found that strengthens the theory of primary magnesite formation in a lagoon environment. Stromatolites were found in the nearest environment of the Fanjiabauzi mining area (Fig. 48-49) during the fieldwork for this paper. Those biogenic, sedimentary rocks are clearly related to high saline, shallow water regions (Fig. 50). Different authors also reported primary sedimentary structures in the massive magnesite deposits of the Liaodong Peninsula, such as cross-bedding, micro-bedding, fossile mudcracks and microcrystalline, sedimentary pyrite layers (Zhu, 1984; Luo, 1990; He, 2009). The most common thesis is that microcrystalline magnesite beds were formed

primary as marine carbonates. As described above, the depositional environment in Proterozoic oceans is interpreted different compared to modern seawater. High Mg-saturation, low O₂ content and high CO₂ partial pressure in the atmosphere makes precipitation directly from seawater possible, although this process is not documented from recent locations. Under these conditions, biogenic activity may also have formed microcrystalline magnesite instead of dolomite or calcite, like postulated for the sedimentary structures found near the Fanjiabauzi talc deposit. Again, this process is highly controversial and not documented for recent algae. Furthermore, biogenic activity and precipitation is only an indicator for the assumed sedimentary milieu, but clearly is not alone responsible for the formation of the giant magnesite deposits in the area.

Argillaceous rocks and carbonates of the area are interpreted as syngenetic. After multiple diagenetic, deformational and metamorphic events during the geological history of the North China Craton, most of the microcrystalline magnesite is recrystallized into sparry magnesite and fine to coarsely grained magnesite marble. Only traces of the primary structures are still present in different locations. When the talc actually was formed during this complex history is not clear yet. Nevertheless, its formation is likely to be closely related to hydrothermal activity linked to the ancient regional thermodynamic metamorphism with several peaks (Zhu, 1984).

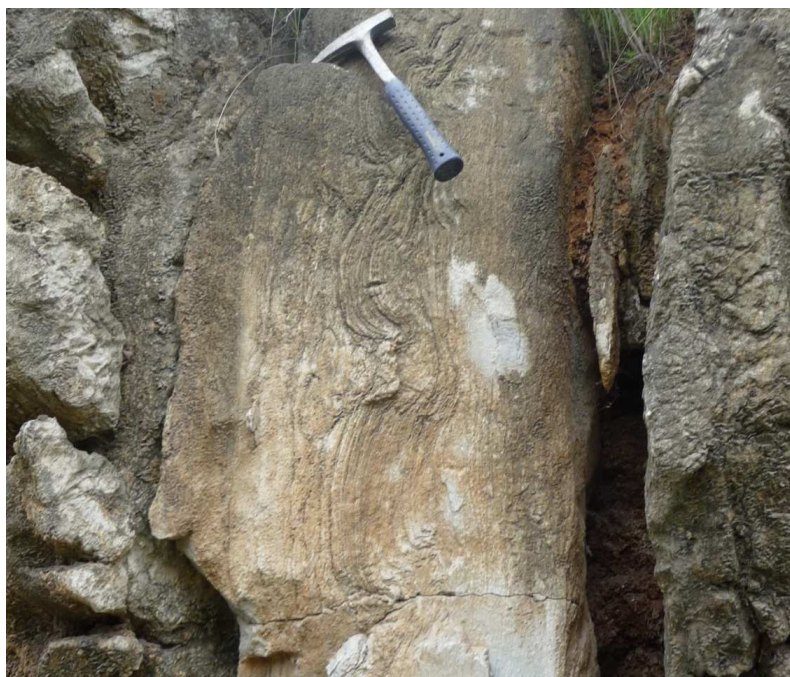


Figure 48: Stromatolites found along the southern borders of the Fanjiabauzi mining area.

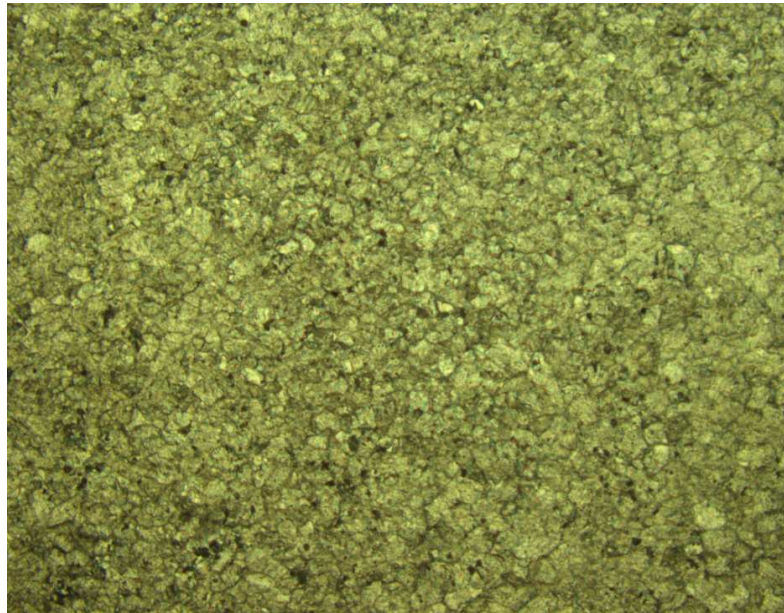


Figure 49: thin-section of fine-grained magnesite, height of picture equals 1,35mm.

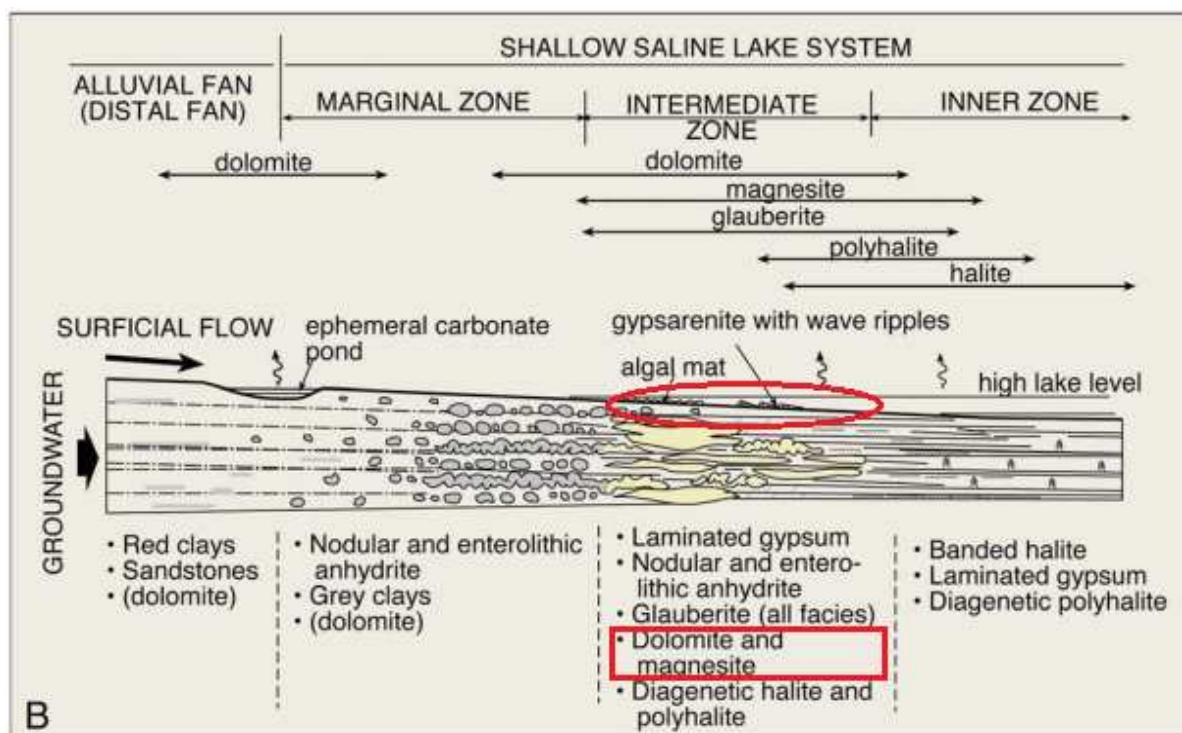


Figure 50: Estimated location of primary magnesite deposition in a high saline, shallow water environment (Warren, 2010).

The carbon isotope distribution for magnesite samples from the Fanjiabauzi ranges in the normal field for a marine evaporitic environment. The average $\delta^{13}\text{C}(\text{PDB})$ is 0.4‰ whereas the normal marine range is between 0.3‰ and 3.5‰. It has to be mentioned that Proterozoic playa and sabkha deposits normally have extraordinary heavy carbon isotope distributions between 7 and 13‰ in average. This is caused by the

global perturbation of the carbon cycle in the Proterozoic (2Ga) and by local phenomena like high bioactivity and evaporation (Melezhik et al, 2001). The lower values for the Fanjiabauzi deposit could be related to later hydrothermal processes involving non-marine solutions. An example for this is the location Sebkha el Mela (Tunisia) with an average $\delta^{13}\text{C}$ of -3‰ (Kralik et al, 1989). The magnesite samples show a tendency to lighter carbon in areas where talc mineralizations are present; this again proves the thesis that later hydrothermal influence changed the isotopic composition of the carbonate beds. The $\delta^{18}\text{O}(\text{PDB})$ value is strongly related to the grade of metamorphism. The samples from Fanjiabauzi can be compared to the values of the deposits Radenthein and Veitsch, which show upper greenschist to amphibolite facies (Fig. 51). An exact determination of the deposit forming processes related to the oxygen isotope distribution is again not possible; the influence of later processes is a factor that cannot be clearly discriminated. Samples from the cogenetic deposits of Dashiqiao (Ta-shi-chiao) and Fanjiabauzi show good correlation for $\delta^{13}\text{C}$, but significantly diverging $\delta^{18}\text{O}$ ratios. It is obvious that the average values for other large playa and sabkha deposits like Barton Farm or the Coorong Lagoon also show high variance. Nevertheless, it can be assumed that there is a general tendency to lighter oxygen with increasing age of the deposit.

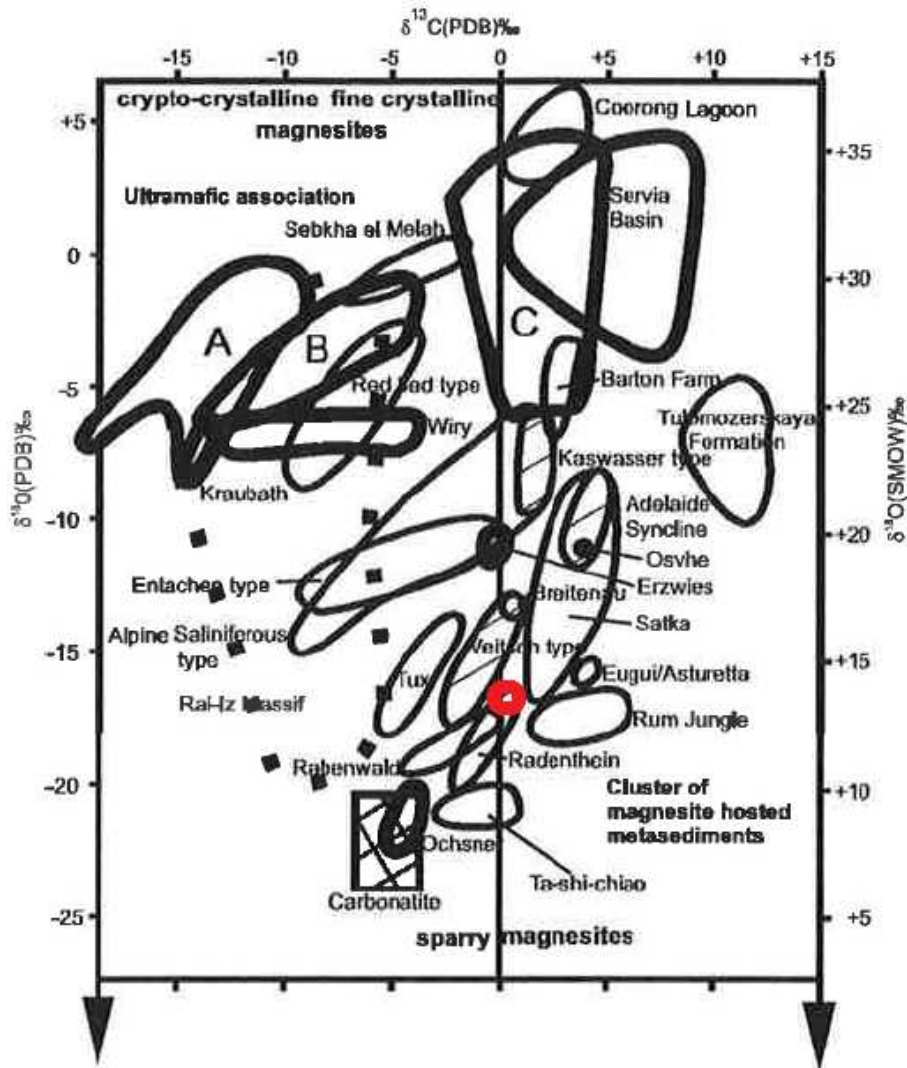


Figure 51: $\delta^{18}\text{O}$ - $\delta^{13}\text{C}$ -plot for selected magnesite deposits (after Kralik et al, 1989; Schroll, 1997; Schroll et al, 1999). The red mark represents the samples from the Fanjiabauzi deposit.

Statistically, most of the Chinese mineral deposits were formed during the Mesozoic, although mineralizations related to almost every historic period from the Archean to the Cenozoic are documented. In general, the Chinese mineral deposits are related to ten distinct metallogenic periods by several authors (Wan, 2010):

- Archean and Paleoproterozoic
- Meso- and Neoproterozoic
- Early Paleozoic
- Late Paleozoic
- Indosinian (Triassic)
- Yanshanian (200-135Ma)

- Sichuanian (135-56Ma)
- North Sinian (56-23Ma)
- Himalayan (23-0.78Ma)
- Neotectonic (0.78)

Unfortunately, there is a lack of publications discussing the genesis of the large Chinese talc deposits in the Liaoning, Guangxi and Shandong Province. In fact, the actual age of mineralization is not determined for most of the important talc occurrences. Therefore, the age of formation of the Fanjiabauzi talc deposit is uncertain. Several other hydrothermal ore deposits in Eastern Liaoning Province were formed in the Indosinian rifting period in the Triassic, but a correlation to deposit forming processes in the Triassic is difficult because of the different orogenic history of host rock and younger mineralizations. The Archean magnesite marbles and granitoids in the region show a complex tectonic setting. For example, there are several geochronologic ages determined for the early Proterozoic granites in the Anshan region, which indicate magmatic events at approximately 3,800Ma (Baijiafen), 3,300Ma (Chentaigou), 3,150Ma (Lishan), 3,000Ma (Anshan), 2,950Ma (Tiejiaohan) and 2,475Ma (Qidashan) (Song et al, 1996). The <3,800Ma granitoids are suggested to be formed by remelting of the 3,800Ma rocks at least partly. Another problem in age determination is the doubtful classification of metallogenic periods which is controversially discussed. Critics argue that the summary of different deformation events occurring at the same geological age into distinct periods like the Indosinian leads to false conclusions concerning the general processes which cause the regional deformation (Carter et al, 2008). The summary obscures the true diversity of geodynamic processes. For example, an active margin setting caused the Triassic events in the South-China block, while in other areas continental accretion regimes dominated (Vietnam) (Carter et al, 2008). Detailed geochronological data from deposits of North-East China rarely exist.

Another, often underestimated part of the research on origins of deposit forming brines is the composition of fluid inclusions from the host rock. The analysis of single inclusions is a difficult task, especially for rocks with a complicated metamorphic history. As inclusions always are affected by changes of geochemical equilibrium, fluid inclusion data has to be viewed critically, because inclusions can represent

different generations of metamorphogenic fluids. Especially isotopic compositions of O and C as well as volatile contents can vary rapidly due to thermobarometric changes. Nevertheless, basic trends can be derived from the chemical composition and element ratios present in the trapped fluids. Good indicators for different depositional facies are incompatible elements like halogens as well as the presence of alkaline and earth alkaline metals (McCaig et al, 2000). Fluid inclusions from the Fanjiabauzi magnesite marble were analyzed using the method of Crush and Leach. This method gives only the bulk composition of inclusions trapped in a given rock sample, which means that all inclusions present in the analyzed sample have the same influence on the results. It is clear that this method is not valuable for inhomogeneous rocks, because fluids from different generations are mixed together. On the other hand side, for relatively homogeneous samples and incompatible elements which are almost not incorporated in metamorphogenic fluid-mineral reactions, this method is fast and gives a good overview over compositional trends.

The fluid composition from the Fanjiabauzi magnesite marble is comparable to the composition of seawater. Lower average salinity is probably caused by freshwater influence, which does not affect the relative element ratios of the brine but reduces the overall concentration. Relatively low Cl/Br ratios and absolute Cl and Na make the influence of dissolved evaporites, especially halite, unlikely and point to low evaporation rates and strong dilution of brines. Generally, Precambrian seawater shows lower Cl concentrations and lower Cl/Br ratios than its recent equivalent, as reported from studies of Kaapvaal seawater (2.2Ga) (Foriel et al, 2004) (Fig. 52). In recent, non-fractionated seawater, the Cl/Br-ratio is about 650, whereas strongly depleted seawater due to precipitation of halite shows ratios between 100 and 90 (McCaffrey et al, 1987). Cl/Br-ratios of Fanjiabauzi brines are between 50 and 100 with only two outliers from samples that represent young shear zones. K is strongly dependent on the ratio between meteoric and marine water, because the average K content of the dissolved load of seawater is about hundred times higher than for freshwater. Fanjiabauzi inclusions are depleted in K, but far above freshwater concentration. A source for high K would be the influence of brines derived from granitic to granodioritic intrusions, which is not the case for the tested samples. The average Li of 0.4ppm fits almost perfectly for seawater (0.2ppm), whereas intrusion related brines have Li concentrations between 10ppm (Reykanes Field, Iceland) and

50ppm (El Tatio, Chile) (Evans, 2008). Continental evaporitic brines vary strongly due to differing freshwater dilution; measured concentrations at the Great Salt Lake in Utah are 30-60ppm Li (Evans, 2008). High Li concentrations are mostly caused by leaching from crustal rocks. Together with Li, other conservative lithophile elements like F and I are related to brines derived from crustal magmatic rocks. The low average I/Cl ratio ($8.3 \cdot 10^{-5}$) of the inclusions from Fanjiabauzi magnesite marble and the average F (28 ppm) are far below the expected values for intrusion related hydrothermal sources (McCaig et al, 2000). Altogether, the chemical composition of the relict fluids in magnesite samples from Fanjiabauzi fits for a lagoonal environment with noticeable freshwater influence in an early evaporitic stage with relatively low salinity. Freshwater influence is also indicated by the low Sr content of magnesite marbles from Fanjiabauzi and neighbouring deposits. The Ba/Sr-ratio for marine species like fossile corals and molluscs as well as modern and ancient oceanic water ranges below 1/1000 (Bowen, 1956), whereas the ratio for magnesite marbles from Qushugou (Aihai Magnesite) is approximately 2:1. Ba/Sr ratios of fluid inclusions were not analyzed. Finally, hydrothermal fluids related to granitic intrusions are unlikely to play a role concerning the fluid composition in the Archean Fanjiabauzi magnesite marbles.

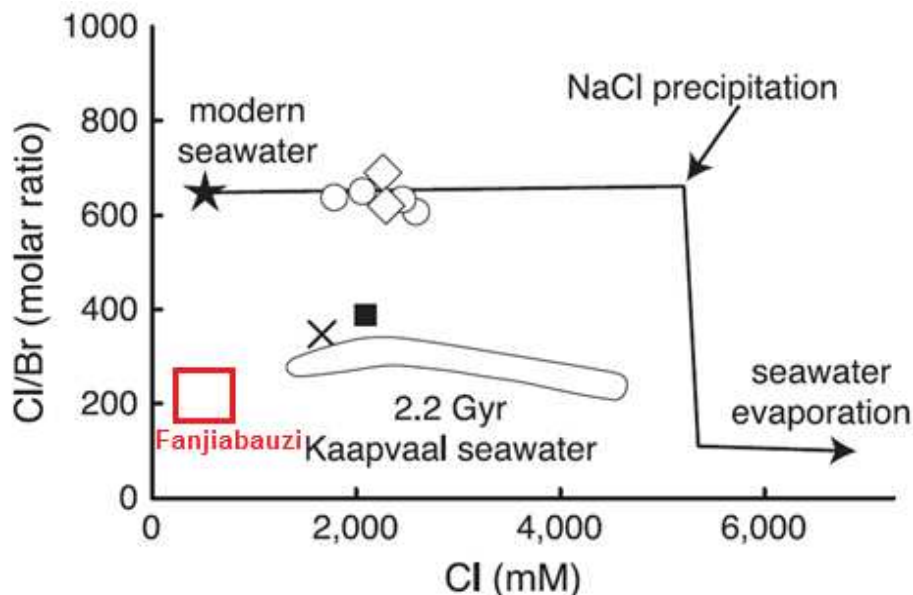


Figure 52: Cl/Br-Cl-plot for different types of seawater modified after Foriel et al, 2004.

4.2 Talc quality and exploration

The chemical analysis of the talc samples collected during the 2010 field work shows very low grades of contamination with trace minerals like mica, also the values for trace elements embedded in the talc structure are very low especially for the grade 1 talc product. This causes the remarkably high grades of whiteness and the low LOI values for the grade 1 samples. The LOI is about 3 to 5 percent higher for grade 2 talc samples; the reason for this increase of volatile components is a higher content of carbonate minerals like magnesite and dolomite, which lose their CO₂ during heating. Higher CaO and MgO values for the average grade 2 talc also prove this higher carbonate content. The contents of other trace elements like FeO and Al₂O₃ are also slightly higher in the average grade 2 talc, although the values in general are typically low, which can be expected for carbonate host talc deposits. These values are mostly controlled by mineral impurities, for example mica or other dyke components, which are mechanically integrated in the talc shear zones. The elements Co, Ni, Cr, Cu and W are throughout under the detection limit, this again proves the absence of ultramafic rocks during the primary talc formation. The only mafic components present at the Aihai talc mine are lamprophyre dykes which are younger than the talc formation and mostly do not influence the quality of the deposit. Only in some parts of the deposit, some dyke components are included into small talc bodies because of tectonic movement. This occurrence does not affect the quality of the mineable talc. Fieldwork clearly shows the relatively younger ages of the lamprophyre dykes that often cut through older talc shear bands. The mafic dyke swarms most likely are a result of crust extension in the late Mesozoic and therefore are related to a young intracontinental rift system at the eastern margin of the NCC (Liu et al, 2009). Few small faults show a dark green to grey filling, which consists of a mixture of talc, magnesite and dyke components like the iron-rich mica chlorite.

The low contents of trace elements, especially rare-earth elements, in the deposit rocks are inconsistent with the idea of igneous rocks as a source for the highly mineralized brines necessary for the talc formation (Schandl et al, 1999). More likely the necessary SiO₂ was derived from underlying sedimentary rocks or siliceous carbonate beds during regional metamorphism (Schandl et al, 1999).

Differences in the coloration of talc affect the grade of whiteness, which is an important quality parameter. Altogether, most talc samples from the Fanjiabauzi mining area show good values for whiteness and yellowness. The reasons for this are the minor impurities in large shear bands. Incorporated carbonate minerals from the surrounding area may influence the chemical composition of grinded talc samples, but have almost no negative effect on the color properties. Dark impurities like mica or pyrite are rare in the high quality talc zones, fine grained pyrite additionally is not as critical as coarse pyrite, because often the pyrite is too small for further grinding. Undestroyed pyrite crystals have almost no negative effect whereas grinded pyrite as a powder is very critical. Pink and white talc show the highest whiteness and combine also very low yellowness indices. Weathering increases the yellowness index while the whiteness still reaches good values up to 95. Yellowness is also the key factor for yellow talc, whiteness is very high for this particular talc samples and averages at 95. The quality of grey talc strongly depends on the grade of impurities; these are often chlorite relicts from dyke material incorporated into shear zones. Measured values spread from above 92 to below 87, depending on the intensity of the grey coloration. Mixtures of yellow, pink and white talc taken from the processing plant for sale show acceptably high whiteness and low yellowness.

The surrounding rocks of the talc deposit consist mostly of magnesite, dolomite and garnet-rich greenschists whereas relatively pure and massive magnesite is the actual host rock of the talc mineralization. Lamprophyre dykes crosscut the massive carbonate layers. The magnesite shows some diagnostic characteristics, which allow to draw conclusions if major amounts of talc are present in the nearest environment. In general, the magnesite in the direct neighborhood of remarkable talc bodies shows a higher purity. There is less contamination with other mineral components like mica, although this pollution is also very minor for magnesite without talc in the nearest environment. This difference is proved by slightly lower Al and Sr values for the talc-host magnesite samples. The values for trace elements included into the magnesite crystal lattice also show a decrease when a talc shear zone with a size relevant for production is close to the sampling spot. The values for Mn, Fe and Ca show the same trend, the reason for the higher Ca contents in non-talc magnesite most likely is caused by small amounts of dolomite admixed with the magnesite rock. Therefore, increasing dolomite contents could indicate the departure from the nearest deposit

environment. In summary, the higher purity of talc-hosting magnesite in comparison to magnesite without talc in the direct neighborhood is evident. The differences in the chemical composition could be helpful for the detection of mineable talc in the actual mining levels, although this can only be an additional support for traditional exploration and requires a constant sampling and testing procedure.

Another potential indicator for talc shear zones is the texture and coloration of the host rock. The magnesite at the borders of large talc bodies has a bright white coloration and a fine-grained, compact fabric. The magnesite occurring further away from the deposit borders has often a slightly grey to yellow coloration and a coarser grained fabric. This is also documented by the measured average whiteness and yellowness indices of magnesite samples from the deposit. The whiteness ranges from 92.6 for fine-grained magnesite near large talc filled shear zones to 89.4 for coarse magnesite without talc in the nearest environment. The yellowness indices also confirm the impression from the fieldwork that the coloration of coarse magnesite gets more yellowish than that of fine grained, compact magnesite. The average yellowness index of coarse magnesite is about three times higher than for fine-grained magnesite near mined shear bands and ranges at 4.5 compared to 1.65. Dolomite occurs often away from the deposit borders whereas at the borders pure magnesite dominates. This correlates with the higher Ca and Fe content of the host rock samples, higher Ca values away from the deposit are caused by dolomite, higher Fe is likely to be caused by pyrite impurities which are more common in dolomite than in the pure magnesite which hosts the talc mineralization. Pure magnesite from the Fanjiabauzi area has to be considered as a valuable deposit part, as the average values for Fe and Ca range far below 1% for unpolluted samples and therefore easily match the product requirements for refractory purposes. Problems for further processing of the Fanjiabauzi magnesite to fireproof products may occur because of high SiO₂ contents. Values above 1.0 to 1.2% affect the mineral chemistry of sinter materials, because high SiO₂ in combination with high CaO causes the formation of monticellite, a mineral of the olivine group with the chemical composition of CaMgSiO₄ with changing contents of Fe substituting Mg. Monticellite has a remarkable low melting point of 1,498°C. In comparison, if the CaO content of the magnesite ore is low, instead of monticellite, forsterite Mg₂SiO₄ is formed during the burning process. Forsterite is the Mg-endmember of the olivine solid solution

series and has a melting point of approximately 1,900°C which is ideal for the production of refractory materials. High SiO₂ particularly occurs in zones were mineralized fluids formed talc and quartz veins and influenced the magnesite chemistry. In zones were no talc was formed, the SiO₂ most likely is also low for magnesite. The Ca and Fe contents of magnesite from Aihai Magnesite and Aihai Talc are comparable (Table 20). Therefore, it can be assumed that the pure magnesite surrounding the Fanjiabauzi talc deposit also can be considered as magnesite ore.

Sampling Area	Sample No.	results [%]	Fe	Mn	Ni	Ca	Sr	Al
Aihai Magnesite	13_2		0,049	0,003	<0,00001	0,601	0,000	0,079
Aihai Magnesite	19_2		0,261	0,018	<0,00001	0,438	<0,000001	0,038
Aihai Magnesite	13_1		0,175	0,008	<0,00001	0,799	0,001	0,379
Aihai Magnesite	15_1		0,123	0,006	<0,00001	0,459	<0,000001	0,043
Aihai Magnesite	15_2		0,145	0,009	<0,00001	0,564	<0,000001	0,034
Aihai Magnesite	16_2		0,090	0,005	<0,00001	0,801	<0,000001	0,056
Aihai Magnesite	8_9		0,706	0,032	<0,00001	0,490	0,000	0,071
Aihai Magnesite	8_4		0,096	0,004	<0,00001	0,394	0,000	0,059
Aihai Magnesite	8_8		0,081	0,004	<0,00001	1,262	0,000	0,094
Aihai Talc	11_3		0,342	0,020	<0,00001	0,555	<0,000001	0,058
Aihai Talc	14_3		0,193	0,010	<0,00001	0,694	0,000	0,060
Aihai Talc	7_1		0,102	0,006	<0,00001	0,858	<0,000001	0,036
Aihai Talc	11_2		0,196	0,010	<0,00001	0,909	<0,000001	0,064
Aihai Talc	16_1		0,165	0,009	<0,00001	0,890	0,000	0,099
Aihai Talc	10_1		0,263	0,013	<0,00001	0,922	<0,000001	0,092

Table 20: Comparison of main element contents for selected magnesite samples from Aihai Talc and Aihai Magnesite.

The SiO₂ contents of selected samples from Aihai Magnesite (Qushugou deposit) are below the important mark of 0.8% for refractory magnesite (Table 21). Nevertheless it has to be mentioned that elevated SiO₂ contents also occur at the Qushugou magnesite deposit and need to be monitored for this purpose.

Analyte	SiO ₂	Al ₂ O ₃	Fe ₂ O ₃ (T)	MnO	MgO	CaO	Na ₂ O	K ₂ O	TiO ₂	P ₂ O ₅	LOI	Total
Unit	%	%	%	%	%	%	%	%	%	%	%	%
Anal Meth	FUS-ICP	FUS-ICP	FUS-ICP	FUS-ICP	FUS-ICP	FUS-ICP	FUS-ICP	FUS-ICP	FUS-ICP	FUS-ICP	FUS-ICP	FUS-ICP
8-1	0,63	0,09	1,09	0,058	46,73	0,58	0,02	0,01	0,008	< 0,01	51,36	100,6
8-4	0,27	0,03	0,17	0,008	48,56	0,33	< 0,01	< 0,01	0,002	0,03	51,59	101
8-8	0,74	0,12	0,17	0,008	47,35	1,11	< 0,01	< 0,01	0,004	0,35	50,57	100,4
8-9	0,47	0,02	0,84	0,049	47,74	0,4	< 0,01	< 0,01	< 0,001	0,07	51,32	100,9
11-2	0,55	0,07	0,24	0,012	47,16	1,14	< 0,01	< 0,01	0,002	0,43	50,78	100,4
13-2	0,47	0,15	0,12	0,006	47,51	0,76	< 0,01	< 0,01	0,004	< 0,01	51,07	100,1
15-1	0,22	0,07	0,33	0,013	47,43	0,45	0,01	0,02	0,002	0,01	51,34	99,91
15-2	0,24	0,04	0,33	0,021	47,78	0,6	< 0,01	< 0,01	0,004	0,07	51,25	100,3
16-1	0,48	0,12	0,22	0,01	47,96	0,59	< 0,01	0,03	0,004	0,02	51,26	100,7
19-2	0,06	0,03	0,57	0,036	47,12	0,33	< 0,01	< 0,01	0,002	< 0,01	51,31	99,48

Table 21: Main element contents of selected magnesite samples from the Qushugou magnesite deposit (Aihai Magnesite).

4.3 Recommendations

4.3.1 Mining and Geo-risks

In contrast to the extraordinary good quality and purity of the high grade talc at the Aihai concession area, the structural situation due to the mining activity is more complicated. The past method of mining unfortunately caused the loss of valuable talc resources due to a comparatively low average recovery rate. This low recovery rate is caused by a lack of future-oriented mine planning as well as the use of inappropriate blasting techniques which destabilize the host rock due to extensive use of explosives. The major reason for the massive geogenic dangers is caused in the unfavorable underground mining method, which causes the development of sinkholes and strongly destabilizes the slope equilibrium (Fig. 53). The situation on the one hand means serious danger for the workers in the underground mines, but also causes economic damage because of very low recovery rates. The amount of talc, which cannot be recovered and therefore finally is lost for the purpose of sale is much bigger than in mines where modern mining technologies are applied. Although the quality of the mined ore is remarkably high in comparison to other talc selling companies, the profit margin is comparatively low.

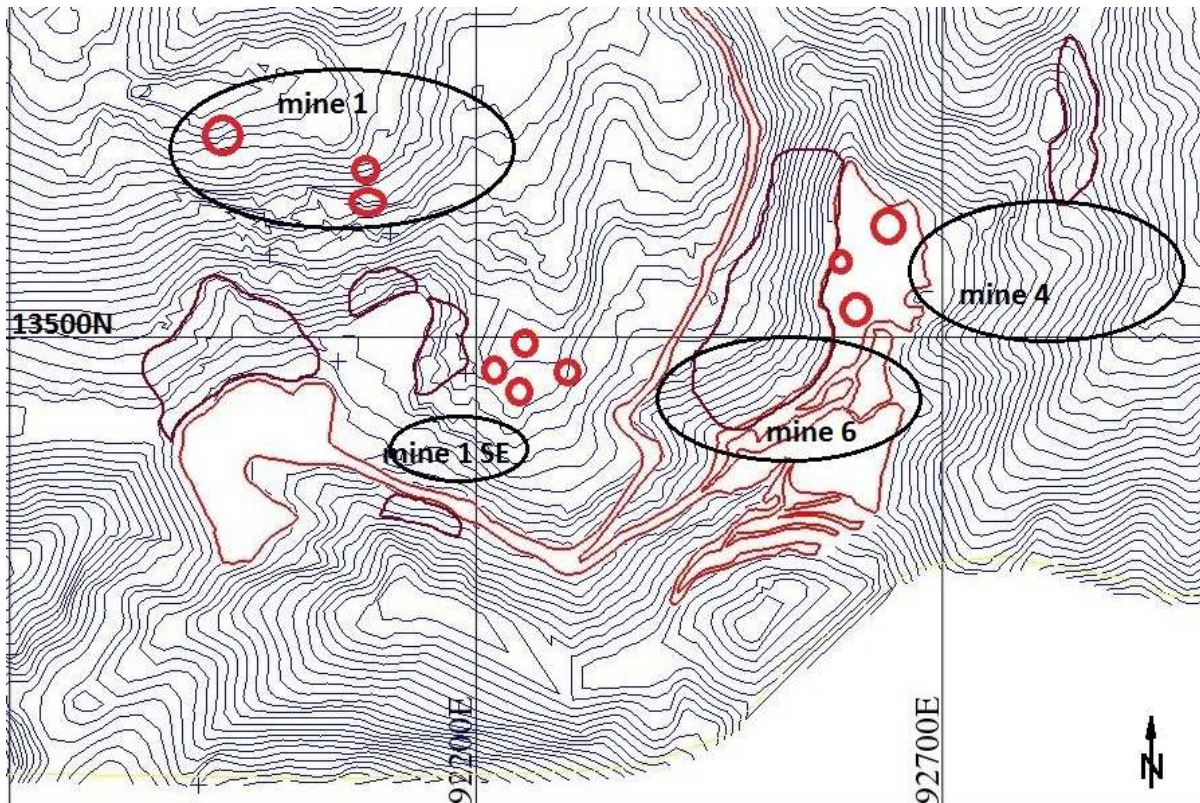


Figure 53: Position of zones with reduced slope stability and sinkholes related to underground mining activity.

The best way to improve the productivity of the Aihai talc mines is the establishment of a new mining concept, using a new underground mining method which includes backfilling of empty tunnels, use of modern blasting techniques and mechanization of the ore extraction. The detailed planning for such a concept should be done by a mining engineer to find out which changes in the production activities make sense for economic reasons. The new open pit in the area above mine 4 opens up the possibility to start up with a new, modern mining method and a plan for the future development of the production. This could reduce the loss of ore as well as the production costs because of more efficient blasting and recovery of talc. After the establishment of the new open pit mine, the complete change from underground to open pit mining should also be taken into consideration, although the evaluation of this possibility has to be done by mining experts. Possible advantages of open pit mining are a high grade of process automation, easier quality control and the increase of productivity. An absolute requirement for a useful concept is the acquisition of more data concerning the size, position and quality distribution of the remaining deposit parts and the ratio between overburden and ore in the area of the new open pit mine. To ensure a long-lasting cost-efficient production, the possible

positions for waste dumps etc. has to be planned in advance and correlated with the evaluation of the slope stability in the selected areas. These criteria are crucial for the realizable production limit and the feasibility of the complete change from underground to open pit mining. Also a critical evaluation of the past and present mining situation including an estimation of the past average recovery rate is essential for the decision between a complete change and the retention of the present method of production.

For the documentation of surface movements and potential mining-induced risks like sinkholes, a map of survey-points is necessary. Such points should be remeasured at least every two months to document possible rapid developments of slope instabilities. It seems that the slope destabilization in the whole concession area got worse between the 2009 and 2010 field work, although without a quantification by exact measurements, there is no possibility for a clear statement or a prognosis of further development in problematic zones. Especially if there is a plan for further open pit mining in the area of mine 6, there is a great potential for problems because of destabilization caused by past underground mining in the mines 6 and 1.

In general, an actual surface map is missing. An adequate surface map is a basic requirement for the planning of extended waste dumps, open pit operation etc. The 2011 drilling program is a great opportunity to gain more information about the quality distribution and remaining talc reserves, the new drill hole information should be implemented into the 2009 drill hole database. The 3D-deposit model should be integrated in the planning process to reduce the loss of ore and to set the stage for a more efficient production. Details like waste dumps, roads etc. have to be planned in advance, otherwise problems like ore pollution during periods with high precipitation or the blockage of open pit expansion are likely to occur in the future.

4.3.2 Sorting

To minimize quality fluctuations of the end-product, a new sorting method should be taken into account. Especially if there is a rapid increase of production due to new open pit operation, the improvement of the whole process-chain is essential to ensure a constant product quality. Modern methods like optical sorting could help to

increase the process automation and at the same time enhance the theoretical output limit of production. It has to be taken into account that the implementation of an optical sorting could be difficult in detail. The finely grained, bright white magnesite hosting talc in massive bodies shows only minor contrast to the talc ore, especially if there is a layer of pulverized talc covering the pebbles. Another technical challenge for the sorting process is the extraction of talc-magnesite-intergrowths from magnesite waste. The borders of talc accretions in finely grained magnesite are irregular in a microscopic scale (Fig. 54), therefore talc and magnesite cannot easily be separated mechanically. On the other hand, the borders are relatively sharp macroscopically and most of the talc bodies are more or less regular and not branched. Therefore, the optical characteristics strongly depend on the perspective and on the fracture plane actually scanned by the optical sensor. Optical parameters are not isotropic for the mixed ore.

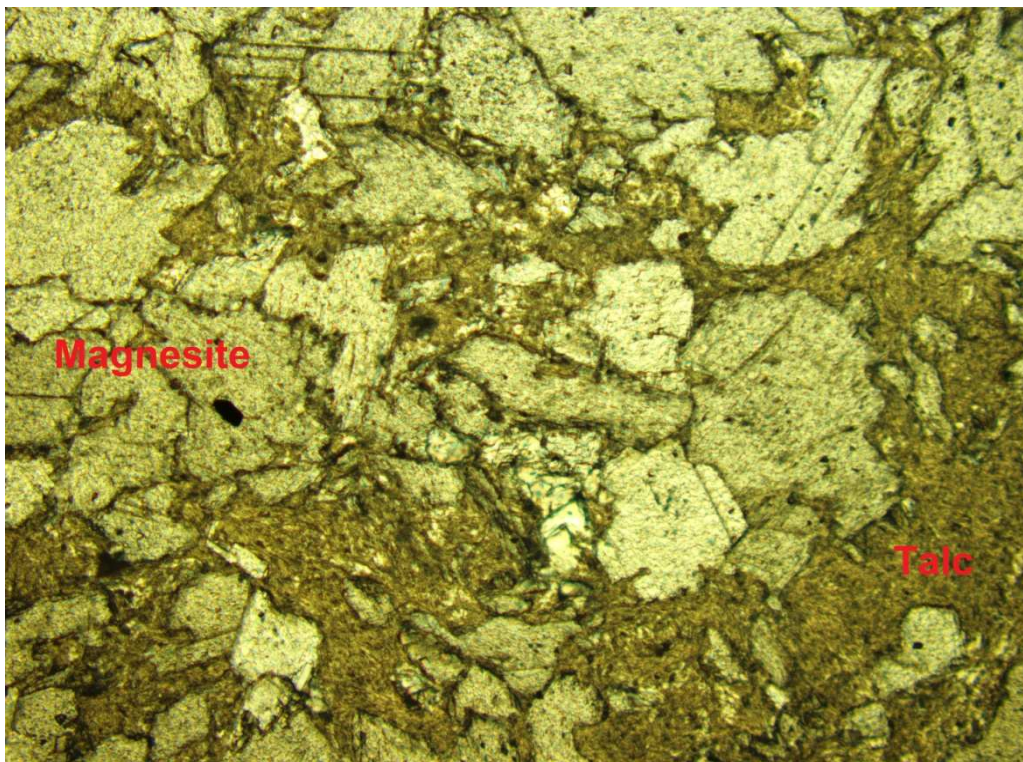


Figure 54: Border zone off talc-magnesite-intergrowth. Height of picture equals 1,35mm.

The discrimination of pure talc, pure magnesite and talc-magnesite-intergrowths with conventional optical methods would therefore require additional conditioning processes like washing of the raw ore. Sorting based on spectrometric sensors or on MW-IR (mid-wave infrared range)-sensors could be a practicable alternative to conventional optical sorting if the mixed ore can be characterized and discriminated

from the burden material. The sorting should be performed in two steps, the first step being the extraction of pure talc, second the separation of mixed ore from the magnesite waste. In general, three basic requirements have to be fulfilled for an ideal optical sorting process (Dehler, 2003):

- The material differs in brightness or coloration (only minor differences are necessary). Conditioning may be necessary (Washing, etc.)
- The material is laid in narrow bands, the air pressure and sorting parameters can be optimized for the different fractions.
- The material can be separated in distinct groups (for example: pure talc and pure magnesite).

If these three requirements are fulfilled, optical sorting works for a wide range of particle sizes (3mm-250mm).

References

Aihai Fanjiabaozi Area- Geological-Topographic Map 1:2000; Aihai Fanjiabaozi Geological Exploration Maps 1:1000; No. 5 Geological Team of Liaoning; Team Leader: Wang Bao Min, Co-Workers: Feng Xiao Yu, Wang Dian Zhong, Ji Hong Jing, He Wei; 2005, 2006.

Aihai Fanjiabaozi Area- Present Situation Map 1:1000; Aihai Mining Department; Team Leader: Xu Guang Tao, Co-Workers: Zhang Mao Ming, Lin Jia Bin; 2009.

Azim Zadeh, A. M., 2009. The genetic model of the Hohentauern/Sunk sparry magnesite deposit (Eastern Alps/ Austria). Dissertation, Institute for Applied Geosciences, University of Leoben, 182.

Baiquan, X., 2011. Microfacies, Carbon and Oxygen Isotopes of the Late Archean Stromatolitic Carbonate Platform of the Kaapvaal Craton, South Africa: Implications for Changes in Paleo-environment. Dissertation der Fachuniversität für Geowissenschaften der LMU München. München, Juni 2011.

Bowen, H., J., M., 1956. Strontium and Barium in seawater and marine organisms. J. mar. biol. Ass. U.K. (1956) 35, 451-460.

Burton, J.H., Price, T.D., 1990. The ratio of barium to strontium as a paleodietary indicator of consumption of marine resources. Journal of Archeological Sciences, Vol. 17, Nr. 5, 547-557.

Carter, A., Clift, P. D., 2008. Was the Indosinian orogeny a Triassic mountain building or a thermotectonic reactivation event? C. R. Geoscience 340 (2008), 83-93.

Chen, C., Cai, K., 2000. Minerogenic System of Magnesian Nonmetallic Deposits in Early Proterozoic Mg-rich Carbonate Formations in Eastern Liaoning Province. Acta Petrologica Sinica 74, 623-631.

Chen C., Lu A., Cai K. & Zhai Y., 2002. Sedimentary characteristics of Mg-rich carbonate formations and minerogenic fluids of magnesite and talc occurrences in early Proterozoic in eastern Liaoning Province, China. *Science China*. 2002, 45; 84-92.

Chen, C., Jiang, S., Cai, K., 2003. Ore-forming Fluids of Talc Deposits in the Early Proterozoic Dashiqiao Formation, Eastern Liaoning Province, China. IGCP 443 (Magnesite and Talc), International Conference of Mineralization in Precambrian Terranes (Nanjing, September 20-28, 2003), Abstract Volume, 44-46.

Chen, C., Jiang, S., Cai, K., Ma, B., 2003. Geology and Geochemistry of Magnesite and Talc Deposits in the Early Proterozoic Mg-rich Carbonate Formations, Eastern Liaoning Province, China. IGCP 443 (Magnesite and Talc), International Conference of Mineralization in Precambrian Terranes (Nanjing, September 20-28, 2003), Abstract Volume, 47-54.

Ciullo P. A., 1996. *Industrial Minerals and Their Uses: a Handbook and Formulary*; 68-72. Published by Noyes Publication, Westwood, New Jersey.

Dehler M., 2003. *Optoelektronische Sortierung von Mineralischen Rohstoffen; Aufbereitungstechnik*, Heft 10, 2003.

Digitized Quality Lines and Underground Ways 1:1000; Aihai Mining Department; Team Leader: Xu Guang Tao, Co-Workers: Wang Yang, Zhang Bao Ming; 2009.

Dill, H.G., 2010. The “chessboard” classification scheme of mineral deposits: Mineralogy and geology from aluminum to zirconium. *Earth-Science Reviews*, 100(2010), 1-420.

Drill Hole Database and corresponding Chemical Analyses; No. 4 Exploration team of Liaoning Geological Survey Bureau; Team Leader: Han Yue Min; Engineers: Lin Ting Ru, Zhang Xin Kui, Co-Workers: Deng Ding He, Gu Shon Qin, Qu Hong Ku, Huang Yao Guang, Zhang Xiang Hu, Liu Guo Zhong, Li Gui Lan, Feng Zheng Shui, Shao Ze Yi, Hon Rui Qiang, Peng Ri Leng; 1966.

European Commission Press Release, Ref. No. IP/12/239, March 13, 2012.

Evans, R.K., 2008. An abundance of Lithium. Unpublished report for the Lithium Corporation of America, 2008.

Foriel, J., Phillipot, P., Rey, P., Somogyi, A., Banks, D., Menez, B., 2004. Biological control of Cl/Br and low sulfate concentration in a 3.5-Gyr-old seawater from North Pole, Western Australia. *Earth and Planetary Science Letters* 228 (2004), 451-463.

Fountain, K., 1992. Liaoning magnesite. *Proceedings 10th Industrial Minerals International Congress*, San Francisco, 65-70.

Gallhofer, D., 2010. Lithologische und geochemische Charakterisierung der Magnesitlagerstätte Breitenau (Grazer Paläozoikum/Ostalpen). Master-thesis, Institute for Applied Geosciences, University of Leoben, 22-24.

Gächter, H., Müller, H., 1989. *Kunststoff-Additive*, 3. Ausgabe, Hanser Verlag, München.

Gondim, A. C., Jiang, S., Y., 2004. Geologic characteristics and genetic models for the talc deposits in Parana and Bahia, Brazil. *Acta Petrologica Sinica*, Vol. 20 (2004), 828-836.

He, Z., Wang, S., Wang, D., He, W., Jiang, F., 2009. Prospecting target around Fanjiabauzi talc deposit in Haicheng City. *Jilin Geology* 2009-03.

Hecht, L., Freiburger, R., Gilg, H.A., Grundmann, G., Kostitsyn, Y.A., 1999. Rare earth element and isotope (C, O, Sr) characteristics of hydrothermal carbonates: genetic implications for dolomite-hosted talc mineralization at Göpfersgrün (Fichtelgebirge, Germany). *Chemical Geology* 155, 115-130.

Jiang, Y., Jiang S., Zhao K., Ni P., Ling H. & Liu D ., 2005. SHRIMP U-Pb zircon dating for lamprophyre from Liaodong Peninsula: Constraints on the initial time of

Mesozoic lithosphere thinning beneath eastern China. *Chinese Science Bulletin* 55, 22, 2612-2620.

Kittel, H., 1998. *Lehrbuch der Lacke und Beschichtungen*, Band 2, 2. Auflage, Hirzel Verlag.

Kralik, M., Ahron, P., Schroll, E., Zachmann, V., 1989. Carbon and oxygen isotope systematics of magnesites in magnesite formation. *Monograph Ser. Mineral Deposits* 28, 207-224.

Hayashi, H., Saburo, A., Suzuki, M., 1978. Semiquantitative chemical analysis of asbestos fibers and clay minerals with an analytical electron microscope. *Clays and Clay Minerals*, Vol. 26, No. 3, 181-188.

Li, S.Z., Han, Z.Z., Liu, Y.J., Yang, Z.S., Ma, R., 2001. Regional metamorphism of the Liaohe Group: implications for continental dynamics. *Geol. Rev.* 47, 9–18.

Liu, S., Ruizhong, H., Shan, G., Caixia, F., Bobin, Y., Guangying, F., Youqiang, Q., Tao, W., Coulson, I. M., 2009. Petrogenesis of Late Mesozoic mafic dykes in the Jiaodong Peninsula, eastern North China Craton and implications for the foundering of lower crust. *Lithos* 113 (2009) 621-639

Lu, S., Zhao, G., Wang, H., Hao, G., 2008. Precambrian metamorphic basement and sedimentary cover of the North China Craton: A review. *Precambrian Research* 160 (2008), 77-93.

Luo, Y., Zhu, J., Wang, Y., 1990. Geological and geochemical features of the ore from the Dashiqiao magnesite deposit. *Mineral deposits*, 1990-01.

McCaffrey, M. A., Lazar, B., Holland, H. D., 1987. The evaporation path of seawater and coprecipitation of Br⁻ and K⁺ with halite. *J. Sediment. Petrol.* 57, 928-937.

McCaig, A.M., Tritlla, J., Banks, D.A., 2000. Fluid mixing and recycling during Pyrenean thrusting: Evidence from fluid inclusion halogen ratios. *Geochimica et Cosmochimica Acta* Vol. 64, Nr. 19 (2000), 3395-3412.

Melezhik, V.A., Fallick, A.E., Medvedev, P-V., Makarikhin, V.V., 2001. Paleoproterozoic magnesite: lithological and isotopic evidence for playa/sabkha environments, *Sedimentology* 48, 379-397.

Misch, D., 2009. 3D-Modelling of the Aihai Talc Deposit, Liaoning Province of China. Bachelor-Thesis, Institute for Applied Geosciences, University of Leoben.

Misch, D., Pluch, H., 2009. 3D-Modelling of the Aihai Talc Deposit, Liaoning Province of China. Unpublished Report for Aihai Talc Company Ltd., Institute for Applied Geosciences, University of Leoben.

Misch, D., Pluch, H., 2010. Geology of the Fanjiabauzi Talc Deposit. Poster-presentation at PANGEO 2010, Montanuniversität Leoben, 15.09-19.09.2010.

Mustansar, M., Hussain, S., 2010. A report on talc (soap stone). Minerals and Metals Division, Trade Development Authority of Pakistan (unpublished).

Parseval, P., Jiang, S.Y., Fontan, F., Wang, R.C., Martin, F., Freeet, J., 2004. Geology and ore genesis of the Trimouns talc-chlorite ore deposit, Pyrenees, France. *Acta Petrologica Sinica*, Vol. 20 (2004), 877-886.

Prochaska, W., 1999. Die Bedeutung der chemischen Zusammensetzung von Einschlussfluiden und laugbaren Salzen für die Genese von hydrothermalen und sedimentären Karbonatgesteinen der Ostalpen. *Mittl. Österr. Geol. Ges.* 90 (1997), 175-183.

Prochaska, W., 1988. Geologie, Geochemie und Genese der Ostalpinen Talklagerstätten. Habilitationsschrift eingereicht an der Montanuniversität Leoben.

Prochaska, W., 1989. Geologische und geochemische Untersuchungen an der Talklagerstätte Lassing (Steiermark). *Arch. f. Lagerst. Forsch. Geol. B.-A.*, Band 10 (Festband für O. M. Friedrich), S.99-114.

Qiu, X., 2002. Collisional orogenic belt and metallogenetic divisions. *Geological Bulletin of China* 21(10), 675-681.

Schandl, E.S., Sharara, N.A., Gorton, M.P., 1999. The origin of the Atshan talc deposit in the Hamata area, Eastern Desert, Egypt: A geochemical and mineralogical study. *The Canadian Mineralogist*, Vol. 37, 1211-1227.

Schandl, E.S., Gorton, M.P., Sharara, N.A., 2002. The origin of major talc deposits in the Eastern Desert of Egypt: relict fragments of a metamorphosed carbonate horizon? *Journal of African Earth Sciences* 34, 259-273.

Schmidt, H., 1984. China - the magnesite giant. *Industrial Minerals* 203, 27-45.

Schroll, E., 1997. Abschnitt V: Geochemische und geochronologische Daten und Erläuterungen. In: Weber, L., *Handbuch der Lagerstätten der Erze und Industriemineralien und Energierohstoffe Österreichs*, Archiv Lagerstättenforschung 19, GBA Wien, 395-542.

Schroll, E., Andras, P., Chovan, M., 1999. A first attempt to geochemically compare ore deposits of the Western Carpathians and the Eastern Alps. *Geological Carpathica*, Bratislava, Special Issue 50, 192-194.

Song, B., Nutman, A. P., Liu, D., Wu, J., 1996. 3800 to 2500 Ma crustal evolution in the Anshan area of Liaoning Province, northeastern China. *Precambrian Research*, Vol. 78 Nr. 1-3, 79-94.

Veizer, J., Hoefs, J., 1976. The nature of O^{18}/O^{16} and C^{13}/C^{12} secular trends in sedimentary carbonate rocks. *Geochimica et Cosmochimica Acta* 40, 905-914.

Wan, T., 2010. *The Tectonics of China – Data, Maps and Evolution*. Higher Education Press Beijing and Springer Verlag Berlin-Heidelberg, 340-384.

Warren, J.K., 2010. Evaporites through time: Tectonic, climatic and eustatic controls in marine and nonmarine deposits. *Earth-Science Reviews*, 98(2010), 217-268.

Weber, L., Zsak, G., Reichl, C., Schatz, M., 2009. Minerals Production, World-Mining-Data 2009, Volume 24.

Weber, L., Zsak, G., Reichl, C., Schatz, M., 2010. Minerals Production, World-Mining-Data 2010, Volume 25.

Weber, L., Zsak, G., Reichl, C., Schatz, M., 2011. Minerals Production, World-Mining-Data 2011, Volume 26.

Weber, L., Zsak, G., Reichl, C., Schatz, M., 2012. Minerals Production, World-Mining-Data 2012, Volume 27.

Wilamowski, A., Wiewiora, A., 2004. Chemical diversity of talcs in relation to their origin. *Acta Mineralogica-Petrographica*, Vol 45/2, 35-39.

Wilkinson, J.J., 2001. Fluid inclusions in hydrothermal ore deposits. *Lithos* 55 (2001), 229-272.

Yin, A., Nie, S., 1996. Phanerozoic palinspastic reconstruction of China and its neighboring regions. Yin, A., Harrison, T.M.(Eds.), *The Tectonic Evolution of Asia*. Cambridge University Press, New York, 285–442.

Zhai, Y., Deng, J., Tang, Z., Xiao, R., Song, H., Peng, R., Sun, Z., Wang, J., 2004. Metallogenic Systems on the Paleocontinental Margin of the North China Craton, *Acta Geologica Sinica*, No. 2, Vol. 78, 592-603.

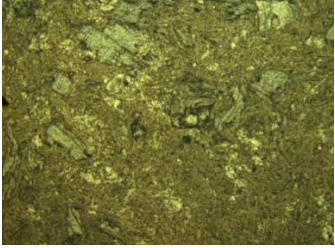
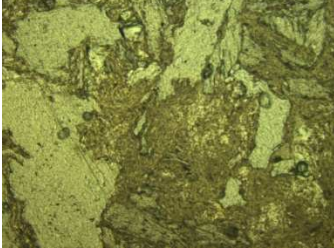

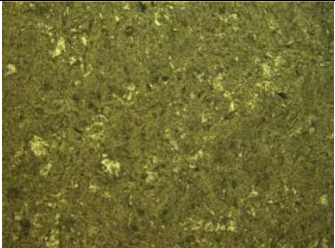
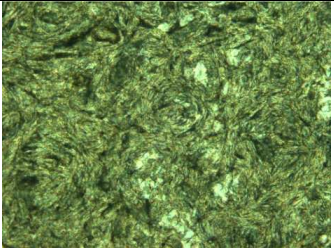
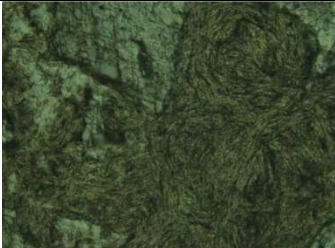
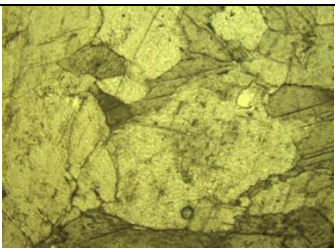
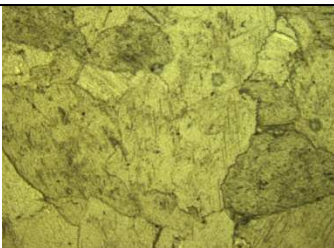
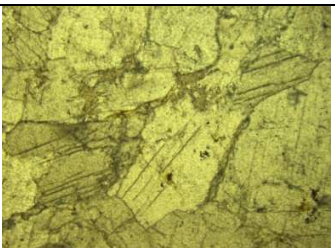
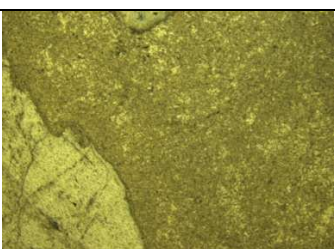
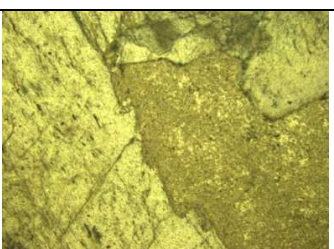
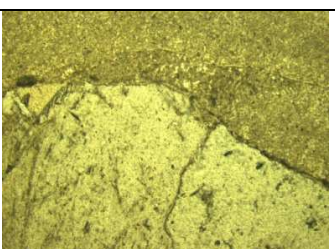
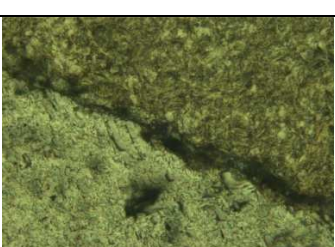
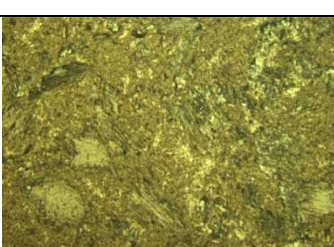
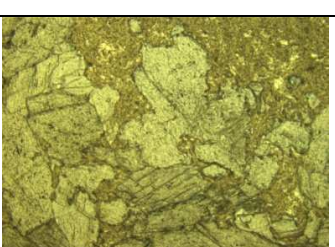
Zhao, G.C., 2001. Palaeoproterozoic assembly of the North China Craton. *Geol. Mag.* 138, 87–91.

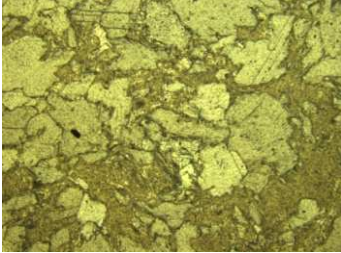

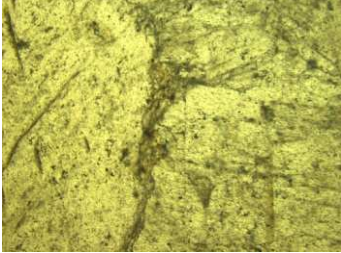
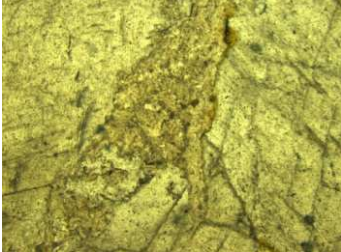
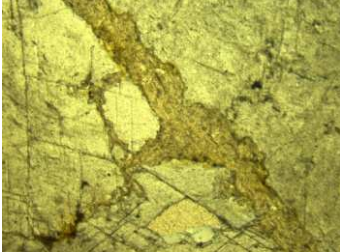
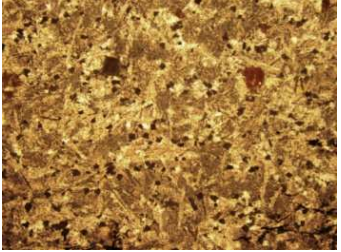
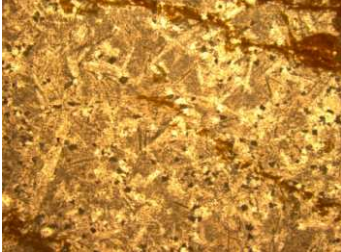
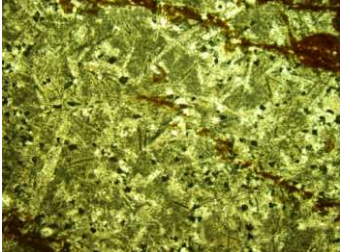
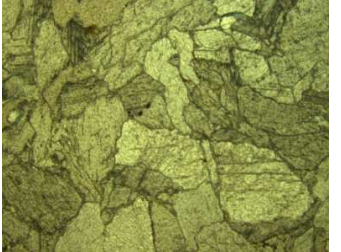
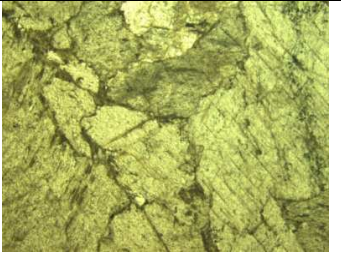
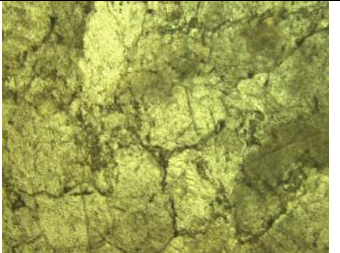
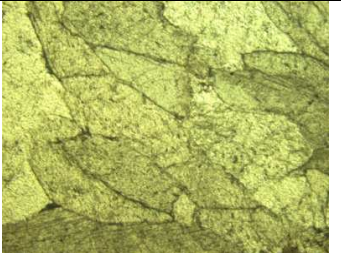
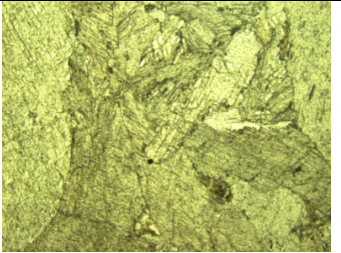

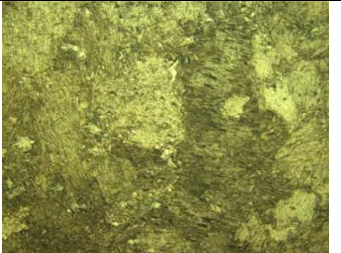
Zhu, G., 1984. The geologic characteristics of talcmagnesite deposits and their origin in the Liaodong Peninsula. *Journal of Jiling University (Earth Science Edition)*, 1984-02.

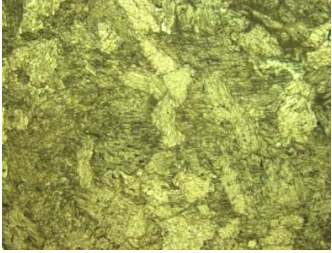

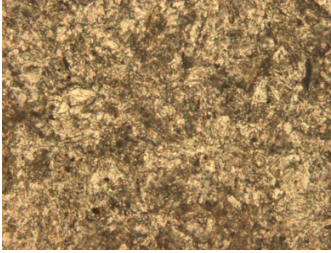
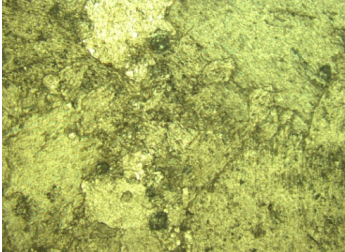
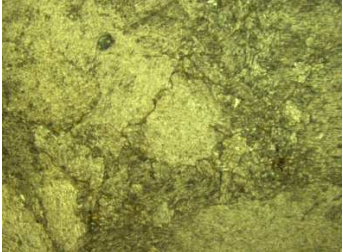

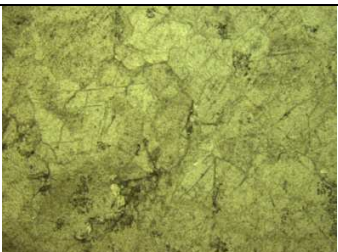
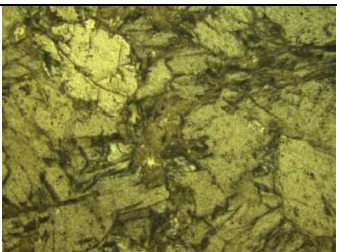
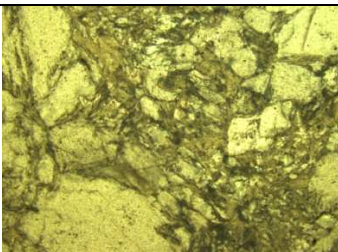
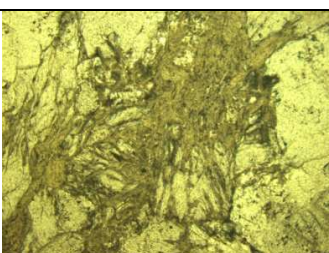
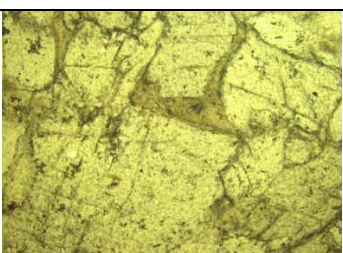
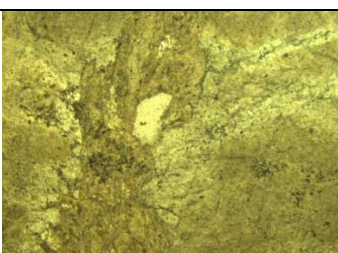
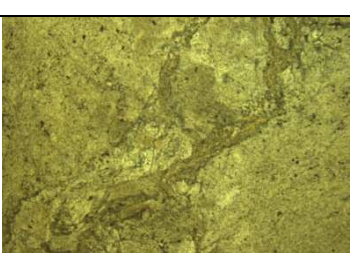
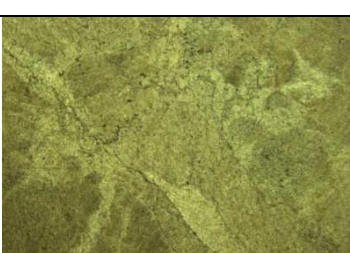
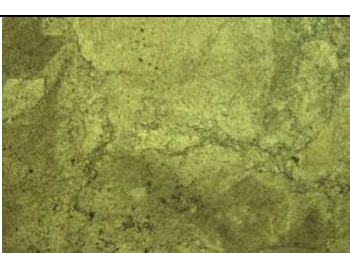
Zhuang, J. X., 2010. Focus on Latest Chinese Talc Trends. Report of the Deputy Secretary in General, China Talc Association.

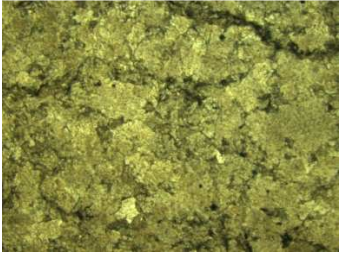
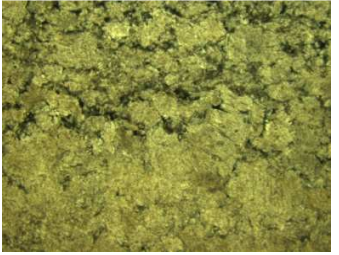
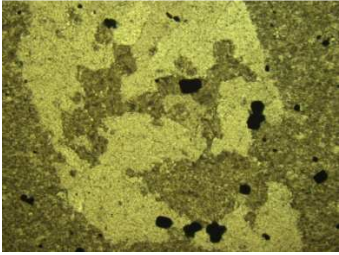
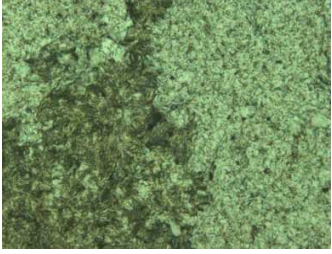
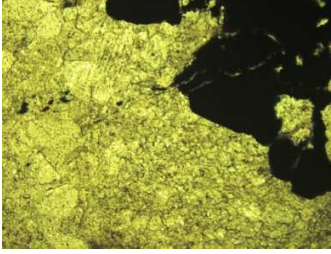
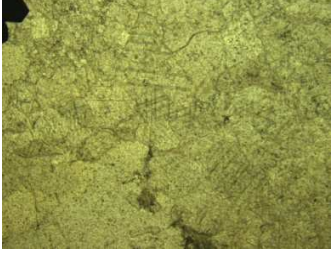
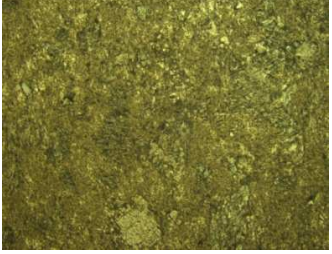
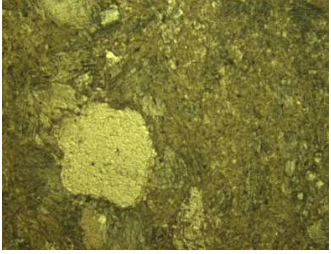
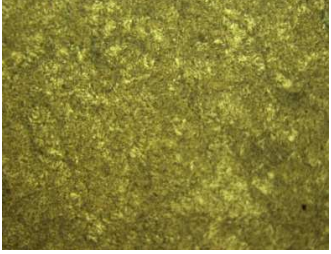
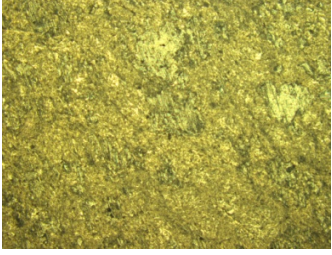
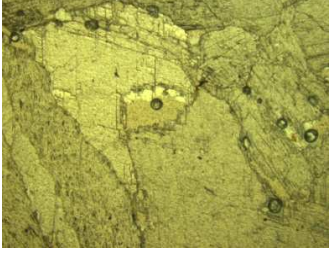
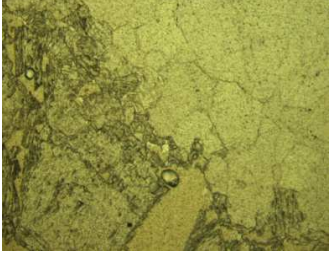
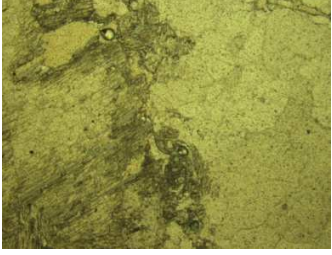

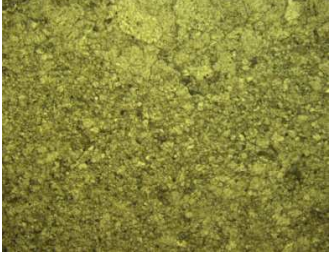
5 Appendix

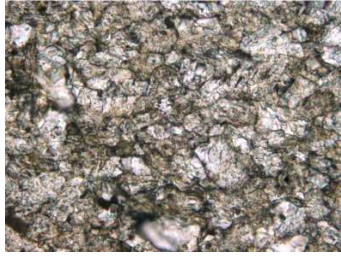
5.1 Thin-Sections (see detailed description below)

 1_1_10x_1	 1_1_10x_2	 1_1_10x_3
 1_1_10x_4	 1_1_50x_1	 1_1_50x_2
 1_2_10x_1	 1_2_10x_2	 1_2_10x_3
 1_2_10x_4	 1_2_10x_5	 1_2_10x_6
 1_2_50x_1	 1_3_10x_1	 1_3_10x_2

		
1_3_10x_3	1_3_50x_1	2_1_10x_1
		
2_1_10x_2	2_1_10x_3	6_1_10x_1
		
6_1_10x_2	6_1_10x_3	6_5_10x_1
		
7_1_10x_1	7_1_10x_2	8_1_10x_1
		
8_1_10x_2	8_1_10x_3	10_1_10x_1

		
10_1_10x_2	11_1_10x_1	11_1_50x_1
		
11_3_10x_1	11_3_10x_2	12_1_10x_1
		
14_3_10x_1	15_2_10x_1	15_2_10x_2
		
15_2_10x_3	15_2_10x_4	15_4_10x_1
		
15_4_10x_2	16_1_10x_1	16_1_10x_2

		
17_1_10x_1	17_1_10x_2	24_1_10x_1
		
24_1_50x_1	25_1_10x_1	25_1_10x_2
		
26_3_10x_1	26_3_10x_2	26_3_10x_3
		
26_3_10x_4	27_1_10x_1	27_1_10x_2
		
27_1_10x_3	35_1_10x_1	35_1_10x_2

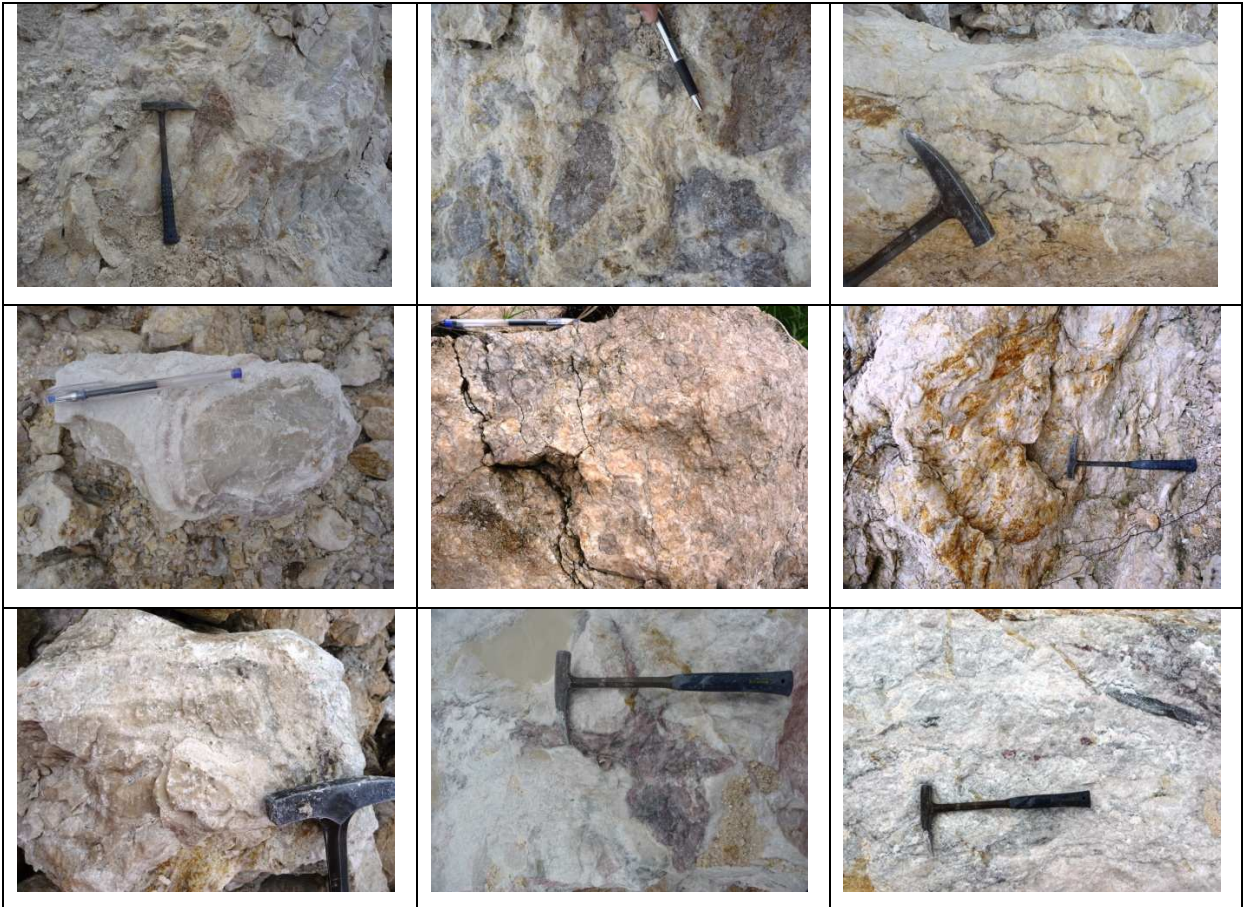


35_1_50x_1

Height of picture equals 1,35mm for 10x and 0,27mm for 50x optical enlargement.

1_1	Talc in fine-grained magnesite
1_2	Intergrowth of talc with coarse grained magnesite
1_3	Zoned intergrowth of fine grained magnesite with talc accretions
2_1	Sparry magnesite with talc in intergranular space
6_1	Lamprophyre dyke
7_1	Sparry magnesite
6_5	Silicified magnesite
8_1	Sparry magnesite
10_1	Magnesite from hanging wall of lamprophyre dyke
11_1	Layered, fine-grained carbonate
11_3	Magnesite, hanging wall of layered fine-grained carbonate
12_1	Silicified magnesite layer
14_3	Magnesite near massive talc shear band
15_2	Magnesite near massive talc shear band
15_4	Magnesite near small talc shear bands
16_1	Magnesite with no talc in the surrounding area
17_1	Carbonate-rich banded schist
24_1	Intermixture of talc and magnesite from young fault
25_1	Dolomite with pyrite
26_3	Contact of talc and magnesite
27_1	Magnesite with younger magnesite dykes
35_1	Fine-grained magnesite with relict structure of biogenic origin

5.2 Outcrops (see detailed description below)



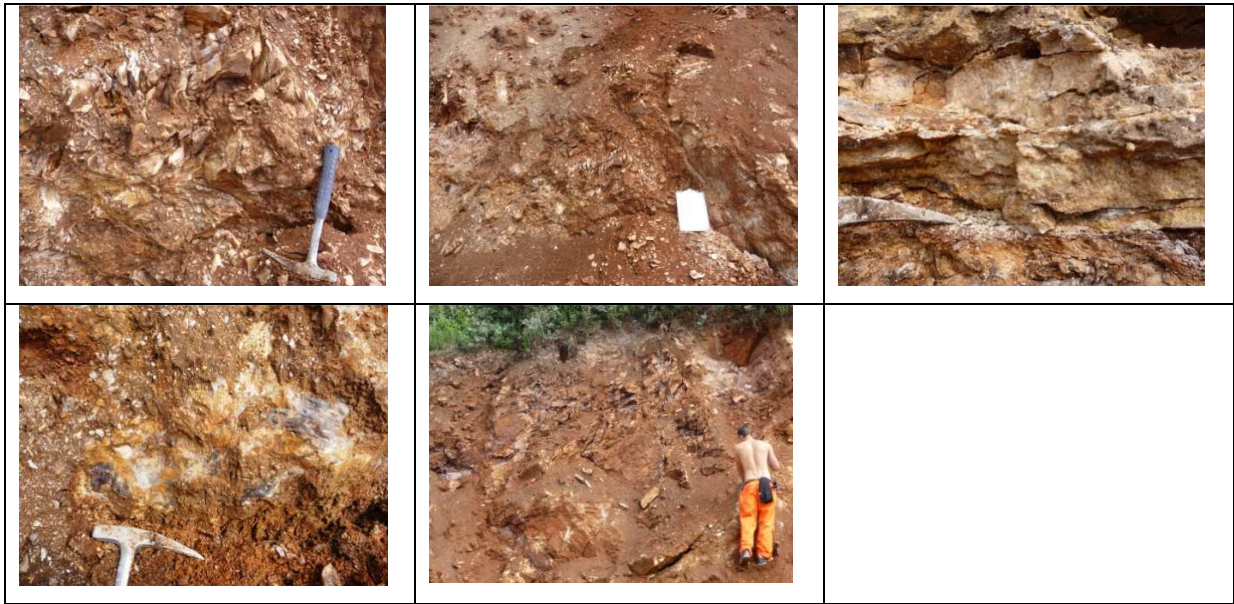
Outcrop 1



Outcrop 2



Outcrop 3



Outcrop 4



Outcrop 5



Outcrop 6



Outcrop 7



Outcrop 8



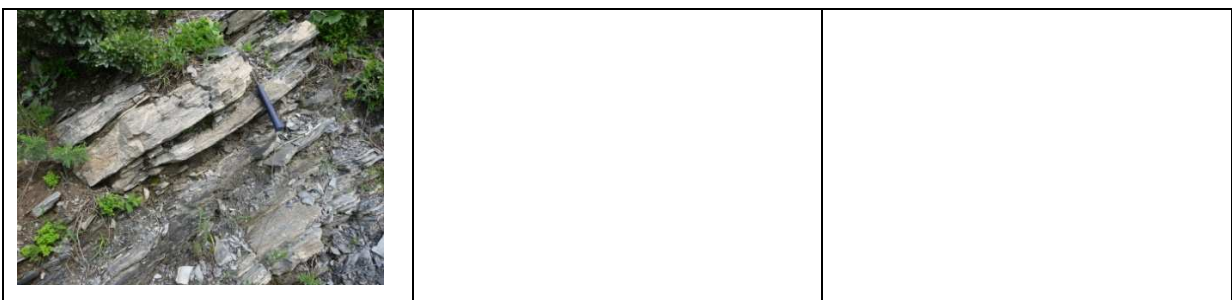
Outcrop 9



Outcrop 10



Outcrop 11



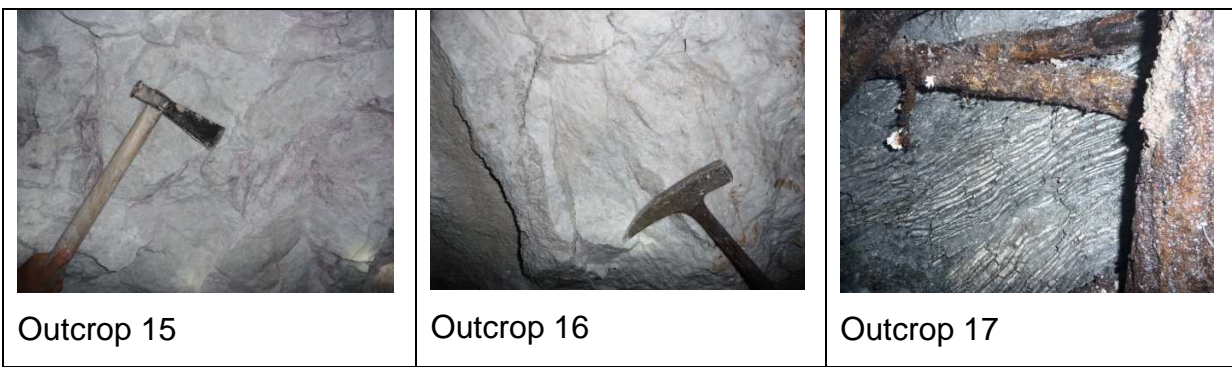
Outcrop 12



Outcrop 13



Outcrop 14



Outcrop 15

Outcrop 16

Outcrop 17



Outcrop 19



Outcrop 20



Outcrop 21



Outcrop 23



Outcrop 24



Outcrop 25



Outcrop 26



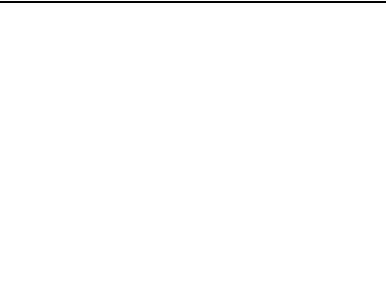
Outcrop 27



Outcrop 29



Outcrop 31



Outcrop 34





Outcrop 35



Outcrop 36

1

Undeformed magnesite with talc intercalations (pink).

2 types of magnesite:

- Fine-crystalline, talc accretions with irregular borders
- Sparry magnesite with talc in intergranular space

Samples:

1_1: Talc-accretion in fine-crystalline magnesite

1_2: Intergrowth talc - sparry magnesite

1_3: Zoned intergrowth fine-crystalline magnesite – talc accretion

1_4: Sparry magnesite with talc in intergranular space

2

Sparry magnesite, layered with grey talc in intergranular space (talc replaces magnesite).

Samples:

2_1: Sparry magnesite with grey talc (replacement?)

3

Transition between sparry magnesite with talc in intergranular space and compact, coarse grained magnesite with distinct talc accretions.

4

Strongly weathered magnesite with dolomite(?) in small dykes. Footwall: talc shear bands intercalating with fine-crystalline unweathered magnesite. Unweathered magnesite also shows undeformed talc accretions. Red weathered material from lamprophyre dyke (hanging wall).

Samples:

4_1: Talc from shear band

5

Talc layer (white-grey, 2,5m), potential connection to new open pit. Minor magnesite relicts in large talc shear zone. Hanging wall: Magnesite with talc accretions (undeformed) and small shear bands.

Samples:

5_1: Talc from large shear zone

6

Lamprophyre dyke crosscuts sparry magnesite with minor talc. Magnesite strongly weathered, with small Dolomite(?) dykes (1,5m on both sides of Lamprophyre dyke).

Dyke also crosscuts talc shear zone (Lamprophyre dyke younger than talc accumulation!). Talc admixture at Dyke borders (mobilized from older shear zone?).

Samples:

6_1: Lamprophyre, middle of dyke

6_2: Lamprophyre, border of dyke

6_3: Transition from dyke to talc shear band

6_4: talc shear band

6_5: Siliceous magnesite 1

6_6: Siliceous magnesite 2

7

Radiating talc(?), crystals 4-8cm, white-pink, in joints of coarse magnesite. Magnesite with small talc accretions (2cm).

Samples:

7_1: Radiating talc

8

Layered magnesite, coarse (xx 0,5-0,8cm), no talc in primary structure. Along schistosity chert and minor talc layers (grey).

Samples:

8_1: Magnesite+chert(?)

9

Lamprophyre dyke, almost parallel to primary bedding of magnesite. Magnesite at border zone strongly silicified, talc layer at transition zone between dyke and

sourrounding magnesite. Dyke seems to rise along former talc shear zone (weak zone). Network of small dykes in the sourrounding area of primary dyke (3m).

Samples:

9_1: Lamprophyre, middle of dyke

9_2: Transition lamprophyre – talc, border of dyke

10

Hanging wall of dyke: sparry magnesite without talc.

Samples:

10_1: Magnesite, hanging wall of dyke

11

Fine sedimentary layers (Carbonate?). Stalky (xx 2-4cm) and rounded (garnet?, xx 1cm) crystals. Primary(?), undisturbed contact to sparry magnesite on both sides. Sparry magnesite without talc.

Samples:

11_1: Layered Carbonate (?)

11_2: Magnesite, Footwall of layered beds (1m)

11_3: Magnesite, Hanging wall of layered beds (1m)

12

Hanging wall of fine sedimentary beds. Strongly silified, banded carbonate (silified marble?). Sourrounding magnesite shows no talc (deposit border?).

Samples:

12_1: silified Carbonate-layer

13

Schistous layer (10m). Network of nonconform dykes (20-40cm, carbonate ?).

Samples:

13_1: Schist

14

Mine 1, level 90, talc grade 2, pink + grey.

Samples:

14_1: Talc from actual mining

14_2: Talc from actual mining

14_3: Magnesite, Footwall of talc shear band

15

Mine1, level 84. Talc shear bands (1-5cm) in compact magnesite with undeformed talc accretions (primary ?). Footwall of massive Talc shear zone (mined). Grade 1 talc embedded into grade 2 talc.

Samples:

15_1: Talc, grade1, pink (top quality)

15_2: Magnesite from border of mined shear zone

15_3: Talc from small shear band, footwall of massive shear zone

15_4: Magnesite beneath small shear bands

16

Mine 1, level 84. Fine-grained, compact magnesite without talc. Magnesite shows high whiteness.

16_1: Magnesite, m1, l84, no talc

17

Second adit of mine 1: 15-20m layer of fine grained, banded, pyllitic schist (carbonate-rich). Footwall border of deposit in the area of mine 1.

Samples:

17_1: Banded, carbonate-rich schist

18

Talc samples from processing plant (correlation with different mines).

Samples:

18_1: mine 6, grey, grade 1

18_2: mine 4, grade 1, color D60 (mixture of colors)

18_3: mine 6, grade 1, white-yellow (mixture of white and yellow components)

19

Aihai mine 3 (outside of Fanjiabauzi area). Lamprophyre dyke crosscuts talc-rich magnesite, talc accumulation in shear zones older than dyke.

Samples:

19_1: talc, mine 3, old open pit area

19_2: talc, mine 3

19_3: undeformed, primary talc accumulation in magnesite

19_4: talc from old open pit area (15-20m talc-rich zone)

20

Mine 4, level 187, talc grade 2 from actual mining.

Samples:

20_1: talc from actual mining, m4, l187, grade 2

20_2: magnesite, footwall of mined shear band

21

Mine 4, level 176, Dyke material ground into talc-bearing fault. Grey coloration of fault material.

22

Small talc-bearing shear bands, parallel to primary magnesite bedding.

23

Mine 4, level 176, grade 1 talc.

Samples:

23_1: talc, m4, l176, grade 1

24

Fault filled with grey material, dyke components ground into fault and mechanically admixed with talc (younger than first talc accumulation in large shear zones).

Samples:

24_1: Fault material

25

Dolomite-layer, footwall of deposit body. Dolomite shows irregular borders to magnesite, fine magnesite dykes crosscut into dolomite bed.

Samples:

25_1: Pyrite-bearing dolomite, m4, I170

26

Open pit (new); Strongly tectonized talc body, strongly weathered (brownish coloration). Talc seems to be more massive and not as platy as in other deposit parts (underground mines). Magnesite is mostly bright white and shows distinct talc accumulations of up to 30cm in diameter (primary mineralization?). Magnesite is fine-crystalline (xx max. 0,3cm), talc only occurs in accumulations, not in intergranular space.

Samples:

26_1: brownish talc, open pit

26_2: brownish talc, surface

26_3: Talc – magnesite contact

27

Mine 6, Level 222. Network of young(?) magnesite dykes in older magnesite, 2m beneath lamprophyre dyke. Near of dyke talc-bearing shear bands.

Samples:

27_1: Magnesite + young(?) magnesite dykes

28

Mine 6, Level 222. Grey talc, grade 2 (beginning of new talc layer). Talc in coarse grained magnesite, magnesite shows massive talc accumulations up to 30cm in diameter.

Samples:

28_1: Talc, m6, l222, grade 2. Poor quality!

29

Talc layer, grade 1. At least 2m of top quality talc. Mainly grey coloration, transition to pink. Good example of completely tectonized sliding planes.

Samples:

29_1: Talc, m6, l222, grade 1

30

Talc layer, grade 2 (punctual grade 1, sampled).

Samples:

30_1: Talc, m6, l222, grade 1

31

Talc layer (thickness several meters), white-grey talc of good quality (grade1, punctual grade 2 and pyrite content).

Samples:

31_1: Talc, m6, l230

32

Transition dyke – magnesite – talc.

Samples:

32_1: Transition dyke – magnesite – talc

33

Young (?), kryptocrystalline magnesite in small dykes crosscuts older magnesite.

Samples:

33_1: young (?) magnesite dykes in older magnesite

34

Southern surroundings of Fanjiabauzi concession area (along train tracks): Outcrop of massive (10m) talc-bearing shear zone. Talc shows pink coloration, occurs in small massive bodies and platy as shear talc. Magnesite is bright-white and fine-crystalline (as observed near most of the mined talc layers).

35

Southern surroundings of Fanjiabauzi concession area (along train tracks):
Magnesite fine-layered, stromatolites (?). Stromatolite (?) layers conform to surrounding magnesite bedding.

Samples:

35_1: fine, layered carbonate, stromatolite (?)

35_2: fine, layered carbonate, stromatolite (?)

36

Fine, layered carbonate (stromatolite ?) alternating with coarse sparry magnesite (xx up to 8cm). Fine, laminated carbonate seems to be recrystallized into sparry magnesite (irregular borders). No talc in this area, no deformation.

Outcrop	Dip Dir.	Dip (°)	Comment
1	N	40-50	Surroundings of tectonized area
2	NNO	40-50	Sparry magnesite
3	N	40-70	Sparry magnesite
4	N	40-50	Weathered magnesite
5	N	40-50	Talc layer
6	N	40-50	Lamprophyre dyke
7	/	/	Radiating talc crystals in magnesite joint
8	N	40-50	Coarse, compact magnesite
9	N	40-50	Lamprophyre dyke
10	/	/	Sparry magnesite
11	NNW	40	fine, layered carbonate
12	NNW	20-40	Silicified marble (?)
13	/	/	Homogeneous, fine-crystalline schist
14	/	/	Talc, mine 1
15	/	/	Talc, mine 1
16	/	/	Magnesite
17	S	40-50	Layered, carbonate-rich schist
18	/	/	Talc samples from processing plant!
19	N-NE	40-50	Lamprophyre dyke, mine 3!
20	/	/	Talc, mine 4
21	NNW	70	Grey filling in young (?) fault (talc-bearing)
22	N	70	Small talc-bearing shear bands
23	SSW	40-50	Talc, mine 4
24	/	/	Grey filling in young (?) fault (talc-bearing)
25	/	/	Dolomite, mine 4
26	N-O/SO	30-70	Strongly tectonized talc from open pit!
27	N	50-70	Small shear bands
28	SW	40-50	Talc, mine 6
29	NNO	40-50	Talc, mine 6
30	NNO	40-50	Talc, mine 6
31	NNW	50-70	Talc, mine 6
32	/	/	Transition dyke - magnesite - talc
33	/	/	Young(?) magn. dykes in older magnesite
34	N-S	85-90	Shear zone in fine-crystalline magn.
35	SSO	70	Stromatolites (?) in sparry magn.
36	N	70	Stromatolites (?)

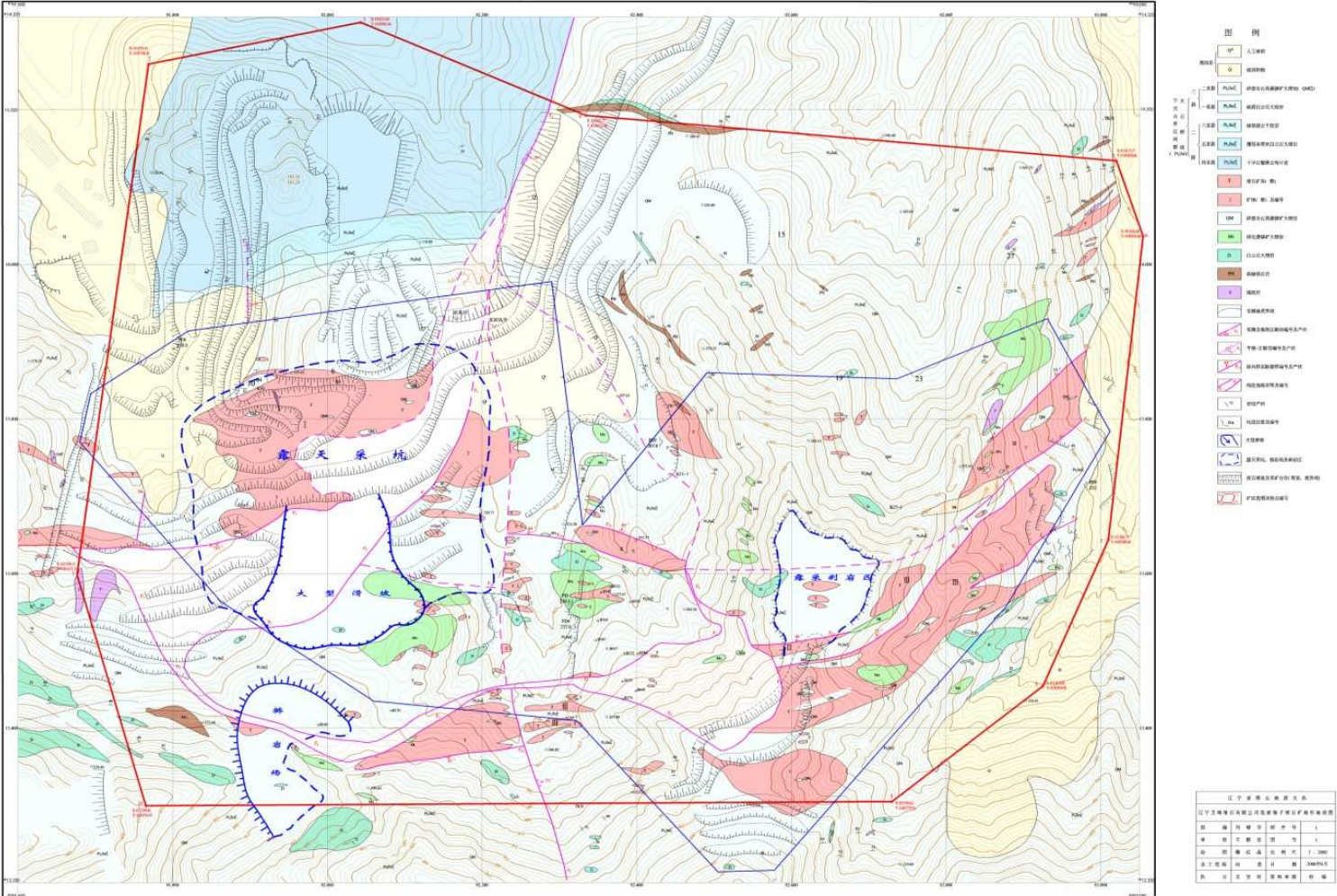
5.3 Mining subsidence damages (for detailed information see chapters “Geo-risks” above)





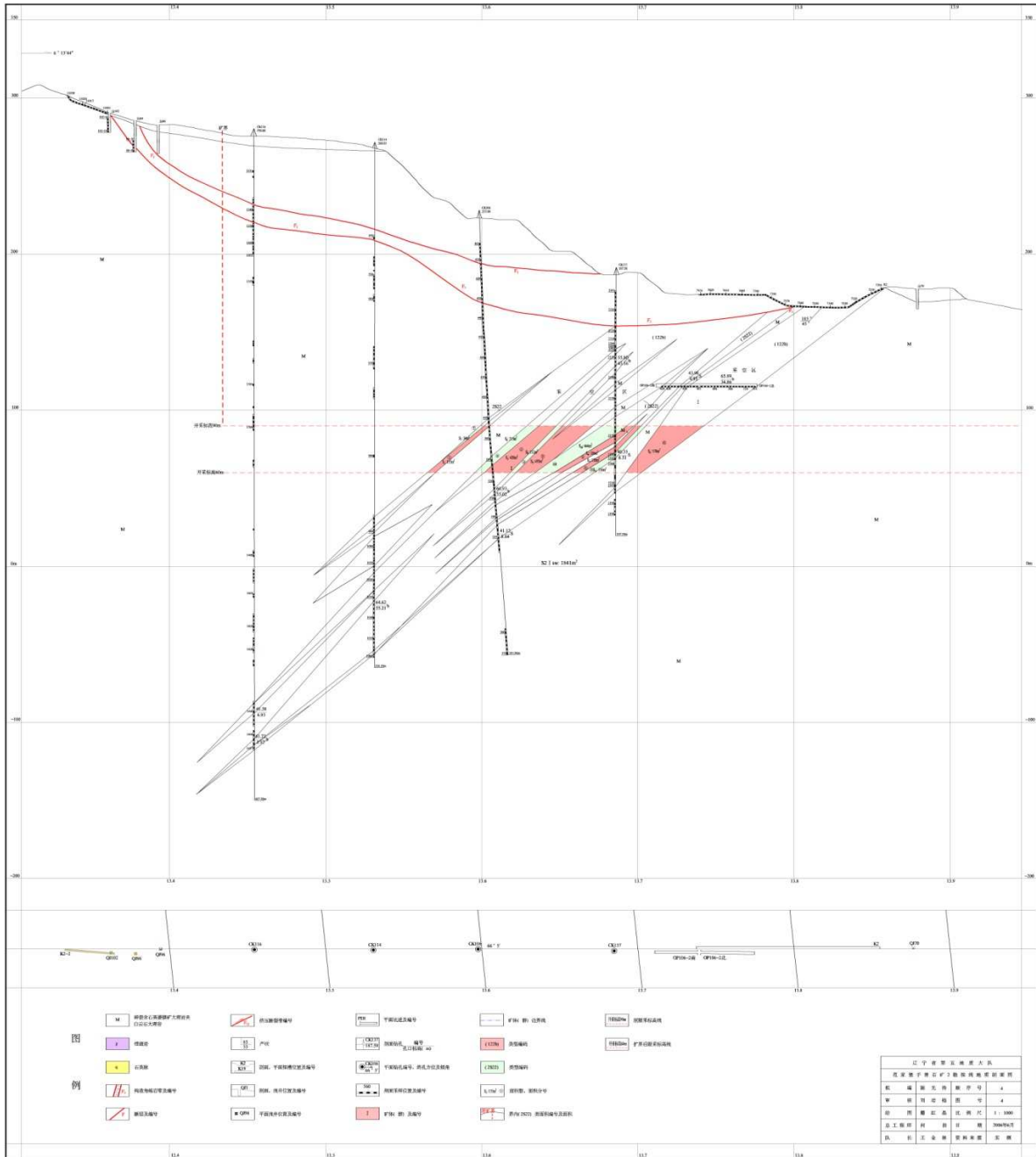
5.4 Maps and Sections (provided by geological staff of Aihai Talc Company Ltd. (see references))

辽宁艾海滑石有限公司范家堡子滑石矿地形地质图



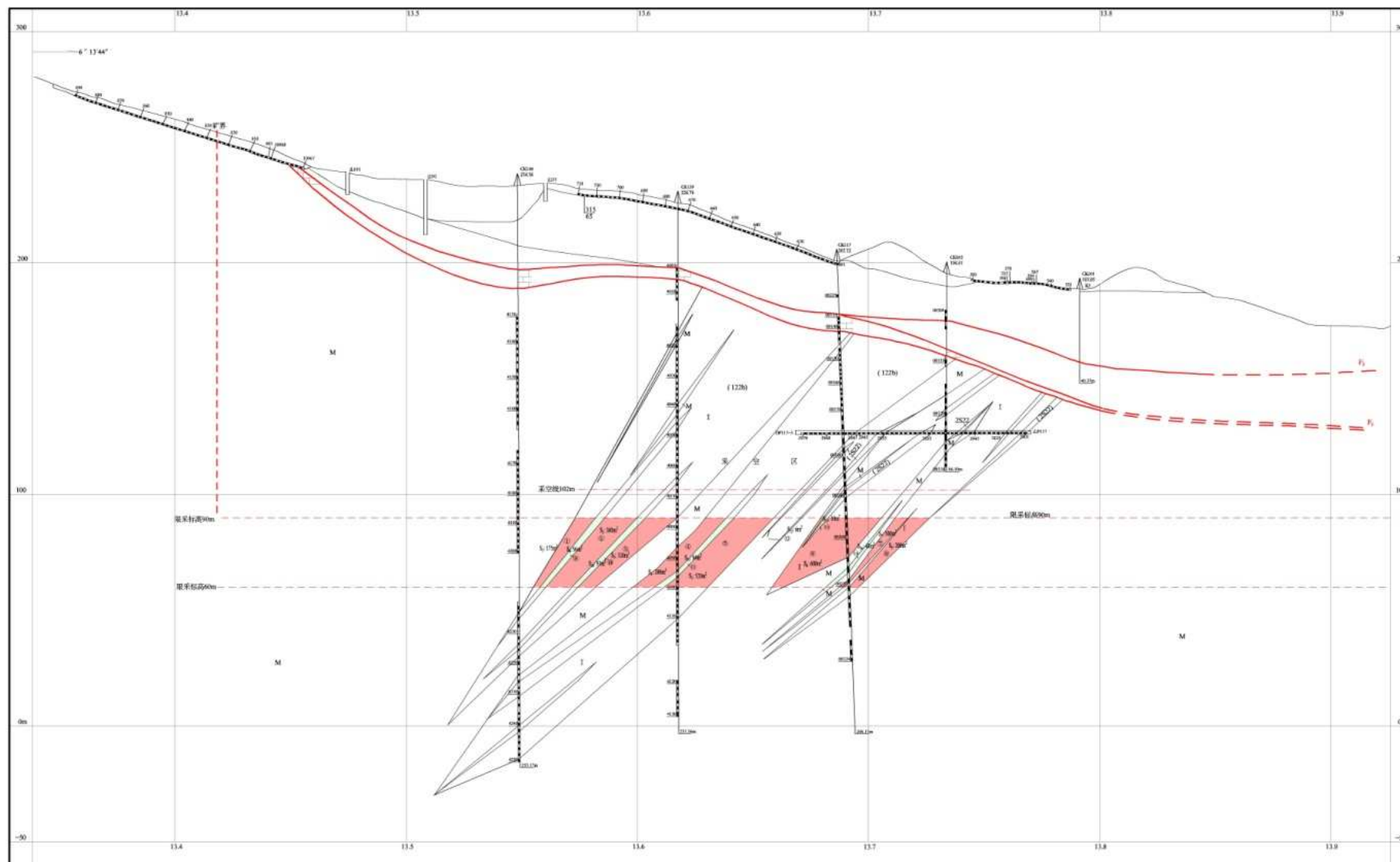
范家堡子滑石矿2勘探线地质剖面图

比例尺 1:1000



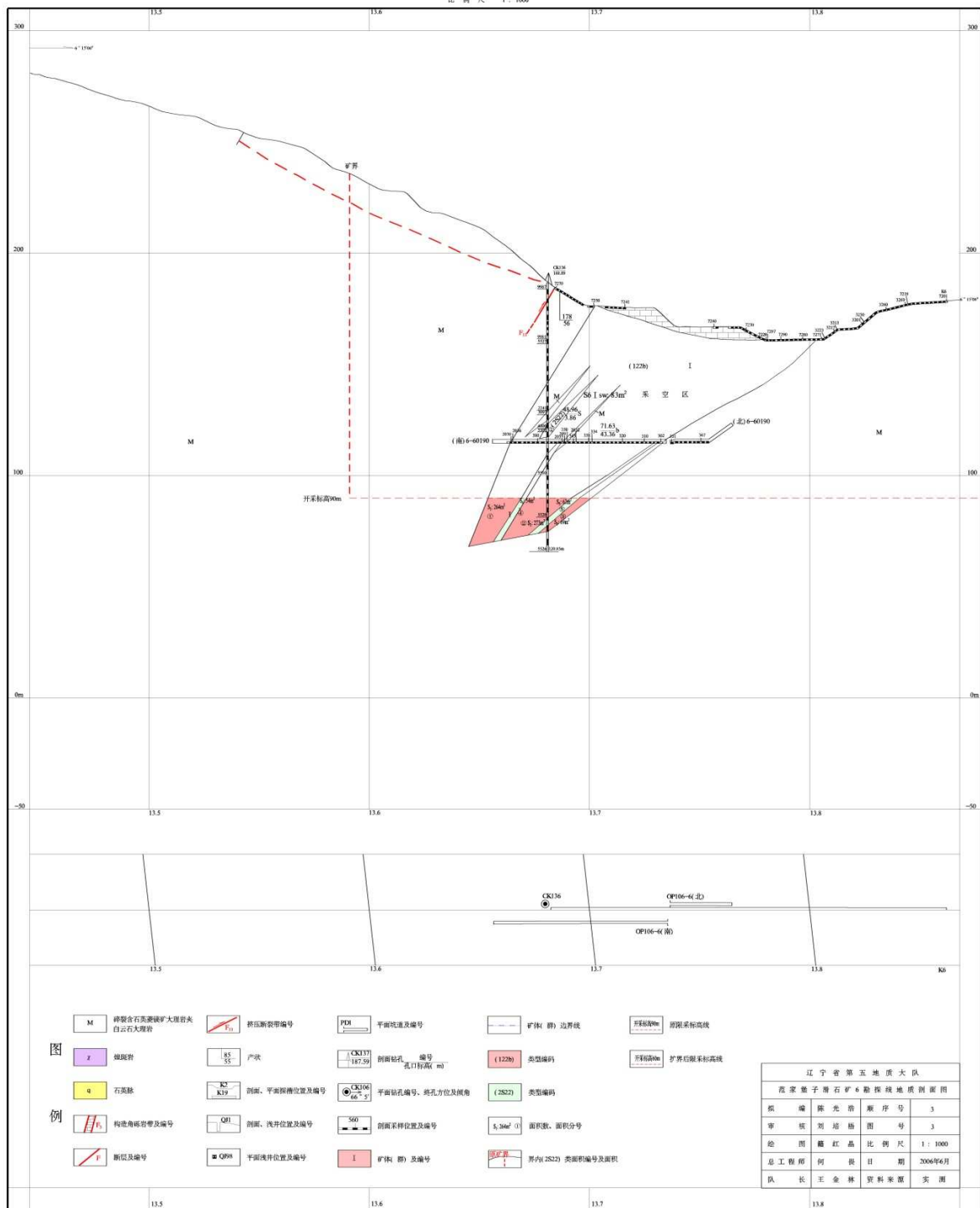
范家堡子滑石矿3勘探线地质剖面图

比例尺 1:1000



范家堡子滑石矿6勘探线地质剖面图

比例尺 1:1000



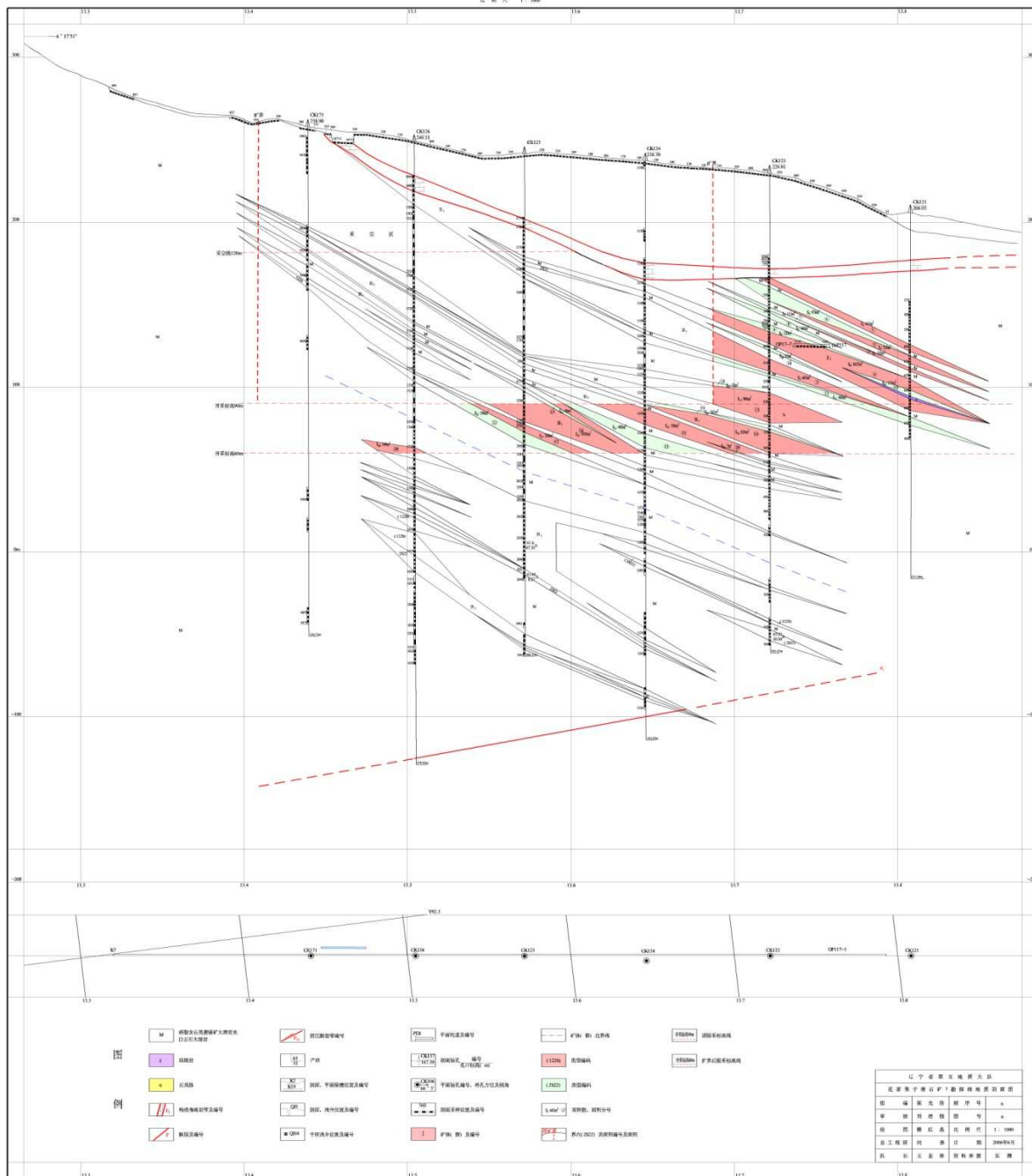
图例

- | | | | | | | | | | | |
|---|--------------------|--|--------------|-------|-----------|--|------------|----------|-------|-------|
| M | 碎斑含石英质砂岩大理岩夹白云石大理岩 | | 挤压断裂带编号 | PDX | 平面线迹及编号 | | 矿体(群)边界线 | | 开探标高线 | |
| X | 断层岩 | | 产状 | CK107 | 剖面钻孔 编号 | | (1228) | 类型编码 | | 开探标高线 |
| q | 石英脉 | | 剖面、平面测井位置及编号 | CK106 | 剖面钻孔 编号 | | (2821) | 类型编码 | | 开探标高线 |
| | 构造角砾带及编号 | | 剖面、洗井位置及编号 | 560 | 剖面采样位置及编号 | | 5.34m² (1) | 面积数、面积分号 | | 开探标高线 |
| | 裂隙及编号 | | 平面测井位置及编号 | I | 矿体(群)及编号 | | 5.34m² (1) | 面积数、面积分号 | | 开探标高线 |

辽宁省第五地质大队			
范家堡子滑石矿6勘探线地质剖面图			
编 号	编 号	顺 序 号	3
审 核	刘 培 培	图 号	3
绘 图	葛 磊	比 例 尺	1:1000
总 工 程 师	何 县	日 期	2006年6月
队 长	王 金 林	资 料 来 源	实 测

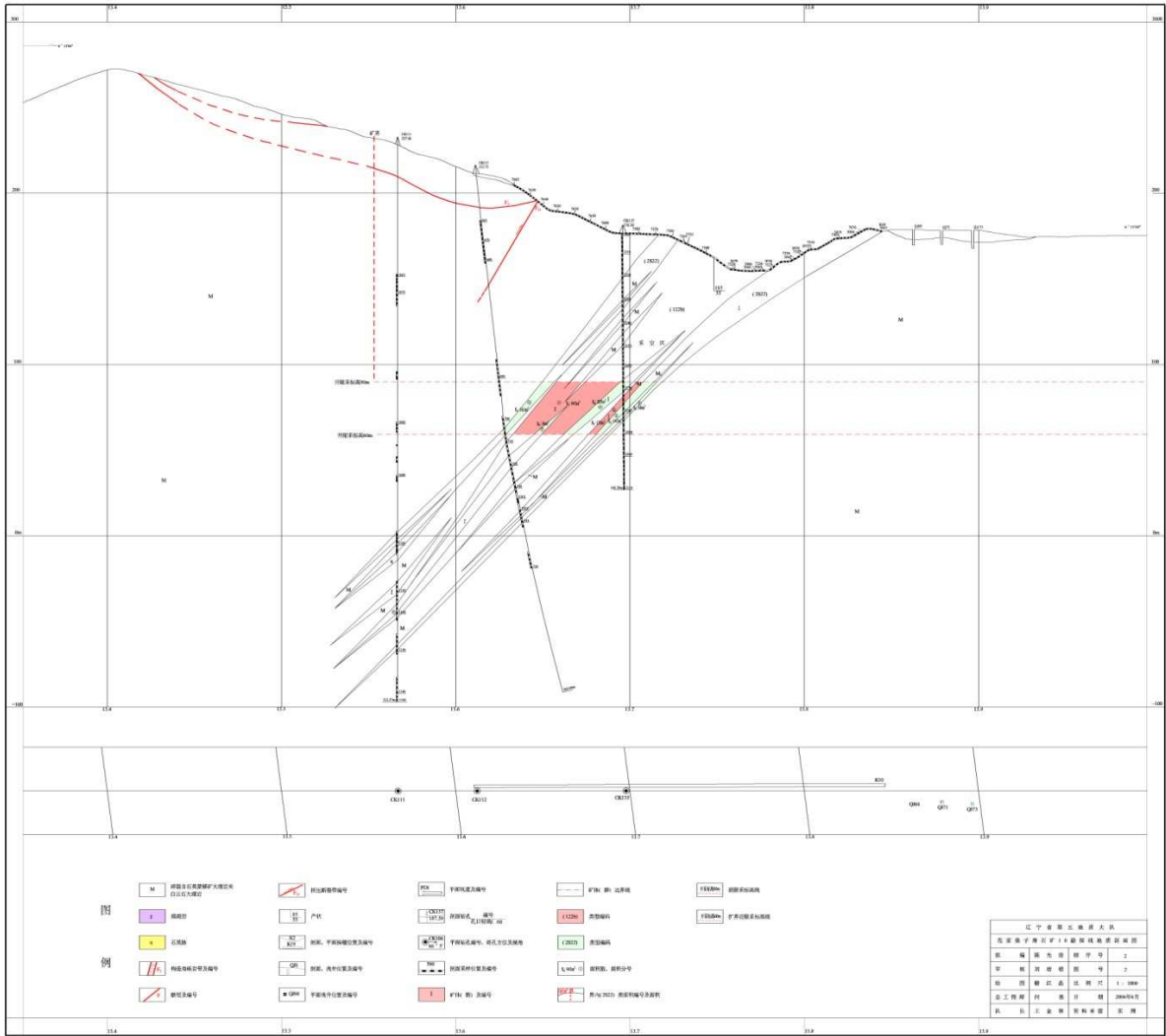
范家堡子滑石矿7勘探线地质剖面图

比例尺 1:1000



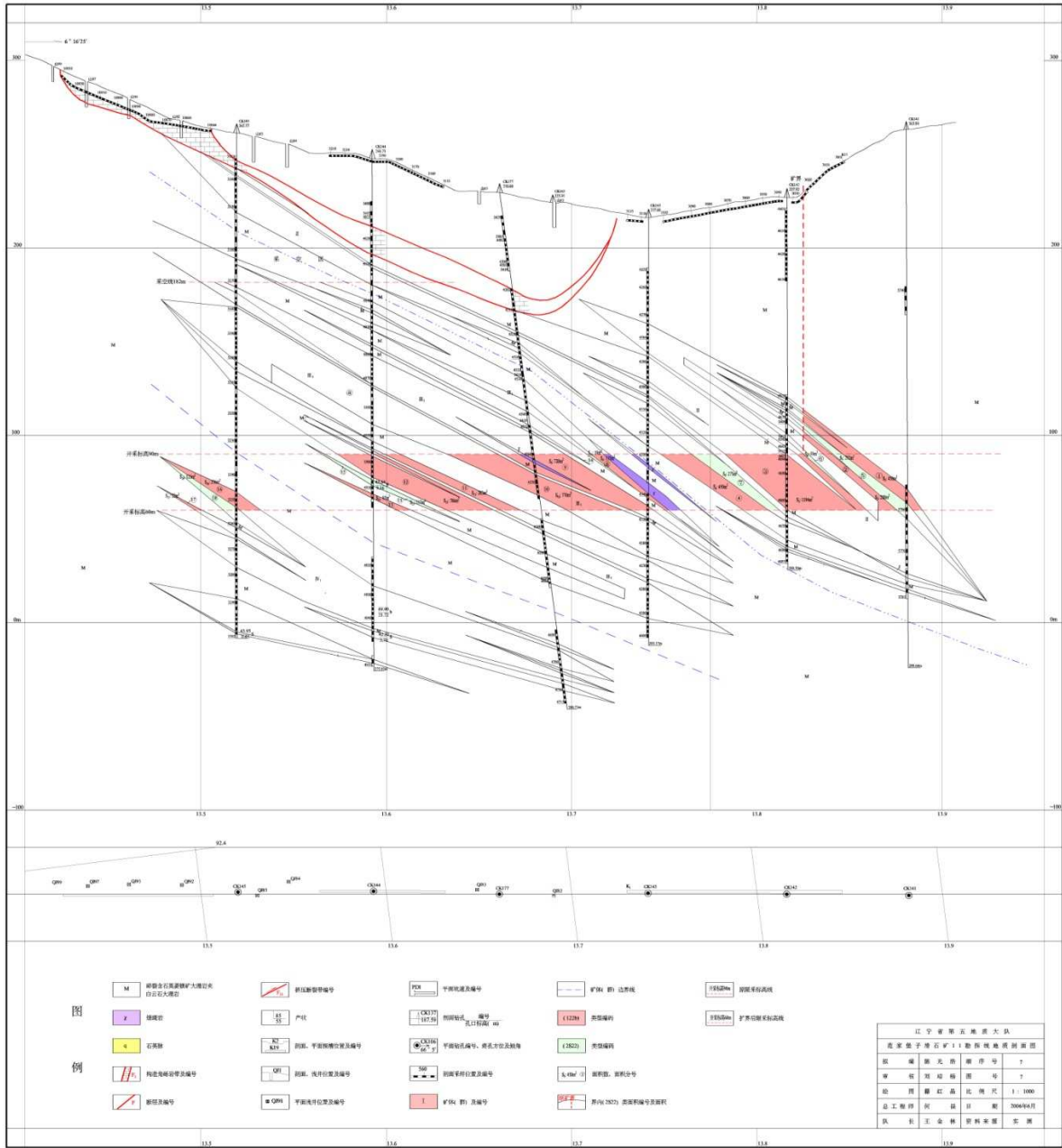
范家堡子滑石矿10勘探线地质剖面图

比例尺 1:100



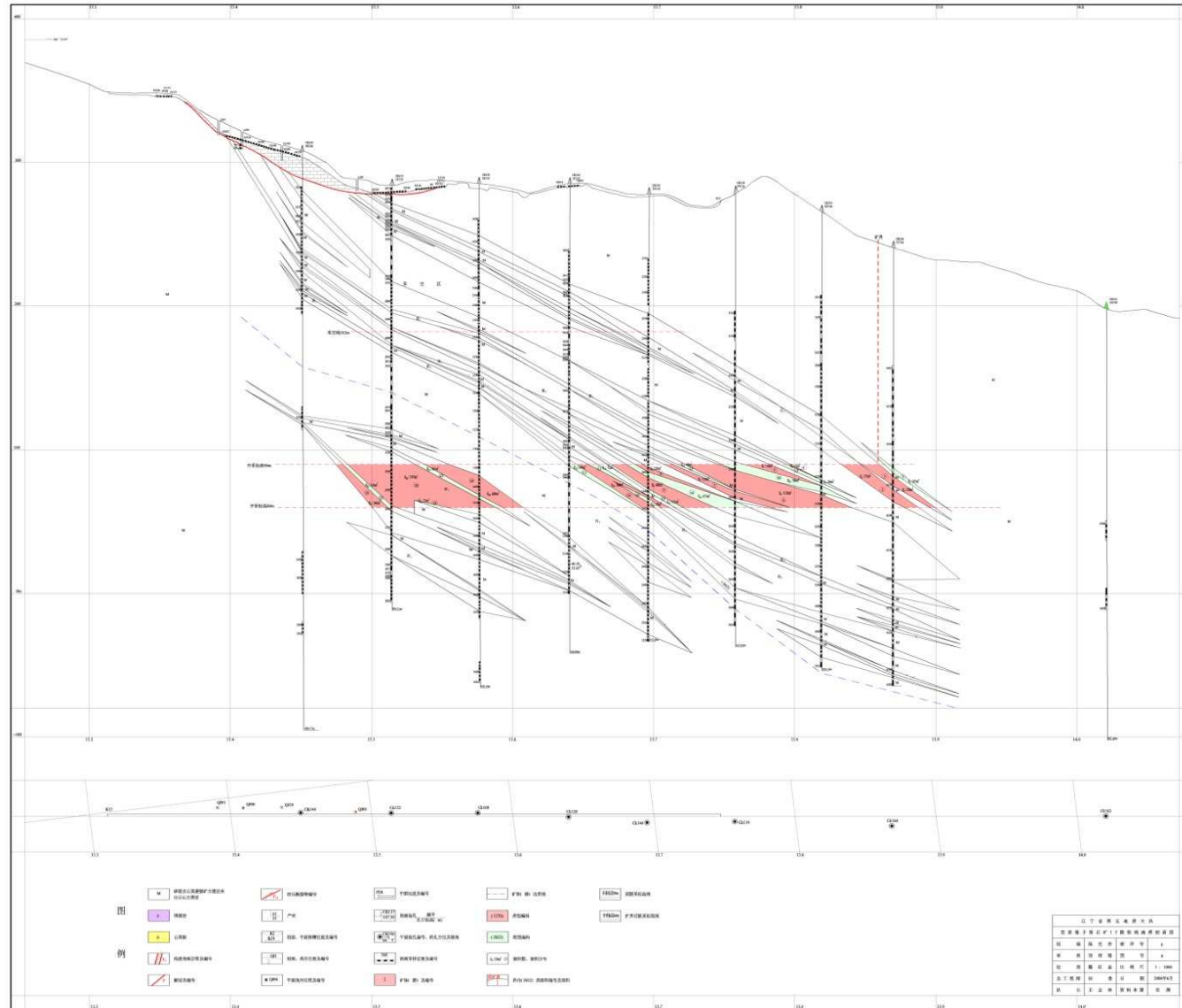
范家堡子滑石矿11勘探线地质剖面图

比例尺 1:1000



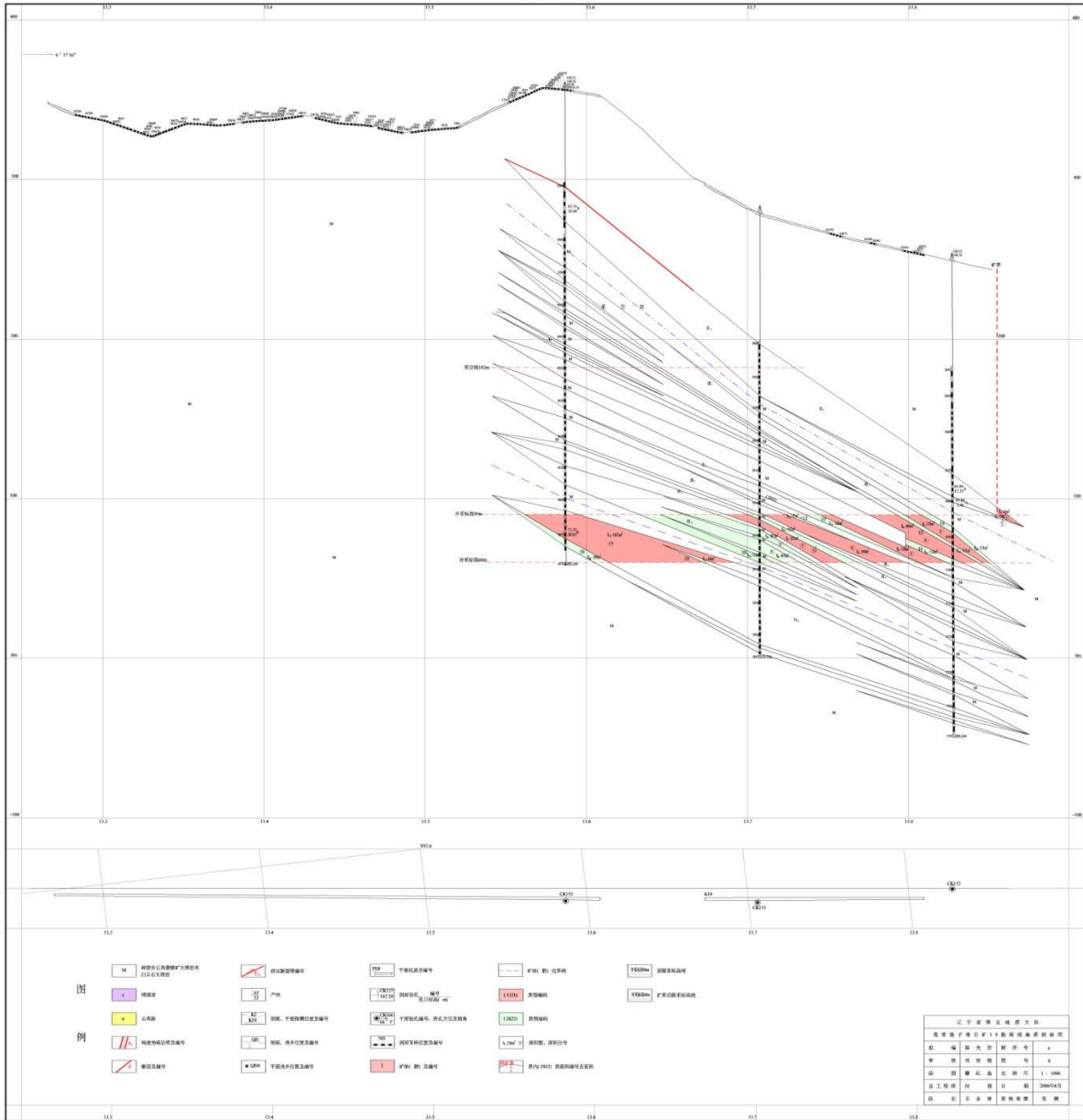
范家堡子滑石矿15勘探线地质剖面图

比例尺 1:1000



范家堡子滑石矿19勘探线地质剖面图

比例尺 1:1000



图例

- M 滑石矿体
- V 构造
- Y 断层
- H 褶皱
- 折线及编号

图例

- 断层带编号
- 产状
- 褶皱、平卧褶皱带编号
- 褶皱、背斜褶皱带编号
- 平卧及平卧褶皱带编号

图例

- 平卧褶皱带编号
- 背斜褶皱带编号
- 平卧褶皱带、背斜褶皱带、平卧褶皱带
- 背斜褶皱带、背斜褶皱带
- 平卧褶皱带、背斜褶皱带
- 矿体、构造带

图例

- 矿体、构造带
- 矿体、构造带
- 矿体、构造带
- 背斜褶皱带、背斜褶皱带

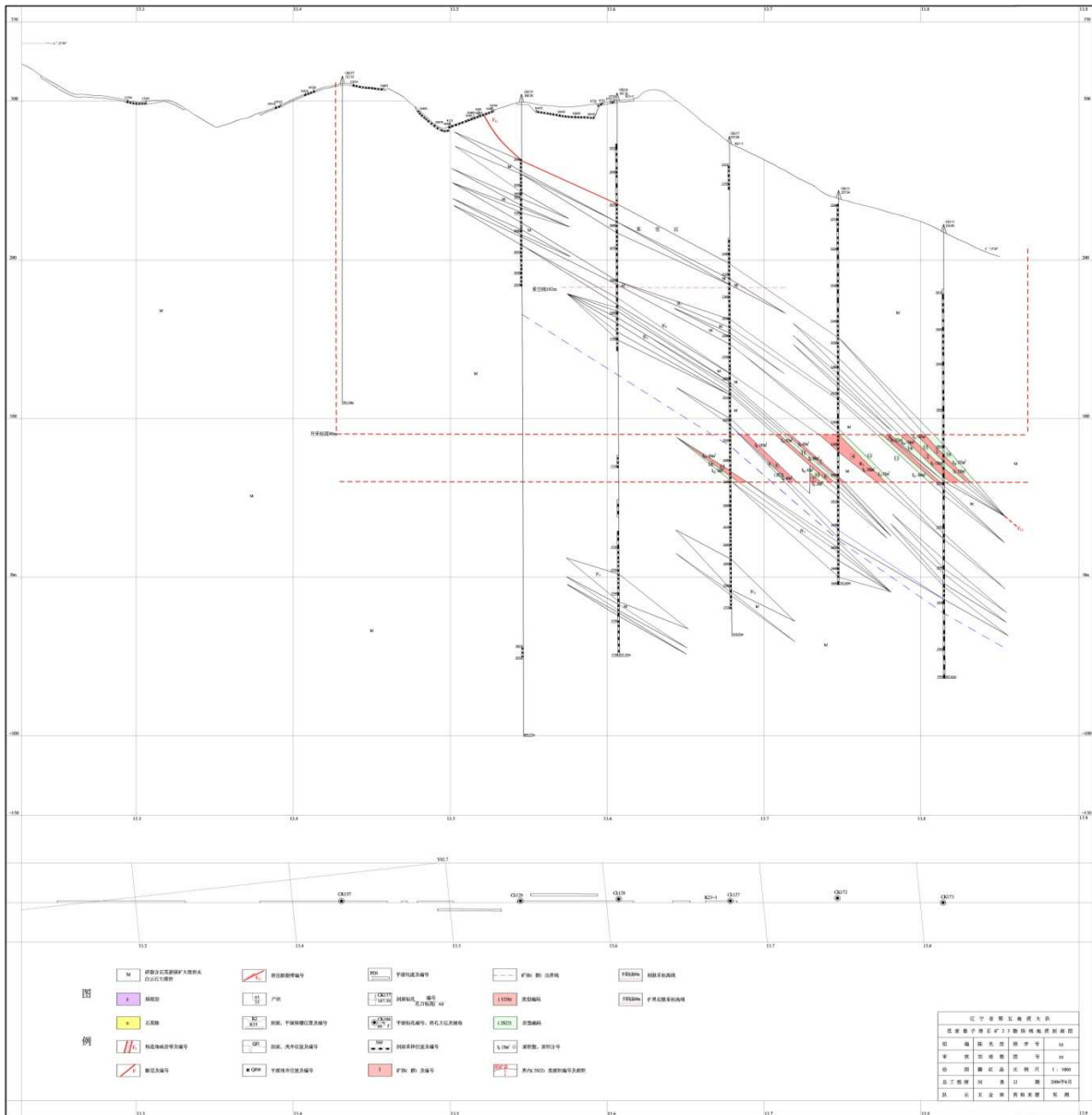
图例

- 构造带编号
- 构造带编号
- 构造带编号
- 背斜褶皱带、背斜褶皱带

辽宁省地质研究所	
范家堡子滑石矿19勘探线地质剖面图	
地质部	地质部
工程地质部	工程地质部
总工程师	总工程师
设计日期	设计日期
比例尺	比例尺
地质部	地质部
地质部	地质部

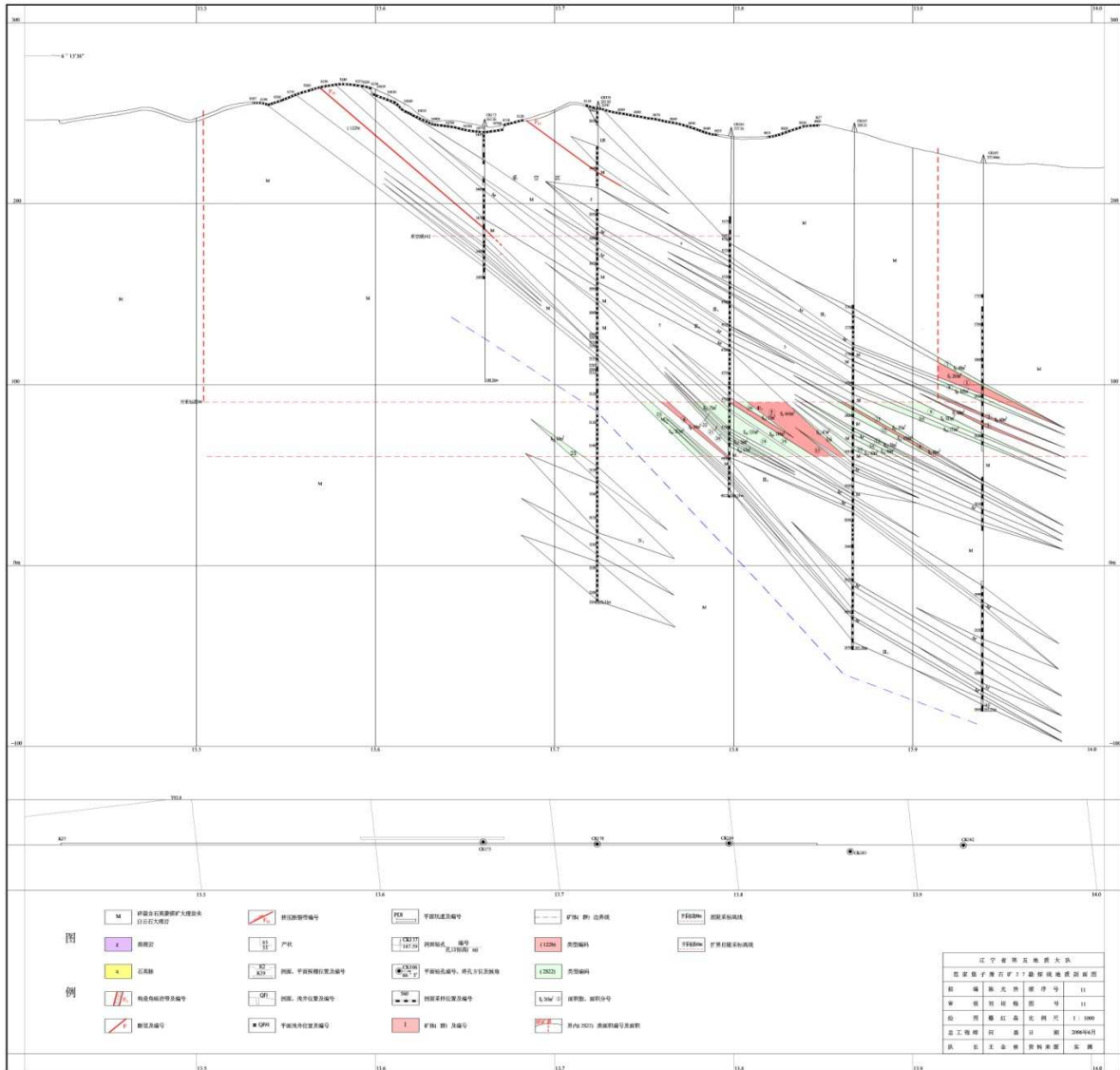
范家堡子滑石矿2-3勘探线地质剖面图

比例尺 1:1000

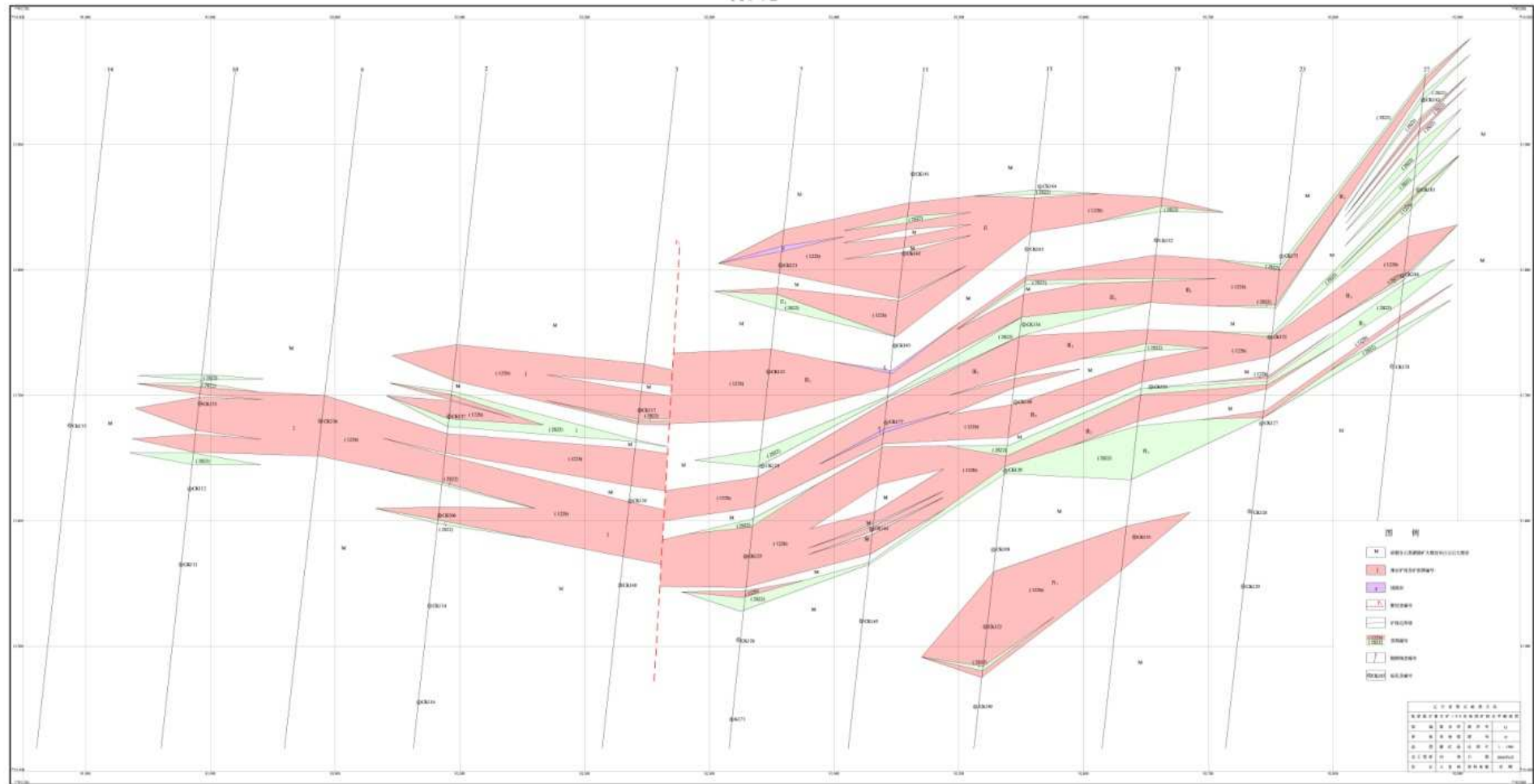


范家堡子滑石矿2.7勘探线地质剖面图

比例尺 1:1000

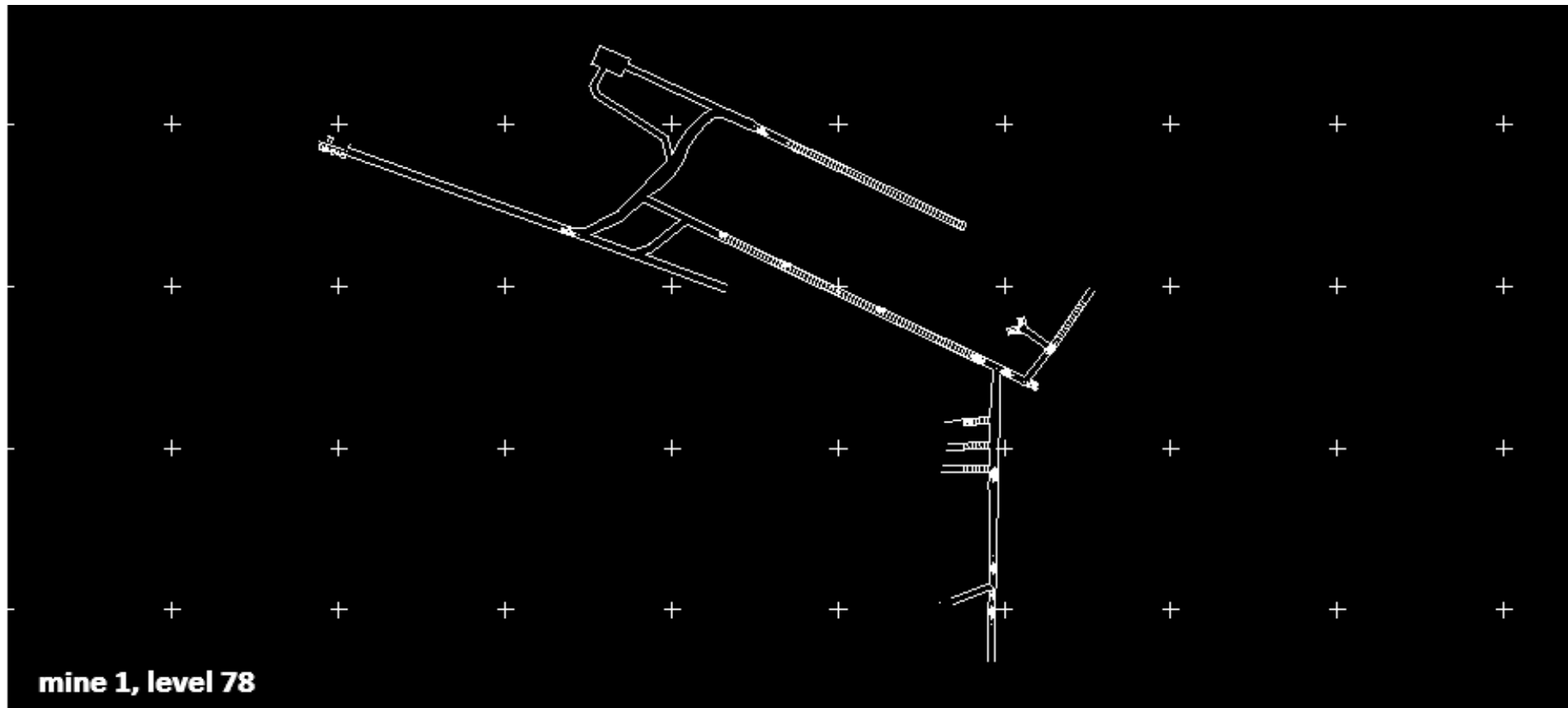


范家堡子滑石矿+90米标高矿体水平断面图



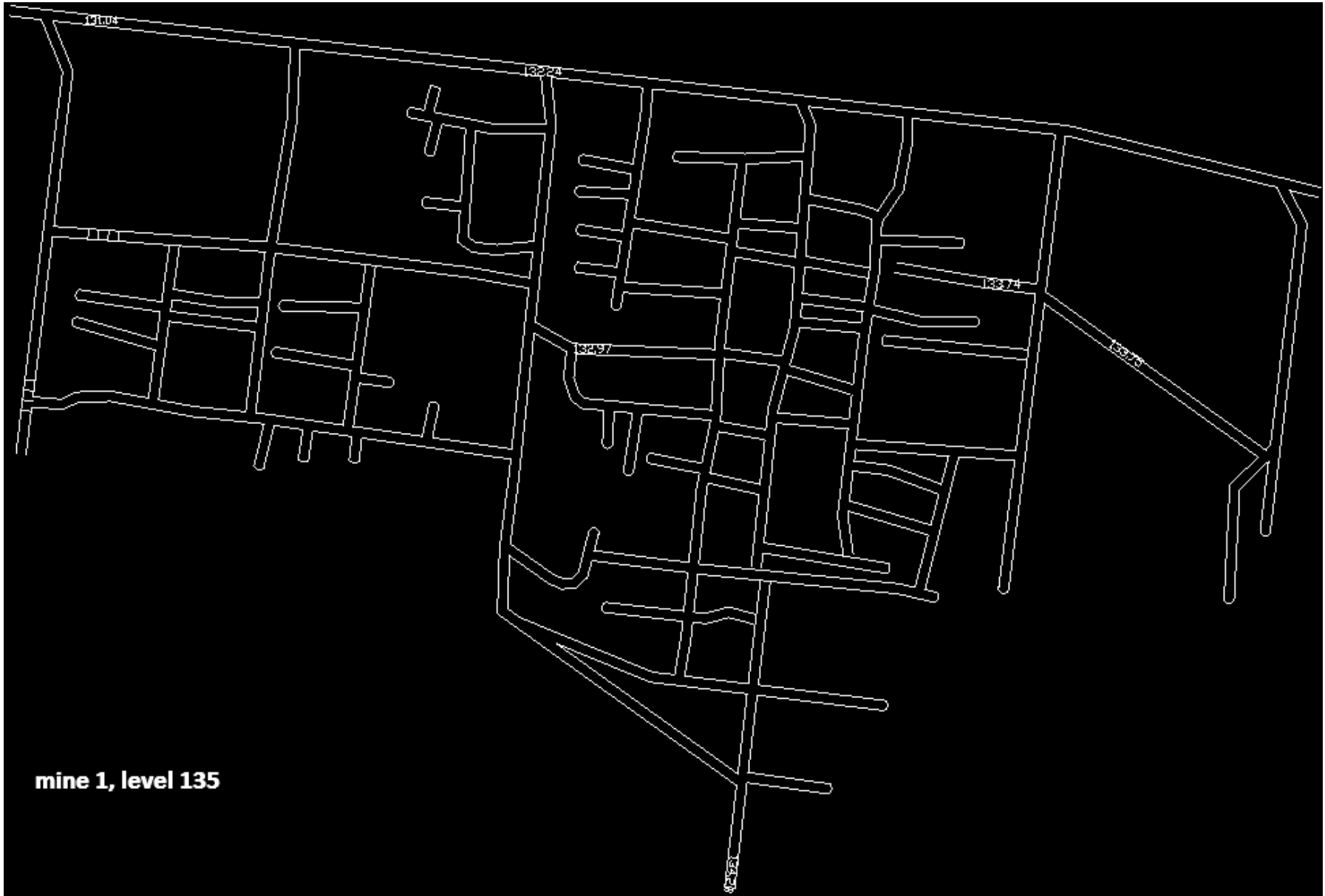
5.5 Mining levels (more detailed information retrievable from digital 3D deposit model (Misch & Pluch, 2009))

5.5.1 Mine 1









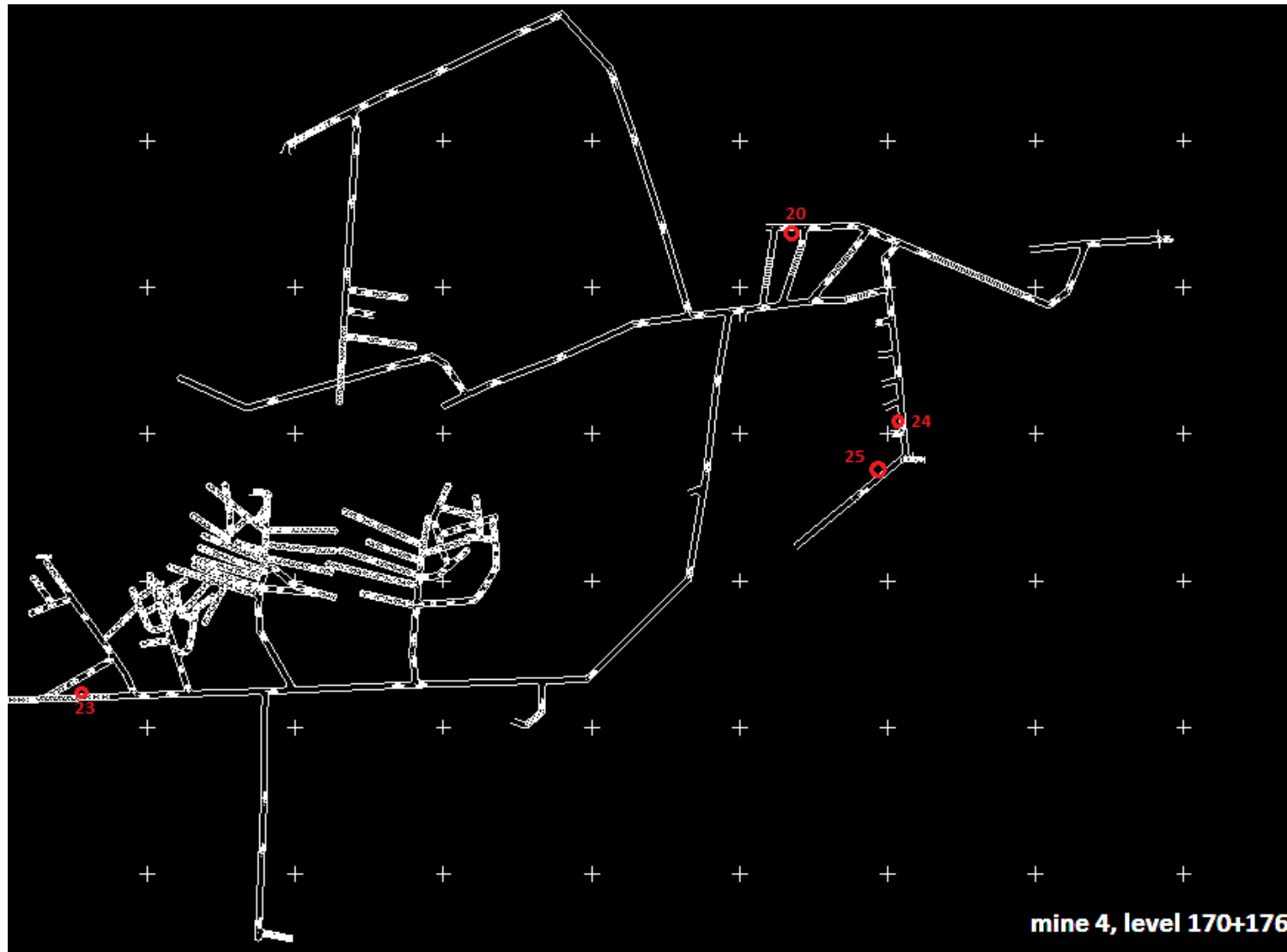


mine 1, level 138



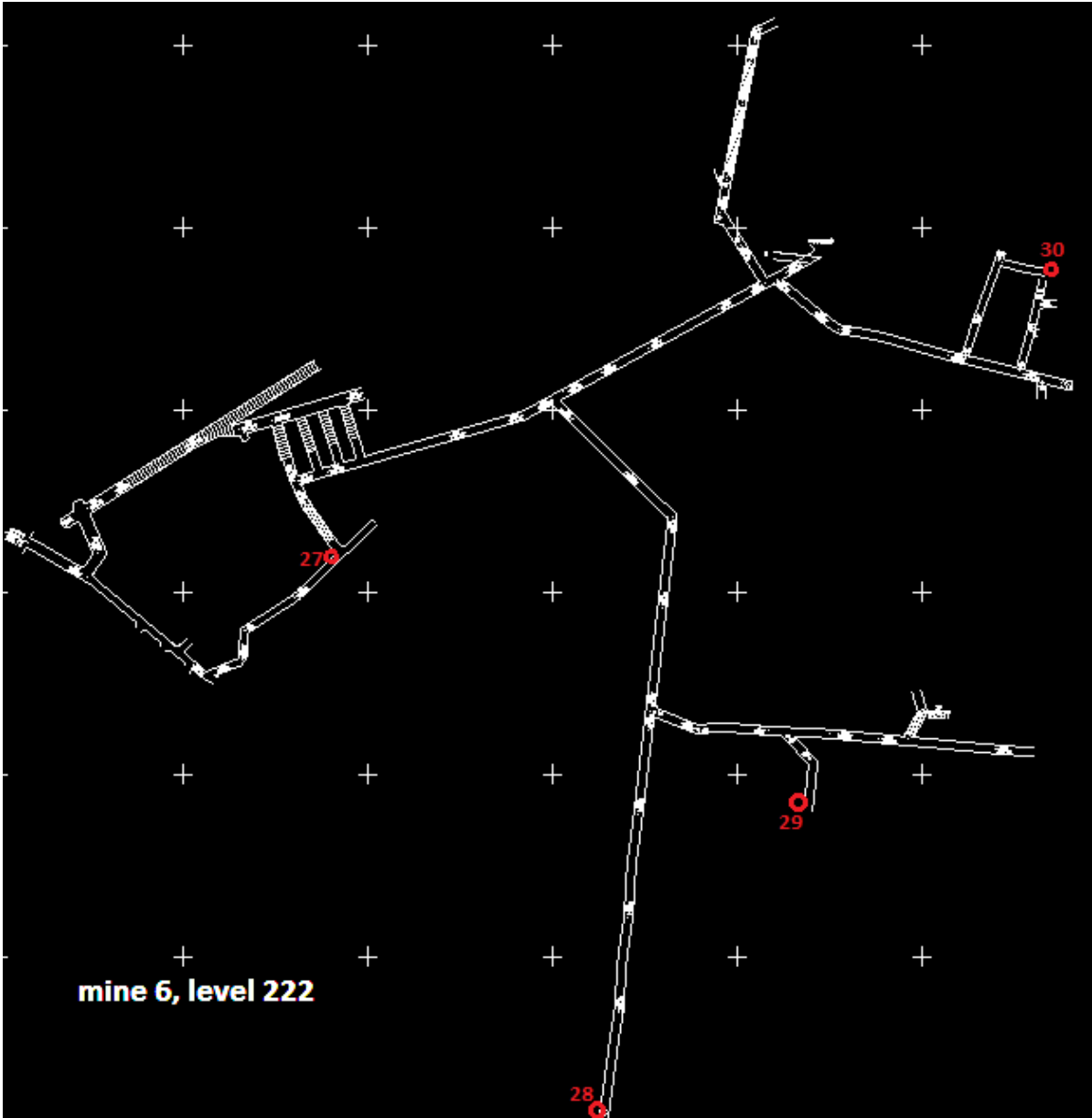


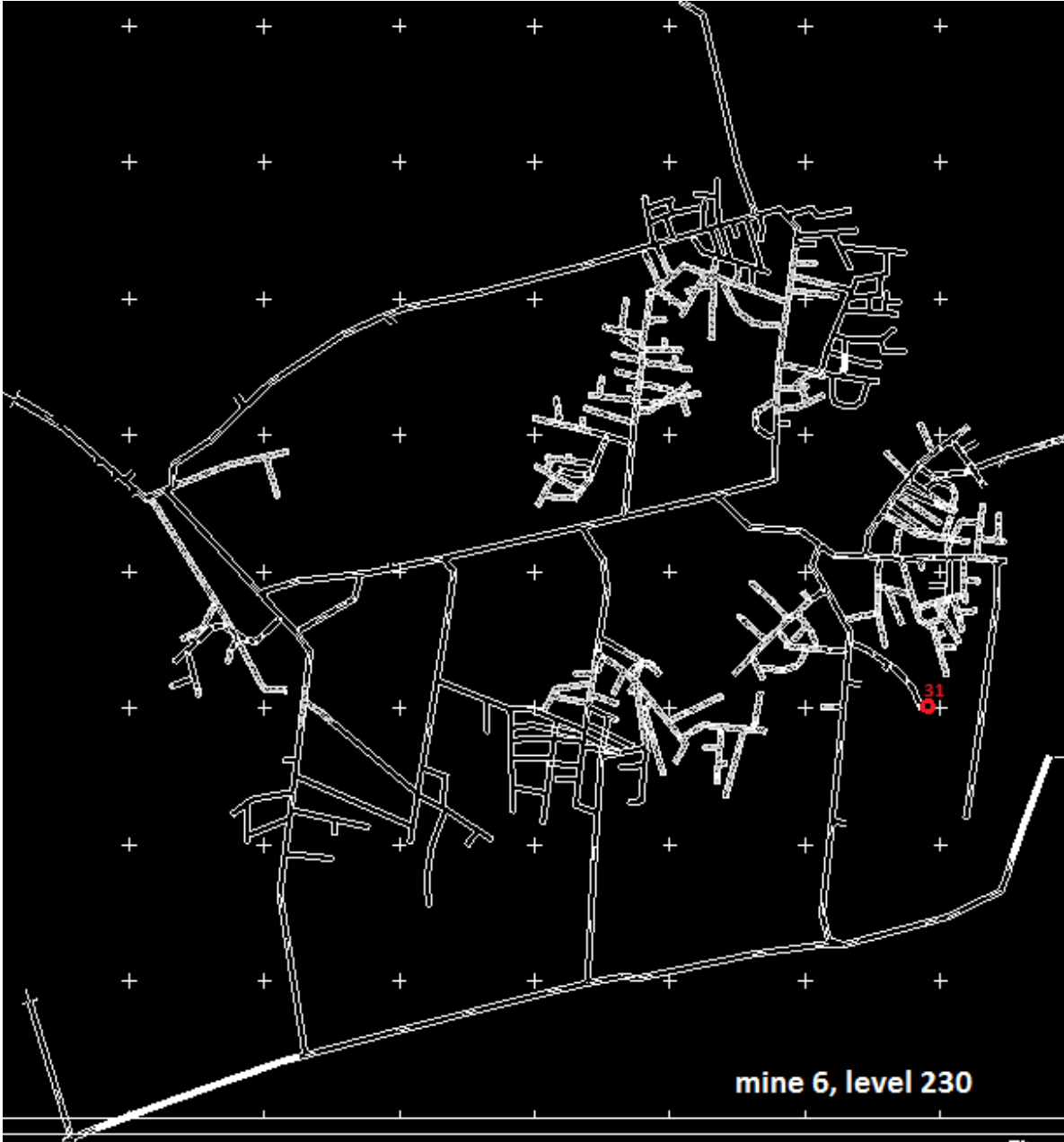
5.5.2 Mine 4





5.5.3 Mine 6





5.6 Chemical Analysis

5.6.1 Talc main elements

Analyte	SiO2	Al2O3	Fe2O3(T)	MnO	MgO	CaO	Na2O	K2O	TiO2	P2O5	LOI	Total
Unit	%	%	%	%	%	%	%	%	%	%	%	%
Detect Limit	0.01	0.01	0.01	0.001	0.01	0.01	0.01	0.01	0.001	0.01		0.01
Method	FUS-ICP	FUS-ICP	FUS-ICP	FUS-ICP	FUS-ICP	FUS-ICP	FUS-ICP	FUS-ICP	FUS-ICP	FUS-ICP	FUS-ICP	FUS-ICP
4_1	63.27	0.04	0.25	< 0.001	30.51	0.06	< 0.01	< 0.01	< 0.001	0.05	4.67	98.84
5_1	42.06	0.05	0.35	0.006	35.73	0.16	< 0.01	< 0.01	< 0.001	0.07	20.71	99.15
1_4	50.78	0.04	0.19	< 0.001	33.83	0.08	< 0.01	< 0.01	< 0.001	< 0.01	13.82	98.76
14_1	55.65	0.08	0.09	< 0.001	32.89	0.24	< 0.01	< 0.01	0.002	0.1	9.69	98.76
14_2	57.99	0.04	0.06	< 0.001	32.64	0.2	< 0.01	< 0.01	< 0.001	0.13	7.75	98.8
15_1	62.3	0.02	0.05	< 0.001	31.43	0.15	< 0.01	< 0.01	< 0.001	0.13	4.8	98.87
15_3	57.22	0.03	0.07	< 0.001	32.9	0.13	< 0.01	< 0.01	< 0.001	0.07	8.71	99.14
18_1	62.6	0.04	0.1	< 0.001	31.89	0.12	< 0.01	< 0.01	< 0.001	0.11	4.83	99.68
18_2	62.23	0.09	0.12	< 0.001	31.67	0.35	< 0.01	< 0.01	0.002	0.06	4.97	99.5
18_3	61.47	0.03	0.17	< 0.001	31.3	0.19	< 0.01	< 0.01	< 0.001	0.17	4.8	98.12
19_1	61.95	0.04	0.22	< 0.001	31.6	0.01	< 0.01	< 0.01	< 0.001	< 0.01	4.96	98.77
19_2	63.26	0.03	0.2	< 0.001	32.2	0.02	< 0.01	< 0.01	< 0.001	< 0.01	4.87	100.6
19_4	43.68	< 0.01	0.18	< 0.001	35.61	0.08	< 0.01	< 0.01	< 0.001	< 0.01	19.2	98.78
20_1	57.23	0.04	0.11	< 0.001	32.08	0.99	< 0.01	< 0.01	< 0.001	0.08	8.09	98.63
23_1	62.46	0.03	0.11	< 0.001	31.01	0.22	< 0.01	< 0.01	< 0.001	0.12	4.97	98.92
26_1	61.6	0.02	0.19	< 0.001	31.88	0.19	< 0.01	< 0.01	< 0.001	0.12	5.63	99.62
26_2	62.89	0.01	0.31	< 0.001	31.56	0.02	< 0.01	< 0.01	< 0.001	< 0.01	4.63	99.4
28_1	34.93	13.28	0.63	< 0.001	35.33	0.19	< 0.01	< 0.01	0.421	0.06	16.15	> 101.0
29_1	62.24	0.06	0.09	< 0.001	31.25	0.08	< 0.01	< 0.01	< 0.001	0.05	4.89	98.65
30_1	62.52	0.06	0.08	< 0.001	31.15	0.15	< 0.01	< 0.01	0.001	0.08	4.72	98.78
31_1	62.17	0.05	0.18	< 0.001	31.38	0.03	< 0.01	< 0.01	< 0.001	< 0.01	4.72	98.53

5.6.2 Talc trace elements

Analyte Symbol	Sc	Be	V	Ba	Sr	Y	Zr	Cr	Co	Ni	Cu	Zn	Ga	Ge
Unit Symbol	ppm	ppm	ppm	ppm	ppm	ppm	ppm	ppm	ppm	ppm	ppm	ppm	ppm	ppm
Detection Limit	1	1	5	3	2	2	4	20	1	20	10	30	1	1
Analysis Method	FUS-ICP	FUS-ICP	FUS-ICP	FUS-ICP	FUS-ICP	FUS-ICP	FUS-ICP	FUS-MS	FUS-MS	FUS-MS	FUS-MS	FUS-MS	FUS-MS	FUS-MS
4_1	<1	<1	5	5	<2	<2	6	<20	<1	<20	<10	<30	<1	<1
5_1	<1	<1	6	4	<2	2	5	<20	<1	<20	<10	<30	<1	<1
1_4	<1	<1	5	5	<2	<2	4	<20	<1	<20	<10	<30	<1	<1
14_1	<1	<1	5	5	<2	<2	6	<20	<1	<20	<10	<30	<1	<1
14_2	<1	<1	<5	4	<2	<2	4	<20	<1	<20	<10	<30	<1	<1
15_1	<1	<1	8	4	<2	<2	5	<20	<1	<20	<10	<30	<1	<1
15_3	<1	<1	<5	4	<2	<2	5	<20	<1	<20	<10	<30	<1	<1
18_1	<1	<1	6	4	<2	<2	<4	<20	2	<20	<10	<30	1	<1
18_2	<1	<1	<5	5	10	<2	7	<20	<1	<20	<10	<30	<1	<1
18_3	<1	<1	6	4	<2	<2	6	<20	<1	<20	<10	<30	<1	2
19_1	<1	<1	6	4	<2	<2	5	<20	<1	30	<10	<30	<1	<1
19_2	<1	<1	<5	4	<2	<2	26	<20	<1	20	<10	<30	<1	<1
19_4	<1	<1	<5	4	<2	<2	5	<20	<1	<20	<10	<30	3	<1
20_1	<1	<1	<5	4	<2	<2	7	<20	<1	<20	<10	<30	<1	<1
23_1	<1	<1	<5	4	<2	<2	5	<20	<1	<20	<10	<30	<1	<1
26_1	<1	<1	<5	4	<2	<2	6	<20	3	<20	<10	<30	1	1
26_2	<1	<1	<5	4	<2	<2	5	<20	2	<20	<10	<30	3	<1
28_1	5	<1	58	5	<2	3	187	60	3	<20	<10	<30	15	<1
29_1	<1	<1	5	4	<2	<2	10	<20	<1	<20	<10	<30	<1	<1
30_1	<1	<1	<5	4	<2	<2	5	<20	<1	<20	<10	<30	<1	<1
31_1	<1	<1	<5	4	<2	<2	<4	<20	1	<20	<10	<30	<1	<1

Analyte Symbol	As	Rb	Nb	Mo	Ag	In	Sn	Sb	Cs	La	Ce	Pr	Nd	Sm
Unit Symbol	ppm	ppm	ppm	ppm	ppm	ppm	ppm	ppm	ppm	ppm	ppm	ppm	ppm	ppm
Detection Limit	5	2	1	2	0.5	0.2	1	0.5	0.5	0.1	0.1	0.05	0.1	0.1
Analysis Method	FUS-MS	FUS-MS	FUS-MS	FUS-MS	FUS-MS	FUS-MS	FUS-MS	FUS-MS	FUS-MS	FUS-MS	FUS-MS	FUS-MS	FUS-MS	FUS-MS
4_1	<5	<2	<1	<2	<0.5	<0.2	<1	<0.5	<0.5	<0.1	<0.1	<0.05	<0.1	<0.1
5_1	<5	<2	<1	<2	<0.5	<0.2	<1	<0.5	<0.5	0.1	0.4	0.06	0.3	<0.1
1_4	<5	<2	<1	<2	<0.5	<0.2	<1	<0.5	<0.5	0.1	0.2	<0.05	0.2	<0.1
14_1	<5	<2	<1	<2	<0.5	<0.2	<1	<0.5	<0.5	<0.1	0.3	0.05	0.1	<0.1
14_2	<5	<2	<1	<2	<0.5	<0.2	<1	<0.5	<0.5	0.1	0.3	<0.05	0.1	<0.1
15_1	<5	<2	<1	<2	<0.5	<0.2	<1	<0.5	<0.5	<0.1	0.1	<0.05	<0.1	<0.1
15_3	<5	<2	<1	<2	<0.5	<0.2	<1	<0.5	<0.5	<0.1	0.3	<0.05	<0.1	<0.1
18_1	<5	<2	<1	<2	<0.5	<0.2	<1	<0.5	<0.5	<0.1	<0.1	<0.05	<0.1	<0.1
18_2	<5	<2	<1	<2	<0.5	<0.2	<1	<0.5	<0.5	0.1	0.3	<0.05	0.2	<0.1
18_3	<5	<2	<1	<2	<0.5	<0.2	<1	0.5	<0.5	<0.1	<0.1	<0.05	<0.1	<0.1
19_1	<5	<2	<1	<2	<0.5	<0.2	<1	<0.5	<0.5	<0.1	<0.1	<0.05	<0.1	<0.1
19_2	<5	<2	<1	<2	<0.5	<0.2	<1	<0.5	<0.5	<0.1	0.2	<0.05	<0.1	<0.1
19_4	<5	<2	<1	<2	<0.5	<0.2	<1	<0.5	<0.5	0.1	0.4	0.07	0.4	0.1
20_1	<5	<2	<1	<2	<0.5	<0.2	<1	<0.5	<0.5	0.1	0.3	<0.05	0.1	<0.1
23_1	<5	<2	<1	<2	<0.5	<0.2	<1	<0.5	<0.5	0.2	0.5	0.07	0.3	<0.1
26_1	<5	<2	<1	<2	<0.5	<0.2	<1	<0.5	<0.5	0.1	0.3	0.05	0.3	<0.1
26_2	<5	<2	<1	<2	<0.5	<0.2	<1	<0.5	<0.5	<0.1	0.2	<0.05	<0.1	<0.1
28_1	<5	<2	8	<2	<0.5	<0.2	2	<0.5	0.6	0.3	0.8	0.14	0.6	0.2
29_1	<5	<2	<1	<2	<0.5	<0.2	<1	<0.5	<0.5	<0.1	<0.1	<0.05	<0.1	<0.1
30_1	<5	<2	<1	<2	<0.5	<0.2	<1	<0.5	<0.5	<0.1	<0.1	<0.05	<0.1	<0.1
31_1	<5	<2	<1	<2	<0.5	<0.2	<1	<0.5	<0.5	<0.1	<0.1	<0.05	<0.1	<0.1

Analyte Symbol	Eu	Gd	Tb	Dy	Ho	Er	Tm	Yb	Lu	Hf	Ta
Unit Symbol	ppm	ppm	ppm	ppm	ppm	ppm	ppm	ppm	ppm	ppm	ppm
Detection Limit	0.05	0.1	0.1	0.1	0.1	0.1	0.05	0.1	0.04	0.2	0.1
Analysis Method	FUS-MS	FUS-MS	FUS-MS	FUS-MS	FUS-MS	FUS-MS	FUS-MS	FUS-MS	FUS-MS	FUS-MS	FUS-MS
4_1	< 0.05	< 0.1	< 0.1	< 0.1	< 0.1	< 0.1	< 0.05	< 0.1	< 0.04	< 0.2	< 0.1
5_1	< 0.05	< 0.1	< 0.1	< 0.1	< 0.1	< 0.1	< 0.05	< 0.1	< 0.04	< 0.2	< 0.1
1_4	< 0.05	< 0.1	< 0.1	< 0.1	< 0.1	< 0.1	< 0.05	< 0.1	< 0.04	< 0.2	< 0.1
14_1	< 0.05	< 0.1	< 0.1	< 0.1	< 0.1	< 0.1	< 0.05	< 0.1	< 0.04	< 0.2	< 0.1
14_2	< 0.05	< 0.1	< 0.1	< 0.1	< 0.1	< 0.1	< 0.05	< 0.1	< 0.04	< 0.2	< 0.1
15_1	< 0.05	< 0.1	< 0.1	< 0.1	< 0.1	< 0.1	< 0.05	< 0.1	< 0.04	< 0.2	< 0.1
15_3	< 0.05	< 0.1	< 0.1	< 0.1	< 0.1	< 0.1	< 0.05	< 0.1	< 0.04	< 0.2	< 0.1
18_1	< 0.05	< 0.1	< 0.1	< 0.1	< 0.1	< 0.1	< 0.05	< 0.1	< 0.04	< 0.2	0.1
18_2	< 0.05	< 0.1	< 0.1	< 0.1	< 0.1	< 0.1	< 0.05	< 0.1	< 0.04	< 0.2	< 0.1
18_3	< 0.05	< 0.1	< 0.1	< 0.1	< 0.1	< 0.1	< 0.05	< 0.1	< 0.04	< 0.2	< 0.1
19_1	< 0.05	< 0.1	< 0.1	< 0.1	< 0.1	< 0.1	< 0.05	< 0.1	< 0.04	< 0.2	< 0.1
19_2	< 0.05	< 0.1	< 0.1	< 0.1	< 0.1	< 0.1	< 0.05	< 0.1	< 0.04	< 0.2	< 0.1
19_4	< 0.05	0.2	< 0.1	0.2	< 0.1	< 0.1	< 0.05	< 0.1	< 0.04	< 0.2	< 0.1
20_1	< 0.05	< 0.1	< 0.1	< 0.1	< 0.1	< 0.1	< 0.05	< 0.1	< 0.04	< 0.2	< 0.1
23_1	< 0.05	< 0.1	< 0.1	< 0.1	< 0.1	< 0.1	< 0.05	< 0.1	< 0.04	< 0.2	< 0.1
26_1	< 0.05	< 0.1	< 0.1	< 0.1	< 0.1	< 0.1	< 0.05	< 0.1	< 0.04	< 0.2	< 0.1
26_2	< 0.05	< 0.1	< 0.1	< 0.1	< 0.1	< 0.1	< 0.05	< 0.1	< 0.04	< 0.2	< 0.1
28_1	0.06	0.3	< 0.1	0.4	< 0.1	0.4	0.07	0.6	0.11	4.4	0.8
29_1	< 0.05	< 0.1	< 0.1	< 0.1	< 0.1	< 0.1	< 0.05	< 0.1	< 0.04	< 0.2	< 0.1
30_1	< 0.05	< 0.1	< 0.1	< 0.1	< 0.1	< 0.1	< 0.05	< 0.1	< 0.04	< 0.2	< 0.1
31_1	< 0.05	< 0.1	< 0.1	< 0.1	< 0.1	< 0.1	< 0.05	< 0.1	< 0.04	< 0.2	< 0.1

5.6.3 Talc whiteness and yellowness index

sample no.	X	whiteness	Z	x	y	Rem 457 [%]	L*	a*	b*	C*ab	b*/a*	color (rock)	yellowness index
4_1	90,23	95,12	99,99	0,32	0,33	93,35	98,08	0,08	1,37	1,37	16,08	yellow-light brown	2,63
14_2	88,23	92,75	98,63	0,32	0,33	92,00	97,13	0,54	0,61	0,81	1,12	pink	1,58
15_1	89,81	94,49	100,00	0,32	0,33	93,56	97,83	0,41	0,92	1,01	2,26	pink	2,06
15_3	88,36	92,91	98,54	0,32	0,33	91,89	97,19	0,50	0,78	0,93	1,55	pink	1,87
18_1	82,23	86,70	92,55	0,31	0,33	86,32	94,61	0,06	0,35	0,36	6,12	grey	0,74
18_3	89,94	95,00	99,84	0,32	0,33	93,32	98,03	-0,24	1,38	1,40	5,86	yellow	2,42
19_1	87,51	92,37	96,51	0,32	0,33	90,22	96,97	-0,12	1,74	1,75	14,26	brown-grey	3,21
19_2	88,70	93,50	97,82	0,32	0,33	91,34	97,43	0,10	1,67	1,67	17,21	yellow-light brown	3,21
20_1	86,33	90,87	95,86	0,32	0,33	89,47	96,36	0,33	1,12	1,17	3,39	? (powder)	2,39
26_1	86,03	90,60	93,85	0,32	0,34	87,73	96,25	0,25	2,28	2,30	9,20	brown	4,52
29_1	87,69	92,35	97,35	0,32	0,33	90,94	96,96	0,25	1,17	1,20	4,76	grey	2,41
30_1	85,30	89,86	94,67	0,32	0,33	88,42	95,94	0,20	1,20	1,21	6,12	grey-brown	2,45
31_1	87,31	92,13	98,09	0,31	0,33	91,51	96,87	-0,07	0,53	0,53	7,39	white	0,96
D60	86,65	91,39	97,14	0,31	0,33	90,65	96,57	0,01	0,63	0,63	108,12	mix yellow, pink, grey	1,22

5.6.4 Magnesite AAS

Sampling Area	Sample No.	results [%]	Fe	Mn	Ni	Ca	Sr	Al
Aihai Talc	15_2		0,0977	0,0063	<0,00001	0,5337	<0,000001	0,0834
Aihai Talc	15_4		0,1349	0,0073	<0,00001	0,6965	<0,000001	0,0848
Aihai Talc	1_3		0,2407	0,0106	<0,00001	0,3146	<0,000001	0,0430
Aihai Talc	20_2		0,2128	0,0122	<0,00001	0,2961	<0,000001	0,0921
Aihai Talc	26_3		0,2061	0,0068	<0,00001	0,3894	<0,000001	0,0457
		Σ	0,1785	0,0086	<0,00001	0,4461	<0,000001	0,0698

Sampling Area	Sample No.	results [%]	Fe	Mn	Ni	Ca	Sr	Al	
Aihai Magnesite	20_1		0,0128	0,0022	0,0016	21,9659	0,0014	0,0411	
Aihai Magnesite	13_2		0,0493	0,0027	<0,00001	0,6009	0,0005	0,0791	
Aihai Magnesite	19_2		0,2605	0,0175	<0,00001	0,4385	<0,000001	0,0383	
Aihai Magnesite	13_1		0,1748	0,0080	<0,00001	0,7989	0,0007	0,3795	
Aihai Magnesite	15_1		0,1229	0,0060	<0,00001	0,4586	<0,000001	0,0427	
Aihai Magnesite	15_2		0,1448	0,0093	<0,00001	0,5637	<0,000001	0,0343	
Aihai Magnesite	21_2		0,1001	0,0051	<0,00001	5,3370	0,0003	0,0548	
Aihai Magnesite	16_2		0,0905	0,0051	<0,00001	0,8009	<0,000001	0,0561	
Aihai Magnesite	8_9		0,7064	0,0319	<0,00001	0,4904	0,0002	0,0715	
Aihai Magnesite	8_10		1,1121	0,0480	<0,00001	6,8081	0,0041	0,3531	
Aihai Magnesite	8_4		0,0956	0,0039	<0,00001	0,3943	0,0002	0,0592	
Aihai Magnesite	8_8		0,0814	0,0040	<0,00001	1,2624	0,0003	0,0941	
Aihai Talc	11_3		0,3424	0,0200	<0,00001	0,5550	<0,000001	0,0581	
Aihai Talc	14_3		0,1931	0,0100	<0,00001	0,6944	0,0002	0,0604	
Aihai Talc	7_1		0,1016	0,0061	<0,00001	0,8575	<0,000001	0,0363	
Aihai Talc	11_2		0,1962	0,0099	<0,00001	0,9091	<0,000001	0,0638	
Aihai Talc	16_1		0,1646	0,0093	<0,00001	0,8897	0,0001	0,0987	
Aihai Talc	10_1		0,2630	0,0134	<0,00001	0,9222	<0,000001	0,0922	
Aihai Talc	33_1		0,1331	0,0197	<0,00001	17,3677	0,0024	0,0458	
			Σ	0,2287	0,0122	0,0001	3,2692	0,0005	0,0926

5.6.5 Magnesite whiteness and yellowness index

sample no.	X	whiteness	Z	x	y	Rem 457 [%]	L*	a*	b*	C*ab	b*/a*	structure	yellowness index
1_3	87,99	92,74	98,00	0,32	0,33	91,44	97,12	0,12	1,02	1,02	8,70	fine, massive talc (surface)	2,02
7_1	87,34	91,87	97,15	0,32	0,33	90,61	96,77	0,44	0,97	1,06	2,18	fine, massive talc (surface)	2,18
10_1	83,77	88,36	92,40	0,32	0,33	86,31	95,31	-0,01	1,66	1,66	211,75	coarse, no talc	3,19
11_2	86,61	91,15	94,70	0,32	0,33	88,46	96,47	0,36	2,10	2,13	5,89	coarse, no talc	4,24
11_3	84,21	88,63	90,66	0,32	0,34	84,78	95,43	0,34	3,06	3,08	8,94	coarse, no talc	6,08
14_3	85,94	90,58	95,84	0,32	0,33	89,41	96,24	0,11	0,93	0,93	8,07	fine, shearzone talc	1,86
15_2	89,63	94,31	100,30	0,32	0,33	93,52	97,76	0,39	0,60	0,72	1,54	fine, shearzone talc	1,45
15_4	87,92	92,59	98,10	0,32	0,33	91,50	97,06	0,25	0,84	0,88	3,37	fine, shearzone talc	1,80
16_1	88,56	93,36	98,73	0,32	0,33	92,11	97,37	0,08	0,97	0,97	11,60	fine, no talc	1,90
20_2	88,34	93,09	98,77	0,32	0,33	92,14	97,26	0,15	0,75	0,77	5,03	fine, shearzone talc	1,55
26_3	88,45	93,25	97,90	0,32	0,33	91,39	97,33	0,07	1,44	1,44	19,69	fine, massive talc (surface)	2,77
33_1	87,95	92,57	98,30	0,32	0,33	91,67	97,05	0,34	0,70	0,78	2,05	fine, shearzone talc	1,59

5.6.6 Main element content for selected samples from Aihai Magnesite

Analyte	SiO2	Al2O3	Fe2O3(T)	MnO	MgO	CaO	Na2O	K2O	TiO2	P2O5	LOI	Total
Unit	%	%	%	%	%	%	%	%	%	%	%	%
Anal Meth	FUS-ICP	FUS-ICP	FUS-ICP	FUS-ICP	FUS-ICP	FUS-ICP	FUS-ICP	FUS-ICP	FUS-ICP	FUS-ICP	FUS-ICP	FUS-ICP
8-1	0,63	0,09	1,09	0,058	46,73	0,58	0,02	0,01	0,008	< 0,01	51,36	100,6
8-4	0,27	0,03	0,17	0,008	48,56	0,33	< 0,01	< 0,01	0,002	0,03	51,59	101
8-8	0,74	0,12	0,17	0,008	47,35	1,11	< 0,01	< 0,01	0,004	0,35	50,57	100,4
8-9	0,47	0,02	0,84	0,049	47,74	0,4	< 0,01	< 0,01	< 0,001	0,07	51,32	100,9
11-2	0,55	0,07	0,24	0,012	47,16	1,14	< 0,01	< 0,01	0,002	0,43	50,78	100,4
13-2	0,47	0,15	0,12	0,006	47,51	0,76	< 0,01	< 0,01	0,004	< 0,01	51,07	100,1
15-1	0,22	0,07	0,33	0,013	47,43	0,45	0,01	0,02	0,002	0,01	51,34	99,91
15-2	0,24	0,04	0,33	0,021	47,78	0,6	< 0,01	< 0,01	0,004	0,07	51,25	100,3
16-1	0,48	0,12	0,22	0,01	47,96	0,59	< 0,01	0,03	0,004	0,02	51,26	100,7
19-2	0,06	0,03	0,57	0,036	47,12	0,33	< 0,01	< 0,01	0,002	< 0,01	51,31	99,48

5.6.7 Carbon and oxygen isotope distribution of selected magnesite samples from the Fanjiabauzi deposit

Sample No.	d18O/16O VPDB	d13C/12C VPDB
20_2	-16,51237	0,78137
16_1	-17,42927	0,88037
11_2	-17,37147	0,44317
1_3	-16,10627	0,11797
33_1	-17,94047	0,26187
10_1	-17,80427	0,77007
15_4	-17,47447	0,39717
14_3	-16,54597	0,39307
15_2	-17,39417	0,74577
7_1	-18,26997	-0,05573
11_3	-16,72967	0,70487
26_3	-16,46447	-0,35743
11_2	-17,11257	0,05707
20_2	-16,88047	0,63027
16_1	-17,76857	0,81237
1_3	-16,16667	0,11757
33_1	-17,98217	0,27387
10_1	-17,60487	0,87577
15_4	-17,34167	0,40857
14_3	-16,84587	0,60017
26_3	-16,34887	-0,61133
15_2	-17,26387	0,46517
11_3	-16,81627	0,69357
average	-17,13803087	0,408939565

5.7 Structural Data

5.7.1 Mine 1

plane type	dip direction	dip	description	level
f	210	55		90
f	188	50		90
f	178	35		90
f	130	40		90
f	268	45		90
f	310	35		90
f	176	35		90
f	178	40		90
f	198	55		90
f	110	45		90
f	130	45		90
f	110	58		90
f	240	40	large, open fault	90
f	228	40		90
f	108	30		90
f	184	45		90
f	160	45		90
f	152	40		90
f	110	40		90
f	110	55	dextral	90
f	148	45	sinistral	84
f	150	50		84
f	72	75		84
f	340	60		84
f	340	65	Normal fault	84
f	204	40		84
f	92	30		84
f	260	75		84
f	102	88	dextral	84
ss	170	60		90
ss	172	75		90
f	188	50		90
f	178	65	sinistral	90
f	178	60		90
ss,f	178	65		90
ss,f	178	38		90
ss,f	162	50		90
ss,f	176	40		90
f	48	40		90

5.7.2 Mine 4

plane type	dip direction	dip	description	level
f		290	35 Abschiebung, geschlossen, weisse Stoerungslette	187
f		288	40 Abschiebung, geschlossen, weisse Stoerungslette	187
f		270	35 Abschiebung, geschlossen, weisse Stoerungslette	187
l		240	60 Abschiebung, geschlossen, weisse Stoerungslette	187
f		340	25 Seitenverschiebung, sinistral, geschlossen, weisse Stoerungslette, vertalkt	182
f		15	20 Seitenverschiebung, sinistral, geschlossen, weisse Stoerungslette, vertalkt	182
f		30	30 Seitenverschiebung, sinistral, geschlossen, weisse Stoerungslette, vertalkt	182
f		350	15 Seitenverschiebung, sinistral, geschlossen, weisse Stoerungslette, vertalkt	182
f		40	30 Seitenverschiebung, sinistral, geschlossen, weisse Stoerungslette, vertalkt	182
f		40	28 Seitenverschiebung, sinistral, geschlossen, weisse Stoerungslette, vertalkt	182
f		28	28 Seitenverschiebung, sinistral, geschlossen, weisse Stoerungslette, vertalkt	182
l		91	1 Seitenverschiebung, sinistral, geschlossen, weisse Stoerungslette, vertalkt	182
f			Quarzgaenge im Magnesit, Nebengestein Stark verkieselt, M.n.m.	176
f			Diabas, Messung nicht moeglich wegen Stahltraeger	176
f		360	45 geschlossen, ohne Stoerungslette	176
f		70	45 geoeffnet, mit Talk verfuellt (10cm-20cm)	176
f		80	55 geoeffnet, mit Talk verfuellt (10cm-20cm)	176
f		10	45 geschlossen, ohne Stoerungslette	176
f		360	40 geschlossen, ohne Stoerungslette	176
f		28	75	176
f		1	88 Abschiebung, geschlossen, mit Talk verfuellt	176
f		320	55 Harnischflaeche vertalkt	176
f		325	60 Harnischflaeche vertalkt	176
f		100	70 verkieselter Magnesit, geoeffnet, talkfuehrend	176
f		110	40 verkieselter Magnesit, geoeffnet, talkfuehrend	176
f		110	55 Abschiebung, geschlossen, verkieselter Magnesit	176
f		105	60 Abschiebung, geschlossen, verkieselter Magnesit	176
f		305	88 geoeffnet, mit Talk verfuellt, dextral, verkieselter Magnesit	176
f		310	87 geoeffnet, mit Talk verfuellt, dextral, verkieselter Magnesit	176
f		20	50 Seitenverschiebung, dextral, geoeffnet, talkfuehrend	176
f		10	35 Seitenverschiebung, dextral, geoeffnet (10cm-15cm), talkfuehrend	176
l		290	10 Seitenverschiebung, dextral, geoeffnet (10cm-15cm), talkfuehrend	176
f		310	75 Magnesit ist vertalkt und verkieselt, MT-T3	176
f		310	75 Magnesit ist vertalkt und verkieselt, MT-T4	176
f		320	80 Magnesit ist vertalkt und verkieselt, MT-T5	176
f		350	35 Ortsbrust, T3, wert geschaezt	176
f		56	45 geschlossen, dunkelgruener Stoerungslette (Diabas)	176
f		40	45 geschlossen, dunkelgruener Stoerungslette (Diabas)	176
f		60	35 geschlossen, dunkelgruener Stoerungslette (Diabas)	176
f		160	75 Seitenverschiebung, sinistral, geschlossen, weiss-graue Stoerungslette	176
f		160	80 Seitenverschiebung, sinistral, geschlossen, weiss-graue Stoerungslette	176
f		162	76 Seitenverschiebung, sinistral, geschlossen, weiss-graue Stoerungslette	176
f		346	70 Abschiebung, geschlossen	176
f		330	65 Abschiebung, geschlossen	176
ss		300	60 Baenderung im Magnesit, Stoerungen laufen parallel zu ss	176
ss		320	55 Baenderung im Magnesit, Stoerungen laufen parallel zu ss	176
ss		325	40 Baenderung im Magnesit, Stoerungen laufen parallel zu ss	176
ss		318	52 Baenderung im Magnesit, Stoerungen laufen parallel zu ss	176
ss		326	68 Baenderung im Magnesit, Stoerungen laufen parallel zu ss	176
ss		316	72 Baenderung im Magnesit, Stoerungen laufen parallel zu ss	176
ss		348	72 Baenderung im Magnesit, Stoerungen laufen parallel zu ss	176
ss		323	55 Baenderung im Magnesit, Stoerungen laufen parallel zu ss	176
ss		324	74 Baenderung im Magnesit, Stoerungen laufen parallel zu ss	176
f		320	60 Ortsbrust, T3, SiO2-Gehalt zw. 52-57%	176
			Ortsbrust, T1, SiO2-Gehalt zw. 52-57%, M.n.m	176
			Ortsbrust, T1, SiO2-Gehalt zw. 52-57%, M.n.m	176
			Ortsbrust, T1, SiO2-Gehalt zw. 52-57%, M.n.m	176
f		200	68 Stoerungsbrekzie (0.8m-1m), Magnesit, Strecke verlaeuft parallel zur f	176
f		180	50 Stoerungsbrekzie (0.8m-1m), Magnesit, Strecke verlaeuft parallel zur f	176

5.7.3 Mine 6

plane type	dip direction	dip	description	level
f		252	48 stark silif. Magnesit	222
f		256	45 stark silif. Magnesit	222
f		242	40 stark silif. Magnesit	222
f		214	70 stark silif. Magnesit	222
f	ca. W	ca. 50-60	grosse Störungszone, Kataklasit-Magnesit+Talk+qrz-Klasten, ca. 5m mächtig	222
f		5	15 Abschiebung mit Kataklasit	222
f		20	20 Abschiebung mit Kataklasit	222
f		244	40 Magnesit, Störungsbrechie 10cm, dextral	222
f		254	45 vertalkt	222
f		340	70 Ortsbrust, tektonischer Kontakt zw. T3 und MT	222
f		347	75 Ortsbrust, tektonischer Kontakt zw. T3 und MT	222
f		327	80 Ortsbrust, tektonischer Kontakt zw. T3 und MT	222
f		240	40 Störung im Magnesit, mit Störungslette+qrz-Klasten	222
f		235	40 Störung im Magnesit, mit Störungslette+qrz-Klasten	222
s?		210	50 DIABAS?,stark silif., Bänderung, ca. 0,5m mächtig	222
s?		240	55 DIABAS?,stark silif., Bänderung, ca. 0,5m mächtig	222
s?		208	45 DIABAS?,stark silif., Bänderung, ca. 0,5m mächtig	222
s?		222	30 DIABAS?,stark silif., Bänderung, ca. 0,5m mächtig	222
s?		190	55 DIABAS?,stark silif., Bänderung, ca. 0,5m mächtig	222
s?		208	75 Magnesit, stark silif., gebändert	230
s?		280	55 Magnesit, stark silif., gebändert	230
s?		162	50 Bänderung	230
s?		186	55 Bänderung	230
f		344	58 Ortsbrust, T3, ca. 0,4m Talkbänder	230
f		330	50 Störung im Magnesit, Störungsbrechie, im Kontaktbereich Talk	230
f		322	45 Störung im Magnesit, Störungsbrechie, im Kontaktbereich Talk	230
f		302	65 Störung im Magn., mit Talk(T3) ca. 0,4m mächtig	230
f		300	65 Störung im Magn., mit Talk(T3) ca. 0,4m mächtig	230
f		330	18 Störung im Magnesit mit weisser Störungslette	230
			Ortsbrust, T2, keine Messungen möglich	230
f		248	65 Störung mit Störungsbrechie, vertalkt ca. 0,2m, Umgebung stark silif.	230
f		256	72 Störung mit Störungsbrechie, vertalkt ca. 0,2m, Umgebung stark silif.	230
f		258	68 Störung mit Störungsbrechie, vertalkt ca. 0,2m, Umgebung stark silif.	230
f		280	60 T1 umgeben von MT, Umgebung stark silif.	230
f		285	70 T1 umgeben von MT, Umgebung stark silif.	230
f		2	1 Harnischfläche vertalkt, Liegendblock geht nach N	230
f		20	40 Störung im Magnesit 0,1-0,2m vertalkt, Abschbg, geschlossen	230
f		18	35 Störung im Magnesit 0,1-0,2m vertalkt, Abschbg, geschlossen	230
f		18	40 Störung im Magnesit 0,1-0,2m vertalkt, Abschbg, geschlossen	230
f		354	54 Störung im Magnesit 0,1-0,2m vertalkt, Abschbg, geschlossen,qrz	230
f		342	65 Störung im Magnesit 0,1-0,2m vertalkt, Abschbg, geschlossen,qrz	230
f		352	70 Störung im Magnesit 0,1-0,2m vertalkt, Abschbg, geschlossen,qrz	230
f		2	1 nicht vertalkt, Liegendblock geht nach S	230
f		80	65 St. im Magnesit, talkführend 0,1-0,3m, geschlossen	230
f		350	35 Störung im Magnesit, charakteristischer Aufbau siehe Aufzeichnungen	230
f		352	35 Störung im Magnesit, charakteristischer Aufbau siehe Aufzeichnungen	230
f		352	38 Störung im Magnesit, charakteristischer Aufbau siehe Aufzeichnungen	230
f		18	40 Störung im Magnesit, charakteristischer Aufbau siehe Aufzeichnungen	230
f		8	32 Störung im Magnesit, charakteristischer Aufbau siehe Aufzeichnungen	230
f		10	40 Störung im Magnesit, charakteristischer Aufbau siehe Aufzeichnungen	230
f		258	52 Störung im Magnesit, vertalkt 0,1-0,2m, Seitenverschiebung sinistral, geschlos	230
f		252	30 Störung im Magnesit, vertalkt 0,1-0,2m, Seitenverschiebung sinistral, geschlos	230
f		350	45 Quarzgang 5-6m, Umgebung T1	230
f		348	44 Quarzgang 5-6m, Umgebung T2	230
f		2	40 Quarzgang 5-6m, Umgebung T3	230
f			Quarzgang umgeben von T1	230
f			Quarzgang umgeben von T2	230
			Ortsbrust MT	230
			Ortsbrust Magnesit	230
f			Störung mit Lamprophyr	230
f		135	80 Störung mit Lamprophyr	230
f		320	85 Störung mit Lamprophyr	230
f		344	48 Störung im Magnesit, talkführend 0,2-0,3m, geschlossen	230
f		36	45 Störung im Magnesit, talkführend 0,2-0,3m, geschlossen	230
sf		220	65 Dolomit	230
sf		212	75 Dolomit	230
sf		210	80 Dolomit	230

5.8 Drillholes

DH	year	N	O	Z	Max Length	hole_path
ck182	2009	13938	95876	222,44	303,23	LINEAR
ck183	2009	13864	92870	239,31	291,36	LINEAR
ck184	2009	13799	92858	237,16	200,37	LINEAR
ck178	2009	13724	92851	251,93	273,32	LINEAR
ck175	2009	13660	92843	241,26	140,3	LINEAR
ck141	2009	13878	92466	263,84	288,64	LINEAR
ck142	2009	13815	92458	227,92	200,5	LINEAR
ck143	2009	13740	92448	217,08	230,17	LINEAR
ck177	2009	13660	92442	230,6	280,73	LINEAR
ck144	2009	13594	92432	248,75	275,93	LINEAR
ck145	2009	13518	92425	262,57	272	LINEAR
ck152	2009	13826	92660	248,78	300,32	LINEAR
ck151	2009	13707	92659	274,59	279,5	LINEAR
ck153	2009	13586	92640	358,33	300,76	LINEAR
ck123	2009	13718	92348	229,91	291,67	LINEAR
ck121	2009	13806	92356	206,93	223,54	LINEAR
ck124	2009	13644	92342	238,7	352,97	LINEAR
ck125	2009	13570	92330	241,94	306,15	LINEAR
ck126	2009	13504	92323	249,11	378,83	LINEAR
ck171	2009	13440	92315	258,3	310,37	LINEAR
ck162	2009	14020	92582	195,99	297,2	LINEAR
ck164	2009	13869	92567	237,96	303	LINEAR
ck165	2009	13818	92556	265,66	320,15	LINEAR
ck134	2009	13754	92554	279,24	317,45	LINEAR
ck148	2009	13696	92546	275,62	313,1	LINEAR
ck120	2009	13640	92538	282,67	326	LINEAR
ck108	2009	13576	92528	282,52	352	LINEAR
ck122	2009	13514	92521	283,92	296,11	LINEAR
ck149	2009	13451	92514	305,08	400,17	LINEAR
ck173	2009	13816	92760	216,58	282,02	LINEAR
ck172	2009	13748	92750	237,54	243,69	LINEAR
ck127	2009	13681	92748	272,98	310,02	LINEAR
ck128	2009	13608	92737	301,16	351,81	LINEAR
ck129	2009	13547	92730	300,1	400,67	LINEAR
ck157	2009	13431	92717	312,33	202,45	LINEAR
ck109	2009	13718	91544	230,91	134,50	LINEAR
ck105	2009	13614	91532	234,49	150,20	LINEAR
ck137	2009	13686	92092	187,59	167,59	LINEAR
ck106	2009	13598	92082	223,98	281,98	LINEAR
ck114	2009	13530	92074	268,61	334,1	LINEAR
ck116	2009	13454	92066	276	427,29	LINEAR
ck136	2009	13680	91988	186,89	120,9	LINEAR
ck107	2009	13756	91348	211,56	110,23	LINEAR
ck133	2009	13680	91786	161,48	128,1	LINEAR
ck103	2009	13732	92248	196,61	86,1	LINEAR
ck117	2009	13686	92242	202,12	206,13	LINEAR
ck139	2009	13616	92236	226,74	231,36	LINEAR
ck140	2009	13548	92228	234,56	253,17	LINEAR
ck101	2009	13786	92252	103,65	40,37	LINEAR
op106-2 2	2009	13738,373	92097,018	115	36	LINEAR
op106-2 1	2009	13714,508	92094,439	115	24	LINEAR
op117-3	2009	13670,596	92240,388	126	97,47	LINEAR
op106-6	2009	13662,587	91987,286	115	110	LINEAR
op117-7	2009	13736,781	92348,268	124	19	LINEAR